**UNIVERSITÀ
DEGLI STUDI
DI TRIESTE**

**UNIVERSITÀ
DEGLI STUDI
DI UDINE**

**Dottorato di Ricerca Interateneo in
Ingegneria Civile - Ambientale e Architettura**

Curriculum: INGEGNERIA CIVILE
Settore Scientifico Disciplinare: ICAR/09
XXXIV Ciclo

Seismic behavior of RC beam-column joints reinforced with deformed or smooth bars

Ph.D. program Coordinator
Prof. Alberto Sdegno

Thesis Supervisor
Prof.ssa Margherita Pauletta

Thesis Co-Supervisor
Prof. Gaetano Russo

Ph.D. Candidate
Caterina Di Marco

ANNO ACCADEMICO 2020/2021

Abstract

Modern seismic design of reinforced concrete (RC) buildings is based on the capacity design principles, which provide for the dissipation of seismic energy through the development of ductile mechanism in the structural elements. Beam-column joints are critical elements, since they are governed by shear and bond behavior, with low ductility and scarce energy dissipation. In the absence of modern seismic codes prescriptions, many existing RC buildings designed before mid-1970 present structural deficiencies, like no joint shear reinforcement and the use of smooth bars. These deficiencies may lead to develop brittle failure mechanisms and to the sudden collapse of the structure, under earthquake actions.

In this thesis, the experimental seismic behavior of an exterior beam-column joint, designed according to the Italian Building Code for high ductility class, but built without the required horizontal ties in the joint core, to simulate a construction error is investigated. This construction error is plausible because, according to the design prescriptions, the joint panel is very crowded with reinforcement bars and the concrete casting and compaction is objectively difficult. The thesis explains in detail the occurred failure mechanisms due to the construction error.

The correct evaluation of beam-column joints shear strength is of fundamental importance to respect the strength hierarchy and allow the ductile mechanisms development. This thesis focuses on shear strength of interior beam-column joints. In particular, a direct formula which accounts for the contributions of three inclined concrete struts and joint reinforcements, the column horizontal stirrups and intermediate vertical bars, is derived. The coefficients of the contributions are calibrated on the basis of experimental results, present in the literature, and the shear strength proposed expression is validated through the comparison with other existing formulae.

Finally, an overview on seismic behavior of beam-column joints reinforced with smooth bars, collected in the literature, is presented. The tests considered concern both interior and exterior joints and take into account the main features influencing joint behavior, including horizontal reinforcement amount, column axial load and anchorage arrangement solutions. A critical discussion of the damage and failure mechanisms developed in the joints is presented and the possible relationships between the structural inadequacies and the final failure modes are highlighted. Besides, the resisting mechanism contributions to shear strength for joints reinforced with smooth bars are

assessed. This thesis is presented as a useful tool for future aware design of beam-column joints reinforced with deformed bars in new RC buildings, and a comprehensive understanding of behavior of joints with smooth bars, to lead to effective retrofit solutions for existing buildings.

Contents

1. Introduction

Modern earthquake resistant concrete buildings are designed according to Capacity Design principles, which provide for the development of ductile mechanisms in the beams, the "plastic hinges", and for the seismic energy dissipation under reversal cyclic loads, thereby avoiding brittle failure of the structures. According to these principles, beam-column joints are critical elements, because their behavior is governed by shear and bond mechanisms, both characterized by low ductility and limited energy dissipation capacity, which could lead to brittle failures in reinforced concrete (RC) structures under seismic loading.

Seismic codes provide specific and strict provisions and requirements to prevent joint shear failure mechanisms and to ensure adequate dissipation of energy in the ductile elements of the frame. Normally, the codes present recommendations for member proportions, confinement of the column core in the joint region or control of joint shear stresses, ratio of column-to-beam flexural strength at the connection, development of reinforcing bars, and details of columns and beams framing into the joint ([1]-[4]).

Although the detailing requirements differ from one code to another, in general, the amount of shear reinforcement required by modern codes often leads to steel congestion in the joint core, which may cause complications during concrete casting and compaction. The provisions of Eurocode 8 [2] for the design of beam-column connections are based on the strut-and-tie mechanisms, which accounts for the contributions of the diagonal concrete strut of joint horizontal stirrups and vertical reinforcement. In ACI Building Code [1] instead, the design shear strength for beam-column joints only depends on the joint geometrical characteristic and the concrete cylindrical compressive strength. However, both Codes require that column confinement be continued in the joint region, assuring confinement to the diagonal strut. This requirement, together with the presence of beams and columns longitudinal bars, could lead to reinforcement congestion in the joint core. This problem can arise particularly in the exterior beam-column joints, as the longitudinal bars of the converging beam have to be bent into the joint core with 90-degree hooks. This issue is investigated in Chapter 2, which illustrates the analytical study of behavior of RC exterior joint behavior, where a construction error due to reinforcement overcrowding inside the joint is present. Two full-scale identical specimens are realized and tested in the Laboratory for Testing Materials and Structures of the University of Udine, designed according to the Italian Building Code [3] prescriptions for high ductility

structural elements. In order to investigate the consequences of a potential construction error, the specimens are deprived of the code-specified ties inside the joint core. The author investigates if the tested joints are still able to perform ductile behavior, or if shear failure occurs.

Given the importance of shear design of RC beam-column joints, various authors [5]-[17] have tried to predict the strength of these structural elements under seismic loads and proposed empirical and mathematical models to evaluate joint shear strength. However, the shear strength calculation is often based on iterative procedures and the predicting formulae are not always accurate, due to the presence of several resisting mechanisms developed in beam-column joints, during earthquakes. In Chapter 3 a model for shear strength prediction of RC interior joints under seismic actions is presented. A direct formula for interior joint shear strength is derived, accounting for the resisting contributions of three inclined concrete struts and joint reinforcements, the column horizontal stirrups and the vertical intermediate bars. Also a design formula is proposed and its results are compared with those of design formulas provided by codes [1], [2].

Before the mid-1970s, due to the limited extension of the zones classified as seismic, many RC Italian buildings were normally designed to resist to gravity and wind loads only, without considering the seismic action and certain reinforcement arrangements and design details. Hence, many existing RC structures in Italy cannot resist even minor earthquakes, as they present several structural deficiencies, such as the absence of horizontal hoops in the joints, inadequate reinforcement anchorages, and the use of smooth reinforcing bars. This condition of existing RC buildings in Italy is representative of buildings present in other seismic regions of the Mediterranean area, which need to be strengthen to resist seismic actions. To design adequate and safe retrofitting solutions for the built heritage, it is of primary concern to study seismic behavior of beam-column joints in RC structures reinforced with smooth bars. Chapter 4 presents such a study reporting the largest collection possible of experimental results, available in the literature, on beam-column joints, both interior and exterior, representing typical joints of existing RC buildings constructed before the mid- 1970s. Several parameters influencing joint behavior are analyzed, including horizontal reinforcement amount, column axial load and anchorage arrangements. The correlations between the failure modes and the inadequacies of certain reinforcement arrangements and details of the collected joints are investigated. Furthermore, it is deepened the influence of column axial load on joint shear stress at failure and the applicability of existing shear strength expressions for joints with

deformed bars to joints with smooth bars.

2. Seismic behavior of exterior RC beam-column joints without Code-specified ties in the joint core

Beam-column joint design for RC buildings is a critical issue for modern earthquake engineering, because for these structural elements, the current codes provide several geometrical constraints and reinforcement provisions, which may be very complex to implement during the construction phase.

Modern RC buildings are designed according to the Capacity Design principles, which provide for the dissipation of the seismic energy by ensuring the complete development of the plastic hinges of the ductile structural elements and preventing the event of brittle failure mechanisms. According to these design criterions, beam-column joints are critical elements, since their behavior under cyclic actions is governed by brittle failure mechanisms, in particular shear and bond mechanism. For these reasons the codes provide specific detailing requirements, which ensure the dissipation of energy in the plastic hinges adjacent to the joint and prevent joint shear failure.

The design approach regarding beam-column connections varies among the codes, as underlined by Uma and Jain [18] in a critical review of the joint design and detailing requirements of the ACI Code (ACI 318M-02) [19], New Zealand Standards (NZS 3101:1995) [20] and Eurocode 8 (EN 1998-1:2003) [2].

Generally, the codes provide a wide range of recommendations regarding member proportions, adequate confinement in the joint core, joint shear stress control, anchorage development of reinforcing bars and details of the elements framing into the joint ([1]-[4], [20]). The numerical values of the prescribed limits are generally different from one code to another; moreover, distinguished from the ACI Code and New Zealand Standards, Eurocode 8 [2] and also the Italian Building Code [3] classify concrete buildings in two ductility classes: "DCM" (medium ductility class) and "DCH" (high ductility class), with the rules governing the seismic design of structural elements being more demanding for the DCH structures. Notwithstanding the different details required, the several geometrical constraints and reinforcement provisions provided by the current codes are very complex to implement during the construction phase. Actually, the steel gathering, due to the shear reinforcement amount required by modern codes, makes the concrete casting and compaction difficult, particularly for exterior beam-column joints. This specific topic is considered by the author mentioned in the following literature review.

Hwang et al. [21] investigated the role of hoops on shear strength of exterior RC beam-column joints and made an attempt to relieve the reinforcement congestion in the joint core, due to seismic design provisions. On the basis of test results, they observed that a minor amount of transverse reinforcement could be used without significantly affecting the performance of the joint. Moreover, these authors underlined that the different requirements of the Codes about the joint transverse reinforcement depend on the different role attributed to this reinforcement in the shear resisting mechanism. Indeed, New Zealand Standards assume that joint hoops are necessary to transfer tensile force and concur to the truss mechanism to resist shear [20]. ACI Code method [19], instead, supposes that the role of transverse reinforcement is to confine the concrete strut in the joint core and the amount of joint hoops is proportional to the concrete strength.

Hwang and Lee [22] developed a softened strut-and-tie model and they observed from the test results available in the literature that joint hoops unequally participate in resisting shear forces. From this consideration, in their model they assumed that the hoops within the center half of the joint core are fully effective, while the other hoops contribute at a rate of 50%.

Ehsani and Wight [23] carried out experimental tests on exterior beam-column joints, to study the effects of different parameters on the joint seismic response. They observed that additional transverse reinforcement enhances joint shear strength, but makes the sub-assemblage very difficult to construct. In addition to the amount of joint shear reinforcement, the key variables considered by the authors were the flexural strength ratio, defined as the sum of the flexural capacities of beam and columns, and the shear stress in the joint. From experimental evidences, Ehsani and Wight found that the amount of joint transverse reinforcement could be safely reduced when either the flexural strength ratio, the joint shear stress or the anchorage requirements are considerably more conservative than the recommended limits.

Kotsovou and Mouzakis [24] proposed a design method for exterior joints, that satisfies the performance requirements of Eurocodes 2 and 8 ([25] and [2], respectively) through a minor amount of joint reinforcement. In their research, the authors observed that the amount of horizontal hoops, recommended by EC8 to activate the truss mechanism, results in steel congestion in the joint core. Furthermore, their experimental investigations demonstrated that the provisions of EC2 and EC8, for high ductility members, are not capable to avoid diagonal cracking of the joint before the development of a plastic hinge in the adjacent beam.

As previous studies confirmed, Codes' provisions for high ductility design of RC building often lead to construction difficulties due to the presence of heavy reinforcement in the joint core. Hence it is possible that, due to these difficulties, the builder voluntary or accidentally omits parts of the reinforcement, such as the ties for example, in the realization of beam-column joints. Taking into account this possibility, the aim of this research work is to study the response to severe cyclic actions of beam-column joints designed for DCH, but executed in the presence of a plausible construction error, which leads to a minor amount of joint horizontal reinforcement, compared to that of design recommendations.

An exterior joint is selected from a building designed under the condition of high ductility [26] according to the Italian Building Code [3]. Two full-scale identical sub-assemblages, representing this joint, are realized and tested in the Laboratory for Testing Materials and Structures of the University of Udine. The specimens are realized identical to observe their average behavior.

In order to assess the consequences of the potential construction error, the sub-assemblages are deprived of the code-specified ties in the joint core. In particular, the author want to investigate if the considered joint, despite the absence of few ties, is still able to perform a ductile behavior, avoiding shear failure of the joint core. It is taken for granted that a code-conforming joint would have exhibited ductile behavior.

For the definition of the test loading pattern, the forces acting on the beam end and the corresponding vertical displacements are evaluated at the beam cracking, yielding and ultimate strength conditions. After testing, these values are compared to the test results. To assess the development of the plastic hinge in the beam and study the joint failure mode, the yield and the ultimate moments of the beam cross-section are also analytically calculated and compared to the moments derived from the application of the test forces.

To check for the possibility of joint shear failure, the maximum horizontal shear acting in the joint is calculated using the formula proposed by Paulay and Priestley [27] and then it is compared to the joint shear strengths provided by Eurocode 8 [2], the ACI Code [1] and Pauletta et al. [28].

2.1. Experimental program

2.1.1. Specimens details

Two identical full-scale exterior reinforced concrete beam-column joints, labeled J1 and J2, are tested (Fig. 1 and Fig. 2). The test units represent a corner joint of a typical multistory building frame, obtained by removing one of the beams framing into the joint, and cutting the remaining beam and the columns at about mid-span and mid-height, respectively, which correspond approximately to their inflection points. The geometric properties of the specimens, i.e., column height, beam span and dimensions of cross sections, are shown in Fig. 1: the distance of the beam end from the column face is 1770 mm and the overall height of the specimens is 2800 mm. Fig. 1 also shows the column width tapering toward the top along the joint height and the eccentricity between the beam axis and the axes of the top and bottom columns. This eccentricity decreases from 125 mm to 100 mm going from the bottom to the top of the joint panel.

Beam section dimensions are 300x550 mm while column section dimensions are 550x300 mm and 500x300 mm, in the bottom and top columns, respectively.
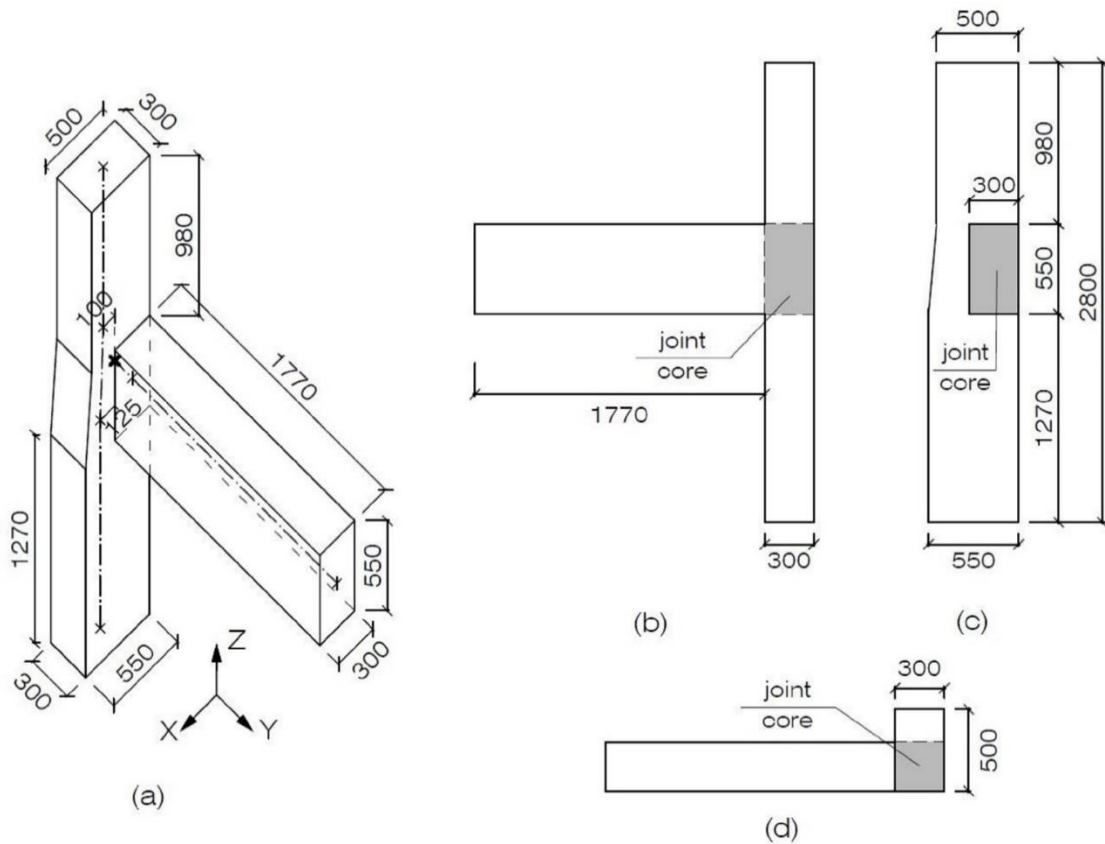
Fig. 1 (a). Axonometric view, (b) lateral view, (c) beam side view and (d) plan view of test specimens.
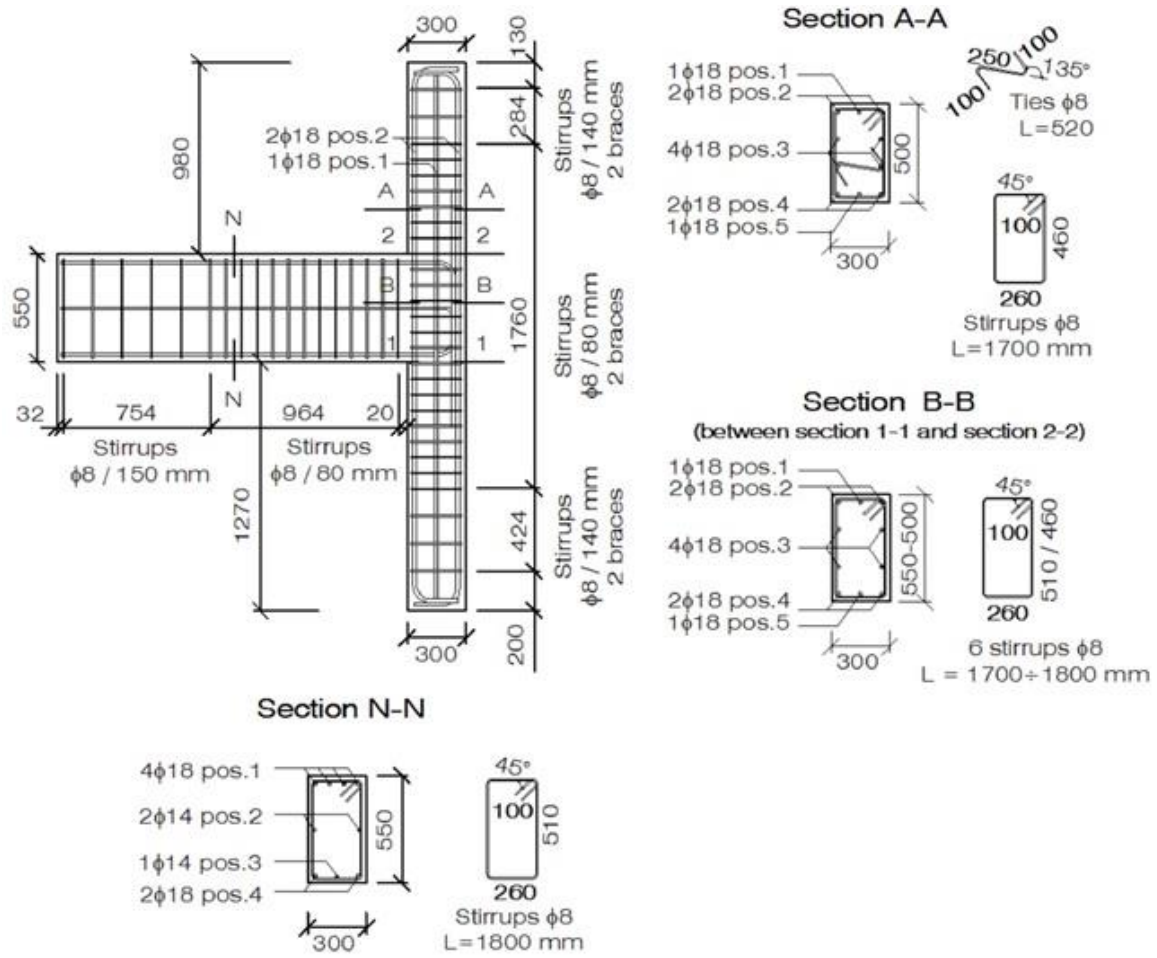
Fig. 2. Reinforcement details of the specimens.

The specimens are cast using concrete with prescribed compressive strength class C25/30 (nominal cylinder strength $f_{c,nom}$ = 25 MPa, nominal cubic strength $R_{c,nom}$ = 30 MPa). The members of the building frame [26], from which the considered joint is extracted, were designed to develop weak-beam strong-column behavior according to high ductility provisions given by the Italian Building Code [3]. The code prescriptions require that the total amount of horizontal hoops in the joint core is at least the same as that of the column in the critical region, and that in the joint core the minimum total area of hoops is

$$\sum A_{sh} = 0.05 \frac{f_{ck} \cdot b_j}{f_{yk}} \cdot s \tag{1}$$

where f_{ck} is the characteristic compressive concrete strength, which in the design stage of the joint was assumed equal to 25 MPa; f_{yk} is the reinforcing hoops characteristic yield strength, equal to 450 MPa; s is the hoops' maximum spacing; and b_j is the effective joint width, defined as follows:

$$b_j = \begin{cases} \min(b_c, b + 0.5h_c) & \text{for } b < b_c \\ \min(b, b_c + 0.5h_c) & \text{for } b \geq b_c \end{cases} \tag{2}$$

with b the beam width, b_c the column width, and h_c the column depth. According to the beam-column joint geometry (Fig. 2), $b = 300$ mm, $b_c = 500$ mm, and $h_c = 300$ mm, hence b_j is equal to 450 mm. By adopting the maximum hoop spacing $s = 80$ mm in the joint core, the minimum area of transverse reinforcement required in the joint core (Eq. (1)) is 100 mm^2. To satisfy Code prescriptions, the transverse reinforcement required in the joint core corresponds to 2 braces of 8 diameter hoops.

The requirement on the minimum total area of horizontal transverse reinforcement in the critical regions of the column is [3]

$$\sum A_{sh} = 0.12 \frac{f_{cd} \cdot b_{st}}{f_{yd}} \cdot s \tag{3}$$

where b_{st} is the distance between the further braces of reinforcement equal to 502 mm in one direction and 252 mm in the other (Fig. 2); f_{cd} is the design compressive concrete strength equal to $\alpha_{cc} \frac{f_{ck}}{\gamma_c}$ with α_{cc} a coefficient taking into account the load's long-term effects on compressive strength, assumed herein equal to 1 [3], because the joints had not been loaded before the tests; γ_c is the partial factor for concrete, assumed herein equal to 1.5 [3]; and f_{yd} is the hoops design yield strength equal to $\frac{f_{yk}}{\gamma_s}$, with $\gamma_s = 1.15$, the partial factor for reinforcing steel. It results $f_{cd} = 14.17$ MPa, and $f_{yd} = 391.3$ MPa. With the maximum adopted spacing $s = 80$ mm, the minimum areas of horizontal reinforcement required for the column section principal directions (Eq. (3)) are 175 mm^2 and 87 mm^2, which correspond to at least 4 braces and 2 braces of 8 diameter reinforcement, parallel to the column section depth and width (Fig. 2), respectively. Since the required area of horizontal reinforcement is greater in the column than in the joint core, and the Italian Building Code [3] requires that the reinforcement in the joint core be at least the same as

that of the column, the latter requirement holds also in the joint. Hence, in the joint core 4 braces are needed in the direction parallel to the column section depth (300 mm in Fig. 2), while, 2 braces are needed in the direction parallel to the column section width (500 mm in Fig. 2).

According to these provisions, beyond the 8 diameter hoop bent around the column longitudinal bars, two ties parallel to the column depth should be put inside the joint core and in the columns and linked to the column vertical intermediate bars, where with "*tie*" it is intended the S-shaped pieces of bar, visible in Fig. 2, section A-A. This would be the beam-column joint configuration without the construction error.

In this way the joint reinforcement would be considerably packed, making the concrete compacting operations difficult. Taking this in account, in order to reproduce the effects of a construction error, specimens are cast completely omitting the S-shaped ties in the joint core, thus reducing by 50% the horizontal reinforcement in the direction parallel to the column section depth. In the column, instead, solely one tie is omitted, thus reducing by 25% the total amount of horizontal reinforcement in the critical regions, in the direction parallel to the column section depth.

Fig. 2 shows the size, amount, arrangement and details of both longitudinal and transverse reinforcements of the beam-column joints being tested. More specifically, Fig. 2 represents the condition where the construction error is present, in fact, no S-shaped ties are present in the joint core (Section B-B) and one tie is present in the column (Section A-A).

It should be noted that, due to the absence of two ties in the joint core and one tie in the column, the sub-assemblage with the reinforcement configuration in Fig. 2 does not satisfy the requirements for high ductility design (Eqs. (1) and (3)) and cannot be considered a high ductility class seismic element. Moreover, it does not satisfy not even the requirements for medium ductility class and should be classified as a non-ductile element.

2.1.2. Materials properties

In order to determine the actual concrete compressive strength at the time of testing (about 2 years after the casting), 4 core samples were extracted (after testing) from undamaged regions of the two specimens: 2 samples from unit J1 (N1.1 and N1.2) and 2 from unit J2 (N2.1 and N2.2). The core samples were then tested according to the UNI EN 12504-1 protocol [27]. The geometric properties, diameter d_s and height h_s, of the core samples

and compression tests results, rupture load and corresponding strength f_c, are reported in Table 1. From this table the mean compressive concrete strength can be derived as: $f_{cm} = \frac{1}{4}\sum_{i=1}^{4} f_{ci} = 49.85$ MPa. The corresponding characteristic concrete compressive strength can be calculated as $f_{ck} = f_{cm} - 8 = 41.85$ MPa [3] and subsequently the design concrete compressive strength $f_{cd} = \alpha_{cc}\frac{f_{ck}}{\gamma_c} = 23.72$ MPa [3]. The concrete elastic modulus in compression, E_c, is calculated from $E_c = 22{,}000 \cdot \left(\frac{f_{cm}}{10}\right)^{0.3}$ [3], which gives $E_c = 35{,}622$ MPa.

Table 1. Geometric properties and compressive strength of core samples.

Specimen	d_s (mm)	h_s (mm)	Load (kN)	f_c (MPa)
N1.1	94	197	390,5	56,3
N1.2	94	195	314,4	45,3
N2.1	94	197	324,3	46,8
N2.2	94	197	353,7	51,0

Steel B450C [3] was used in the specimens both for longitudinal and transverse reinforcement, with characteristic yield tensile strength equal to $f_{y,nom} = f_{yk} = 450$ MPa. To determine the real average value of this strength, the experimental results of tensile tests on 50 bar specimens of diameter 14 mm and 9 of diameter 18 mm, coming from the same manufacturer of those bars used to make the joints, are considered. The obtained average yield strength, calculated on the complete set of 59 specimens, is 527.7 MPa. The corresponding coefficient of variation is equal to 0.047. Steel elastic modulus, E_s, is assumed equal to 210,000 MPa [3].

The design, characteristic and mean values of concrete strength are reported in Table 2 at column (1). The values of steel reinforcement yield strength are reported in column (3).

Table 2. Design, characteristic, and mean values of strength and strain for concrete and reinforcing steel.

	Concrete C25/30		Steel B450C	
	(1)	(2)	(3)	(4)
	(MPa)	(%)	(MPa)	(%)
Design values	f_{cd} 23.72	ε_{cu} 0.35	f_{yd} 407.9	ε_{syd} 0.194
Characteristic values	f_{ck} 41.85	ε_{cu} 0.35	f_{yk} 469.1	ε_{syk} 0.223
Mean values	f_{cm} 49.85	ε_{cu} 0.35	f_{ym} 527.7	ε_{sym} 0.251

2.1.3. Test setup and instrumentation

The test apparatus and boundary conditions of the beam-column joint are shown in Fig. 3. The column ends of the specimens were laterally restrained to the lateral steel reaction frame and the bottom column was supported by a steel pillar anchored to the concrete foundation. A constant axial compression load $N = 327$ kN was applied to the top column by a hydraulic jack with 718 kN capacity (Fig. 3b). A reversed cyclic vertical load was applied to the beam end by a MTS hydraulic actuator with 500 kN capacity, at 1600 mm distance from the column face (Fig. 3a).
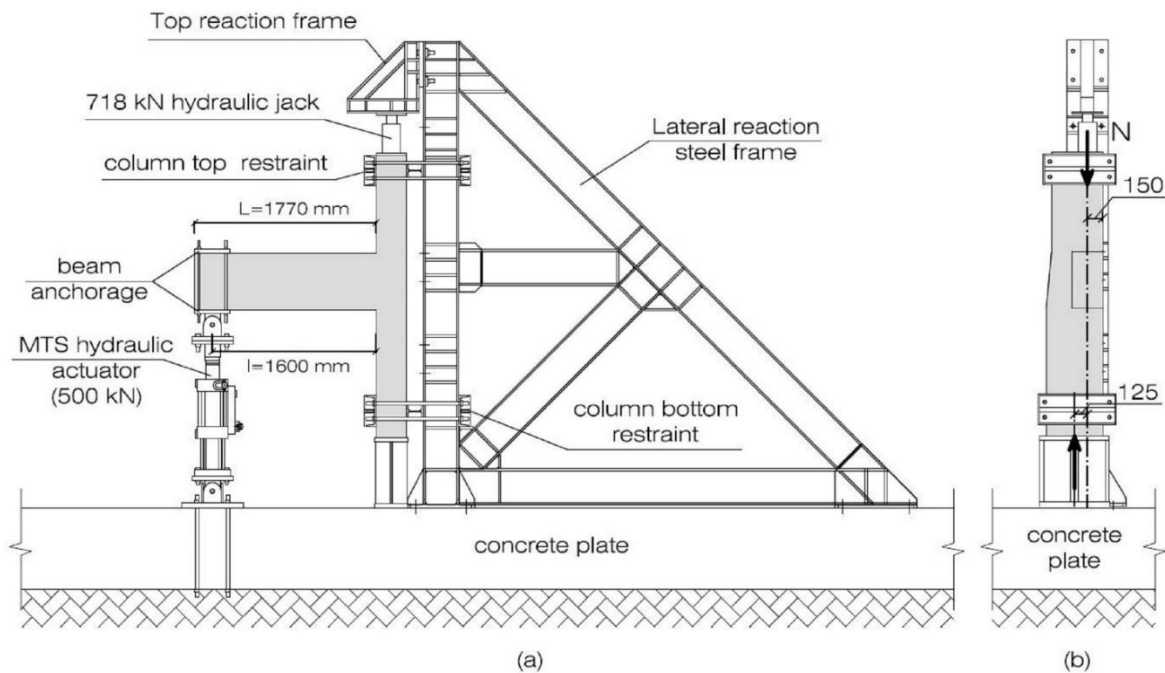
Fig. 3. Test setup: (a) lateral view and (b) beam side view.

The corresponding static scheme of the beam-column sub-assemblage is shown in Fig. 4a.

Potentiometric transducers (denoted by letter P in Fig. 5) were attached to the beam-column joint faces along the diagonal, vertical and horizontal directions to measure joint panel deformations. Inductive transducers (denoted by letter I in Fig. 5) were attached at the beam-column interface to measure top and bottom beam surface deformations and cracks opening within the potential plastic hinge region.

Fig. 4 (a). Static scheme of specimens during cyclic tests; (b) bending moment pattern for downward force.

Fig. 5. Transducers arrangement in the specimens: (a) left lateral and (b) right lateral views, respectively, with respect to the beam axis.

The testing method was displacement-controlled, and the cyclic load simulating the seismic force was quasi-statically applied. The displacement history imposed on the beam free end followed a cyclic sequence, and it was based on displacement increments of 4 mm at each loading step, for displacements from 4 mm (1st step) to 20 mm (5th step), and increments of 10 mm thereafter.

The test was stopped at 60 mm (9th step) for specimen J1, and continued up to 90 mm (12th step) for specimen J2. Each step included 4 load cycles at the same displacement amplitude. The loading rate was kept constant throughout the test and equal to 0.5 mm/s. Since load reversal frequency is defined as the ratio between the load application rate and the displacement, it follows that the frequency decreased step by step.

2.2. Theoretical models for structural behavior prediction

2.2.1. Beam bending moments at first cracking

In order to predict the beam end upward and downward displacements, which induce the opening of the first crack at the beam bottom and top surfaces, it is necessary to determine the beam positive and negative cracking moments, M_{cr}^{+} and M_{cr}^{-}, respectively.

The calculation of the beam positive and negative cracking moments assumes elastic behavior of the beam cross section and a maximum tensile stress in the concrete equal to the concrete flexural tensile strength f_{cfm} (Fig. 6). This strength is calculated by means

of $f_{cfm} = 1.2 \cdot f_{ctm}$ [3], where f_{ctm} is the concrete mean tensile strength, calculated from the characteristic value of compressive strength $f_{ctm} = 0.3 \cdot (f_{ck})^{2/3}$ [3].
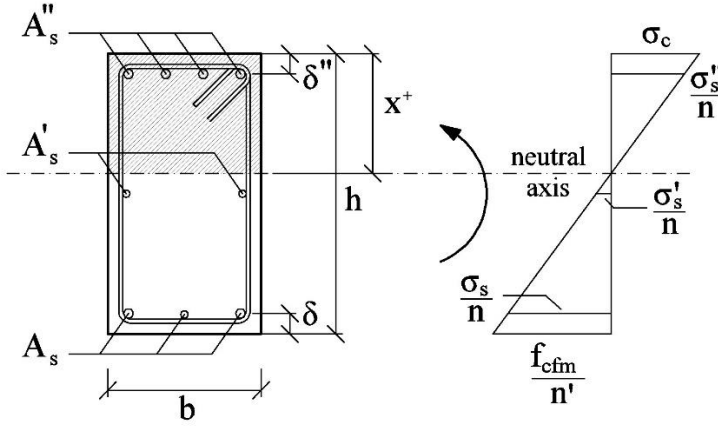
Fig. 6. Homogenized stress distribution in beam cross section at the concrete cracking, for positive bending.

To compute the beam positive and negative cracking moments, the neutral axis depth x is determined by imposing the horizontal equilibrium of the beam internal forces and the strain compatibility conditions. For positive bending moment, the following equation gives the neutral axis depth x^+

$$
\frac{bx^{+2}}{2} - n' \cdot b \frac{(h - x^+)^2}{2} + n \cdot A_s''(x^+ - \delta'') - n \cdot A_s(h - x^+ - \delta) - n
$$
$$
\cdot A_s'\left(\frac{h}{2} - x^+\right) = 0
\tag{4}
$$

where (Fig. 6) b and h are the beam width and height; A_s'', A_s' and A_s are the areas of beam top, middle and bottom longitudinal reinforcing bars, respectively; δ'' and δ are the distances between the centroid of top and bottom beam reinforcements, respectively, to the nearest edge of the beam cross section; and n and n' are the modular ratios given by $n = \frac{E_s}{E_c}$ and $n' = 0.5$.

The positive bending moment, M_{cr}^+, inducing the opening of the first crack at beam bottom surface can be computed as follows:

$$
M_{cr}^+ = \frac{f_{cfm}}{n'} \cdot \frac{I_n^+}{(h - x^+)}
\tag{5}
$$

where $I_n{}^+$ is the moment of inertia about the neutral axis x^+ of the cross section, which is considered completely reactive, since it is not yet cracked.

Analogously, for the negative bending at the time of the first crack opening, the neutral axis depth, x^-, and the corresponding negative cracking moment, M_{cr}^-, are given by the following equations

$$\frac{bx^{-2}}{2} - n' \cdot b \frac{(h - x^-)^2}{2} + n \cdot A_s(x^- - \delta) - n \cdot A_s' \left(\frac{h}{2} - x^-\right) - n \qquad (6)$$
$$\cdot A_s''(h - x^- - \delta'') = 0$$

$$M_{cr}^- = \frac{f_{cfm}}{n'} \cdot \frac{I_n{}^-}{(h-x^-)} \qquad (7)$$

where $I_n{}^-$ is the moment of inertia about the neutral axis x^- of the cross section, considered completely reactive.

The upward and downward forces, F_{cr}^+ and F_{cr}^-, which induce the positive and negative cracking moments in the beam cross section at column interface, can be determined by imposing the rotational equilibrium of the beam with respect to this section, as follows:

$$F_{cr}^+ = \frac{\left(M_{cr}^+ + \frac{qL^2}{2}\right)}{l} \qquad (8)$$

$$F_{cr}^- = \frac{\left(M_{cr}^- - \frac{qL^2}{2}\right)}{l} \qquad (9)$$

where q is the distributed self-weight of the beam; and L and l are the beam clear span and the distance of the actuator applying the force from the column face, respectively (Fig. 3a).

The upward and downward displacements, d_{cr}^+ and d_{cr}^-, applied to the beam end, which induce the formation of the first bottom and top beam cracks, respectively, are determined by solving, through Software SAP 2000, the static scheme shown in Fig. 4a, under the application of the forces given by Eqs. (8) and (9).

The values of the positive and negative cracking moments and the corresponding values of vertical forces and displacements are reported in
Table 3.

Table 3. Positive and negative values of beam bending moments, vertical forces, and beam end displacements at first beam cracking, calculated with the materials' mean strength, and experimental mean values.

	M_{cr}^{+} (kNm)	F_{cr}^{+} (kN)	d_{cr}^{+} (mm)	M_{cr}^{-} (kNm)	F_{cr}^{-} (kN)	d_{cr}^{-} (mm)
Predicted values	91.57	61.27	5.17	-96.19	-56.08	-5.58
Experimental mean values		62.05	4.30		-66.98	-4.81

2.2.2. Beam bending moments at first yield

The yield moments are calculated assuming that yielding occurs due to the plasticization of the longitudinal bars under tensile stresses; it is used the mean value of yield strength and it is assumed that the concrete remains elastic under compression, and concrete tensile contribution is neglected.

For the calculation of the yield moments, the neutral axis depth at the tensile reinforcement first yield can be obtained by imposing the beam internal forces equilibrium and the strain compatibility conditions, similarly to what was done with Eqs. (4) and (6), assuming the tensile steel strain equal to the yielding one.

By writing the rotational equilibrium of the internal forces acting on the beam section with respect to the compression reinforcement, the positive and negative yield moments can be calculated as follows:

$$M_y^{+} = A_s \cdot f_y \left(\frac{h}{2} - \delta\right) + \frac{b \, x^{+2}}{2} \cdot \frac{\varepsilon_y}{(h - x^+ - \delta)} \cdot E_c \left(\frac{h}{2} - \frac{x^+}{3}\right) + A_s'' \cdot E_s$$
$$\cdot \frac{\varepsilon_y}{(h - x^+ - \delta)} \cdot (x^+ - \delta'') \left(\frac{h}{2} - \delta''\right) \tag{10}$$

$$M_y^{-} = A_s'' \cdot f_y \left(\frac{h}{2} - \delta''\right) + \frac{b x^{-2}}{2} \cdot \frac{\varepsilon_y}{(h - x^- - \delta'')} \cdot E_c \left(\frac{h}{2} - \frac{x^-}{3}\right) + A_s \cdot E_s$$
$$\cdot \frac{\varepsilon_y}{(h - x^- - \delta'')} \cdot (x^- - \delta) \left(\frac{h}{2} - \delta\right) \tag{11}$$

where f_y and ε_y are the steel yield strength and strain, respectively, and x^+ and x^- can be calculated from the horizontal equilibrium of the beam internal forces, analogously to Eqs. (4) and (6), assuming the tensile steel strain equal to ε_y.

Table 4 lists the values of the yield moments calculated by adopting the materials' design, characteristic, and mean strengths and strains reported in Table **2** (columns (1), (3) and (4)).

Table 4. Positive and negative values of beam bending moments, vertical forces, beam end displacements and cross section chord rotations at first beam yielding, calculated with design, characteristic, and materials' mean properties, and experimental mean values.

	M_y^+ (kNm)	F_y^+ (kN)	d_y^+ (mm)	θ_y^+ (1/mm)	M_y^- (kNm)	F_y^- (kN)	d_y^- (mm)	θ_y^- (1/mm)
Design values	142.18	92.90	7.73	0.0054	-207.64	-125.74	-11.48	0.0058
Characteristic values	163.50	106.23	8.91	0.0058	-238.79	-145.20	-13.19	0.0062
Mean values	183.94	119.33	10.03	0.0063	-268.64	-163.86	-14.83	0.0068
Experimental mean values		127.05	15.05			-152.70	-17.53	

The upward and downward forces corresponding to the positive and negative yield moments at the beam end are computed as follows (values in Table 4):

$$F_y^+ = \frac{\left(M_y^+ + \frac{qL^2}{2}\right)}{l} \tag{12}$$

$$F_y^- = \frac{\left(M_y^- - \frac{qL^2}{2}\right)}{l} \tag{13}$$

The corresponding displacements, d_y^+ and d_y^- in Table 5, are evaluated through Software SAP 2000, according to the static scheme in Fig. 4a and assuming a linear elastic behavior for steel and concrete. To take into account cracking in the joint elements due to the application of cyclic loading, the moment of inertia and the shear area of beam and column elements are reduced by 70% and 60%, respectively, when introduced into the SAP software.

2.2.3. Ultimate beam bending moments

In order to predict the maximum upward and downward beam end displacements at the flexural collapse of the beam-column interface, occurring at the attainment of the ultimate

strain in tensile reinforcement, ε_{su}, or the ultimate compressive strain in the concrete, ε_{cu}, whichever occurs first, material ductility is considered. More specifically, for steel reinforcement, the bi-linear stress-strain relationship with post-yield behavior described by a ideally plastic branch is adopted, and, for concrete, the equivalent stress-block shown in Fig. 7 is used.
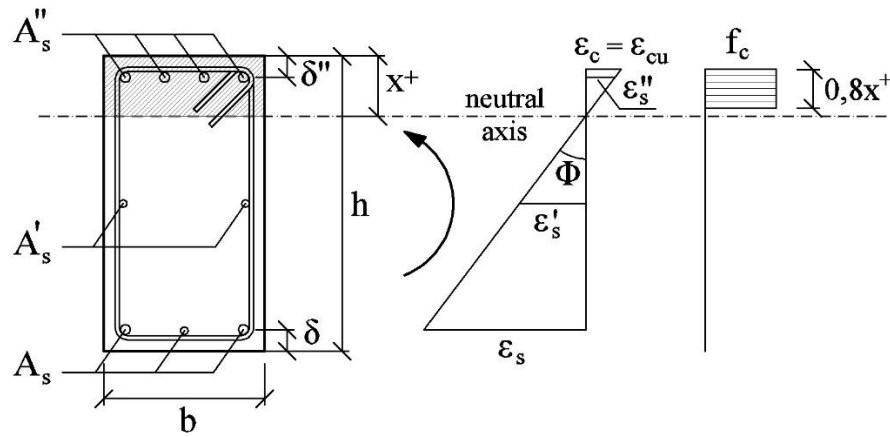
Fig. 7. Assumptions for the calculation of beam ultimate flexural capacity for positive bending moment.

Regarding steel, the design yield strain, ε_{syd}, is derived by dividing the design yield stress (Table **2**, column (3)) by the steel elastic modulus, $E_s = 210,000$ MPa. Analogously, the characteristic and mean yield strains, ε_{syk} and ε_{sym}, are derived using respectively the characteristic and mean stresses reported in Table **2** at column (3). The obtained values of the previous yield strains are reported in column (4) of the same table. Regarding concrete, the design, characteristic and mean values of strengths and strains are listed in Table **2** in columns (1) and (2), respectively.

In the calculation of the beam ultimate bending moments of the considered specimen (Fig. 2), it is found that, under positive and negative moments, the beam failure is attained due to concrete crushing failure, with the tensile reinforcement yielded.

To calculate the ultimate moments, a stress-block is adopted as shown in Fig. 7 for the case of positive moment, where the concrete strength is denoted in general with f_c, which becomes f_{cd}, f_{ck} or f_{cm}, depending on the used value for concrete strength, i.e. design, characteristic or mean value.

The ultimate capacity of the beam for positive bending moment is calculated from the rotational equilibrium of the beam section with respect to the middle longitudinal reinforcement

$$M_u{}^+ = 0.8 \cdot b \cdot x^+ \cdot f_c \cdot \left(\frac{h}{2} - 0.4 \cdot x^+\right) + A_s{}'' \cdot E_s \cdot \varepsilon_s{}'' \cdot \left(\frac{h}{2} - \delta''\right) + A_s \cdot f_y$$
$$\cdot \left(\frac{h}{2} - \delta\right)$$

(14)

with $\varepsilon_s{}''$ the strain in the top beam bars, equal to

$$\varepsilon_s{}'' = \frac{\varepsilon_{cu}}{x^+} \cdot (x^+ - \delta'')$$

(15)

The neutral axis depth x^+ can be determined by imposing the translational equilibrium of the beam section internal forces and the strain compatibility conditions, which, assuming that the middle and bottom reinforcements yield under tensile actions, leads to

$$a_1 \cdot x^{+2} + a_2 \cdot x^+ + a_3 = 0$$

(16)

with

$$a_1 = 0.8 \cdot b \cdot f_c$$

(17)

$$a_2 = -(A_s + A_s{}') \cdot f_y + A_s{}'' \cdot E_s \cdot \varepsilon_{cu}$$

(18)

$$a_3 = -A_s{}'' \cdot E_s \cdot \varepsilon_{cu} \cdot \delta''$$

(19)

Similarly, the ultimate capacity of the beam for negative bending moment is calculated from the rotational equilibrium of the beam section with respect to the middle longitudinal reinforcement

$$M_u{}^- = 0.8 \cdot b \cdot x^- \cdot f_c \cdot \left(\frac{h}{2} - 0.4 \cdot x^-\right) + A_s \cdot E_s \cdot \varepsilon_s \cdot \left(\frac{h}{2} - \delta\right) + A_s{}'' \cdot f_y$$
$$\cdot \left(\frac{h}{2} - \delta''\right)$$

(20)

where

$$\varepsilon_s = \frac{\varepsilon_{cu}}{x^-} \cdot (x^- - \delta)$$ (21)

and the neutral axis depth x^- is calculated by means of Eq. (16) with

$$a_1 = 0.8 \cdot b \cdot f_c$$ (22)

$$a_2 = -(A_s'' + A_s') \cdot f_y + A_s \cdot E_s \cdot \varepsilon_{cu}$$ (23)

$$a_3 = -A_s \cdot E_s \cdot \varepsilon_{cu} \cdot \delta$$ (24)

The upward and downward forces at beam end that induce beam flexural collapse, F_u^+ and F_u^- respectively, can be determined from Eqs. (12) and (13), substituting M_y^+ with M_u^+ from Eq. (14) and M_y^- with M_u^- from Eq. (20).

Table 5 reports the different values for the positive and negative ultimate moments of the beam, M_u^+ and M_u^-, and the corresponding values of vertical loads, F_u^+ and F_u^-, calculated by adopting the design, characteristic, and mean values of material strengths (Table 2).

Table 5. Positive and negative values of beam bending moments, vertical forces, beam end displacements and cross-section chord rotations at ultimate beam flexural conditions, calculated with design, characteristic, and materials' mean properties, and experimental mean values.

	M_u^+ (kNm)	F_u^+ (kN)	d_u^+ (mm)	θ_u^+ (1/mm)	M_u^- (kNm)	F_u^- (kN)	d_u^- (mm)	θ_u^- (1/mm)
Design values	163.49	106.22	50.22	0.0319	-231.91	-140.90	-50.81	0.0280
Characteristic values	190.85	123.32	57.76	0.0363	-270.23	-164.85	-58.51	0.0318
Mean values	215.22	138.55	60.41	0.0377	-304.60	-186.33	-61.39	0.0331
Experimental mean values		142.30	60.90			-175.10	-58.40	

The ultimate beam end displacement inducing the ultimate moment at the beam-column interface, d_u, can be calculated as the sum of the yield and plastic displacements ($d_u = d_y + d_{pl}$). For a cantilever beam, the plastic component of the ultimate displacement at the beam free end, d_{pl}, can be computed as $d_{pl} = (\theta_u - \theta_y) \cdot L_v$, where θ_u and θ_y are

the chord rotation at ultimate and yielding beam conditions, respectively, and L_v is the shear span, given by the moment/shear ratio at the constrained end section.

The value of the total ultimate chord rotation, θ_u, of concrete members with no shear diagonal reinforcement and in absence of axial loads, under cyclic loading, can be calculated using the following expression [29]:

$$\theta_u = \frac{1}{\gamma_{el}} \cdot 0.016 \cdot \left[\frac{\max(0.01; \omega')}{\max(0.01; \omega)} \cdot f_c \right]^{0.225} \cdot \left(\frac{L_v}{h} \right)^{0.35} \cdot 25^{(\alpha \cdot \rho_{sw} \cdot \frac{f_{yw}}{f_c})} \tag{25}$$

where γ_{el} is equal to 1,5 for primary seismic elements; ω' and ω are the mechanical ratios of the compression and tensile longitudinal reinforcements, respectively; f_{yw} is the characteristic yield strength of the transverse reinforcement; and $\rho_{sw} = A_{sw}/(b \cdot s_w)$ is the geometric ratio of the beam transverse reinforcement parallel to the shear direction, with A_{sw} the cross-sectional area of reinforcement and s_w the stirrup spacing.

The value of the total chord rotation at yielding, θ_y, may be computed using the following expression [29]

$$\theta_y = \Phi_y \cdot \frac{L_v}{3} + 0.0013 \cdot \left(1 + 1.5 \cdot \frac{h}{L_v} \right) + 0.13 \cdot \Phi_y \cdot \frac{d_b \cdot f_y}{\sqrt{f_c}} \tag{26}$$

where Φ_y is the yield curvature at the beam constrained section, calculated with reference to the section in Fig. 7 from

$$\Phi_y{}^+ = \frac{\varepsilon_y}{(h - x^+ - \delta)} \tag{27}$$

and

$$\Phi_y{}^- = \frac{\varepsilon_y}{(h - x^- - \delta'')} \tag{28}$$

Different values for the positive and negative chord rotations at yielding and ultimate conditions are calculated by adopting design, characteristic, and mean values of material

strengths, and are reported in Tables 4 and 5, respectively, together with the corresponding values of the ultimate displacement at the beam free end.

2.3. Joint shear strength

To predict the shear strength of the beam-column joint, the design formulae provided by Eurocode 8 [2], ACI Code 352R [4], and the experimental-derived formula proposed by Pauletta et al. [28] are used. The last formula was chosen because it showed a very good capacity for predicting shear strength of exterior beam-column joints. For the detailed calculation, please refer to Appendix A.

2.3.1. Eurocode 8 [2]

According to Eurocode 8 [2], the allowable horizontal shear force in exterior beam-column joints is given by (Code clauses 5.5.3.3, (2)-(3); Code formulae (5.33)-(5.35))

$$
V_{jhd} = \min \begin{cases} 0.8 \cdot \eta f_{cd} b_j h_{jc} \sqrt{1 - \dfrac{\nu_d}{\eta}} \\[4mm] b_j h_{jc} \sqrt{\left(\dfrac{A_{sh} f_{ywd}}{b_j h_{jw}} + f_{ctd} \right)(f_{ctd} + \nu_d f_{cd})} \end{cases} \tag{29}
$$

where $\eta = 0.6 \cdot \left(1 - \frac{f_{ck}}{250}\right)$; b_j is the effective joint width as defined in Eq. (2); ν_d is the normalised axial force in the column above the joint ($\nu_d = \frac{N}{A_c f_{cd}}$ with A_c the gross area of column cross section); h_{jc} is the distance between the extreme layers of column reinforcement; A_{sh} is the area of joint transverse reinforcement; f_{ywd} is the transverse reinforcement design yield strength; and h_{jw} is the distance between top and bottom beam reinforcements.

Table 6 reports the shear strength of the specimens considered, $V_{n,EC8}$, calculated from Eq. (29), by substituting the design strength values of concrete and transverse reinforcement with the materials' mean strength values (Table 2). Regarding the concrete design tensile strength, f_{ctd}, it is substituted by the value of the mean tensile strength equal to $f_{ctm}=0.3f_{ck}^{2/3}$.

23

2.3.2. ACI Code 352R [4]

According to the ACI Code [4], the shear capacity of the exterior beam-column joint depends on the concrete compressive strength and the joint geometry and is given by (Code clause 4.3.1; Code formula (4.7))

$$V_n = 0.083\gamma\sqrt{f_c'}b_j h_c \tag{30}$$

where γ is equal to 12 for joints with a discontinuous column and confined only on one vertical face, f_c' is the compressive concrete strength; h_c is the column depth; and b_j is the effective joint width, which should not exceed the smallest of $\left\{(b_b + b_c)/2;\ b_b + \sum\frac{mh_c}{2};\ b_c\right\}$, with m equal to 0.3 [4]. The resulting value of joint shear capacity, $V_{n,ACI}$, calculated from Eq. (30) is reported in Table 6.

2.3.3. Pauletta et al. [28]

The shear strength formula proposed in [28] is made by the addition of the resisting contributions given by the concrete diagonal strut mechanism (first term in Eq. (31)), the horizontal stirrups (second term) and the vertical intermediate column bars (third term). A detailed description of Pauletta's model is given in chapter 3.2.

$$V_{n[28]} = 0.71\left[\frac{\chi f_c' a_c b_j \cos\vartheta_h}{\alpha} + 0.79 A_h f_{yh} + 0.52\frac{A_v f_{yv}}{\tan\vartheta_h}\right] \tag{31}$$

where χ is the following non-dimensional interpolating function:

$$\chi = 0.74 \cdot \left(\frac{f_c'}{105}\right)^3 - 1.28 \cdot \left(\frac{f_c'}{105}\right)^2 + 0.22 \cdot \left(\frac{f_c'}{105}\right) + 0.87; \tag{32}$$

b_j is the width of the diagonal strut, assumed as the minimum value between the beam width, b, and the column width, b_c; a_c is the depth of the column compression zone, whose value is approximated by [28]

$$a_c = \left(0.25 + 0.85\frac{N}{A_g f_c'}\right)h_c; \tag{33}$$

24

f_c' is the mean compressive concrete strength; A_h and A_v are the total areas of horizontal hoops and vertical intermediate column bars, respectively; f_{yh} is the transverse reinforcement mean yield strength; f_{yv} is the longitudinal column bars mean yield strength; and ϑ_h is the angle of inclination of the diagonal strut, defined as follows:

$$\theta_h = \tan^{-1}\left(\frac{h_b''}{h_c''}\right) \tag{34}$$

with h_b'' the distance between top and bottom beam longitudinal bars, and h_c'' the distance from the centroid of bar extension at the free end of the 90-degree hooked bar to the centroid of longitudinal column reinforcement in the opposite side.

The coefficient α in Eq. (31) is given by the following expression:

$$\alpha = \frac{2HL}{2HL - (2L + h_c)\cdot j_{db}} \cdot \left(1 - \frac{l_h\sqrt{f_c'}}{d_b \cdot f_{bi}}\right) \tag{35}$$

where H is the distance between the upper and lower columns' inflection points; L is the length from section of load application at the beam end to the column face; j_{db} is the beam cross section lever arm; l_h is the length of the column tensile zone under combined compressive and bending stresses, calculated as $l_h = h_c - a_c$; and f_{bi} is the tensile stress in the longitudinal beam reinforcement at joint shear failure, which can be evaluated by means of the following expression:

$$f_{bi} = (0.63 \cdot \omega^{-0.21}) \cdot f_{yb} \tag{36}$$

with f_{yb} the longitudinal reinforcement mean yield strength, and ω the mechanical reinforcement ratio of the tensile longitudinal reinforcement, defined as follows if the beam top longitudinal reinforcement is subjected to tensile stresses:

$$\omega = \frac{A_s'' \cdot f_{yb}}{b_b \cdot h_b \cdot f_c'}, \tag{37}$$

otherwise

$$\omega = \frac{A_s \cdot f_{yb}}{b_b \cdot h_b \cdot f_c'}.$$ (38)

The result obtained from Eq. (31), $V_{n[28]}$, is reported in Table 6.

Table 6. Experimental mean values of joint shear force and joint shear strength values calculated with the formulae of Eurocode 8 [2], ACI Code 352R [4], and Pauletta et al. [28].

Experimental mean values	Eurocode 8 [2]	ACI Code 352R [4]	Pauletta et al. [28]
$V_{n\,exp}$	$V_{n,EC8}$	$V_{n,ACI}$	$V_{n\,[28]}$
(kN)	(kN)	(kN)	(kN)
+368.9; -478.3	507.3	727.8	525.7

2.4. Test results

The results of the cyclic load tests on specimens J1 and J2 are shown in Fig. 8 and Fig. 9, where the four force-displacement cycles for each load step and the envelope curves of the first cycles are reported. The first observation that can be derived from these figures is that, for each load step considered, after the first complete cycle, a loss in strength occurs.
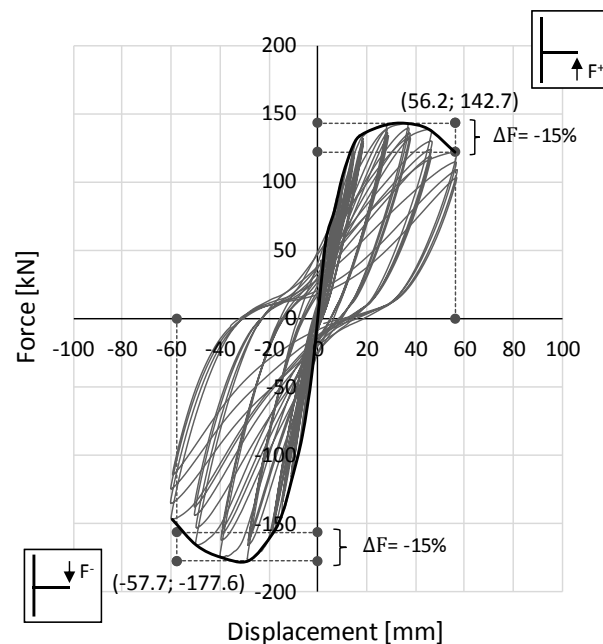
Fig. 9. Force-displacement cycles of specimen J2.

As shown in Fig. 8, specimen J1 attains the negative peak load (-177.6 kN) at about 28 mm displacement, while it attains the positive peak load (+142.7 kN) at about 36 mm displacement. As shown in Fig. 9, specimen J2 attains the negative peak load (-172.6 kN) at about 40 mm displacement, and the positive peak load (+141.8 kN) at about 39 mm displacement. Since the two specimens are identical, the average of these values can be considered representative of both, i.e. -175.1 kN at 34 mm, and +142.3 kN at 37.5 mm.

2.4.1. Cracking patterns development and failure modes

Fig. 10 shows the crack patterns observed at the end of the tests on specimens J1 and J2. Diagonal shear cracking occurred in the joint panel for both specimens, with spalling of the concrete cover in specimen J2, which was subjected to greater displacements. Due to the eccentricity of the joint (Fig. 10), the cracking was more visible on the flat side (Fig. 10a) and less visible on the tapered one (Fig. 10b). Since the shear force entering into the joint is transferred by the beam longitudinal bars, from Fig. 10 it is evident that the force was concentrated at the intersection of the beam with the column, near the flat side of the joint, hence producing more damage on this side, while the damage was slight on the

other side. Moreover, on the flat side the concrete cover was thinner than it was on the tapered side.

(a)   (b)
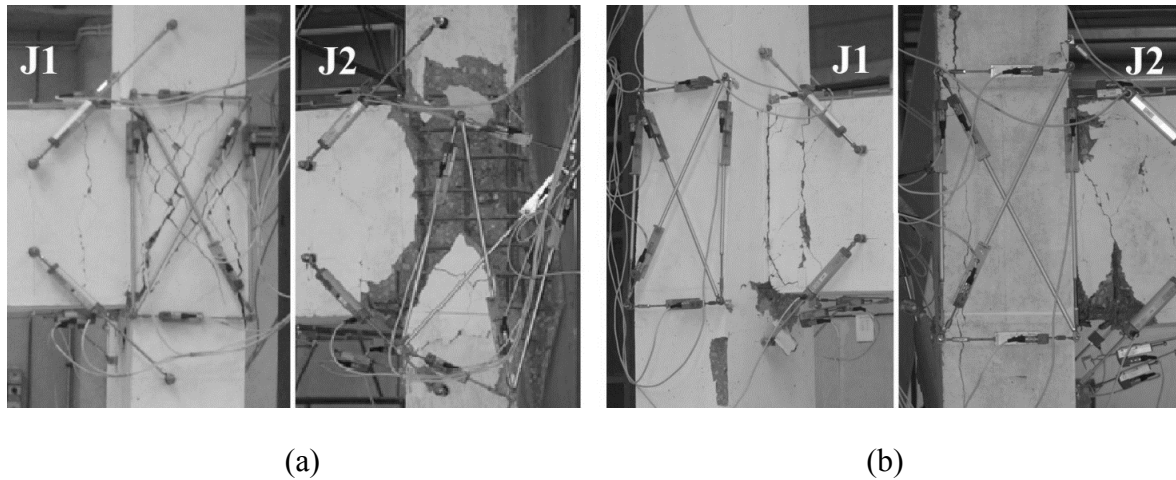
Fig. 10. Crack patterns at the end of the experimental tests (60 mm step for specimen J1 and 90 mm displacement step for specimen J2): (a) on the flat side of the joint (b) on the tapered side of the joint.

During the test, the first diagonal cracks appeared in the joint panel at the 3rd step cycles (12 mm). On the flat side of the joint, transducers P5 and P6 (Fig.5b) revealed that these cracks were closing at the inversion of the load up to the 4th step (20 mm). At the 5th step (30 mm) the cracks began to widen without closing again. Concrete cover loss started in the joint panel during the 7th step cycles (40 mm). At the 8th step cycles (50 mm) in specimen J1 the loss of concrete cover from the joint continued, while in specimen J2 a complete loss of the column cover occurred.

In the beam, flexural cracking occurred (Fig. 10) with yielding of the bars and concrete crushing near the joint. During the test, the first visible vertical cracks appeared in both sub-assemblages in the beam tensile regions next to the column, at the 2nd step cycles (8 mm), as attested by the measurements of transducers I1, I2, I3, and I4 (Fig. 5). The opening and closing of the beam cracks, measured by transducers P13, P14, P15, and P16 (Fig. 5), was clearly observable at the load inversion. The beam bars yielded, giving rise to the development of the plastic hinge in the beam during the 5th step cycles (20 mm). The softening of the load-displacement curves began at the 7th step cycles (40 mm) for negative displacements and the 8th step cycles (50 mm) for positive displacements, as can be seen in Fig. 8 and Fig. 9.

28

The test was stopped at the 60 mm step for specimen J1, while it continued for specimen J2 up to the 90 mm displacement step, to observe the complete failure of the joint (Fig. 10). In specimen J2 at the 70 mm displacement step, the column bars underwent buckling with concrete cracking and detachment (Fig. 11) and, during the third positive half cycle of this step, tensile break of a beam bottom bar occurred (Fig. 12).

The cracking pattern evolution of specimens J1 and J2, described in this chapter, is summarized in Table 7.

Table 7. Cracking pattern evolution of the joint panel and the beam, during the experimental tests of specimens J1 and J2.

Load step displacement	Event	
	Joint damage evolution	Beam damage evolution
8 mm		Vertical cracks appearance
12 mm	First diagonal cracks appearance	
16 mm	Opening and closing cracks at the load inversion	
20 mm		Beam bars yielding and plastic hinge development
30 mm	Permanent diagonal cracks	
40 mm	Joint concrete cover loss	Softening branch for negative cycles
50 mm (J2 only)	Column bars buckling and complete cover loss	Softening branch for positive cycles
70 mm (J2 only)		Tensile break of a bottom bar

Fig. 11. Buckling of the column bars during the 70 mm step for specimen J2.

Fig. 12. Tensile break of a beam bottom bar during the 70 mm step for specimen J2.

2.5. Discussion of test results

2.5.1. Vertical forces at beam cracking, yielding and flexural collapse

Test data obtained from the transducers revealed that first cracks started in the beam bottom region when the beam was subjected to the upward force equal to +57.0 kN for specimen J1 and +67.1 kN for specimen J2 (on average +62.05 kN). The respective

measured displacements were +4.32 mm (J1) and +4.25 mm (J2), whose average value is +4.3 mm. In comparison to the predicted cracking values, previously obtained using the materials' mean strengths (Table 3) and equal to +61.27 kN and +5.17 mm, for positive beam bending moment and displacement, respectively, the error in the prediction of the cracking force is very small (-1.3%), while it is greater in the prediction of the corresponding displacement (+20.2%).

Regarding the cracking of the beam top region, specimen J1 was preliminary subjected to a load cycle of about 4 mm downward displacements. Since from the cycles performed successively during the official test it was not possible to individuate the point of cracking, because no changing in the first cycle slope was visible, probably this specimen developed cracking at the beam top under the load preliminary applied. For specimen J2, first cracks started when the beam was loaded with a downward force equal to -67.0 kN, and a corresponding measured displacement of -4.8 mm. By considering these values for the comparison with the predicted ones in Table 3, which are equal to -56.08 kN and -5.58 mm, respectively, the error in the prediction is -16.2% for the cracking force, while +16.3% for the corresponding displacement.

As regards the yielding conditions, the top beam bars' yielding occurred at the application of forces equal to -153.4 kN (J1) and -152 kN (J2), on average -152.7 kN, with recorded displacements of -17.5 mm (J1) and -17.56 mm (J2), on average -17.53 mm. Bottom beam bars yielded at the application of forces equal to +127.7 kN (J1) and +126.4 kN (J2), on average +127.1 kN, with displacements of +15.35 mm (J1) and +14.8 mm (J2), on average +15.05 mm. The predicted values of beam vertical forces and displacements at first yielding, calculated with materials' mean properties (Table 4), are equal to -163.9 kN and +119.3 kN for negative and positive forces, respectively, and -14.83 mm and +10.03 mm for negative and positive displacements, respectively. By comparing these values with the experimental ones, it results that the error in the prediction of the yielding forces is quite restrained, +7.3% for negative forces and -6.1% for positive forces, respectively, while the error in the prediction of the relative displacements is greater, -15.4% for negative displacements and -33.4% for positive displacements, respectively.

As regards the ultimate conditions, the test results revealed that specimen J1 reached its ultimate strength under the application of -177.6 kN and +142.7 kN forces (Fig. 8). It is assumed herein that the corresponding ultimate displacements are found along the softening branch and are those which correspond to a reduction of the maximum force ΔF of -15%, considering the envelope curves. These are equal to -57.7 mm and +56.2 mm,

respectively. Analogously, in specimen J2 ultimate strengths were attained at the application of -172.6 kN and +141.8 kN forces (Fig. 9), and the ultimate displacements in the softening branch were equal to -59.1 mm and +65.6 mm, respectively. The mean values are -175.1 kN and +142.3 kN for negative and positive ultimate applied forces, respectively, and the corresponding mean values of displacements are -58.4 mm and +60.9 mm, respectively.

The theoretical forces applied at the beam end inducing flexural collapse are determined by Eqs. (12) and (13). In these equations the ultimate moments obtained from Eq. (14) and (20) are used instead of M_y. Moreover, to calculate the collapse forces, different strengths and strains for steel and concrete are considered, i.e. design, characteristic and mean values as reported in Table 5. The relative beam end displacements are calculated, as mentioned before, by summing the yield displacement component, obtained from software SAP 2000 NL by means of the linear static analysis, to the plastic displacement component. By comparing these values to the measured ones, it emerges that the use of materials' mean properties results in a better approximation of the joint test units' behavior, with the predicting values of -186.3 kN and +138.6 kN, for negative and positive ultimate forces, respectively, and -61.4 mm and +60.4 mm for negative and positive corresponding displacements.

The error in the prediction of the ultimate joint conditions is +6.4% and -2.6% for negative and positive forces, respectively, while the error in the prediction of the ultimate displacements is smaller and it is equal to +0.8% for negative displacements and -0.8% for positive displacements.

Two experimental force-displacement envelope curves of the first cycles of specimen J1 and J2 are shown in Fig. 13, for a visual comparison between the experimental curves of the two specimens, and to compare the test results with the predicted yielding and ultimate conditions, previously predicted and listed in Table 4 and Table 5, respectively.
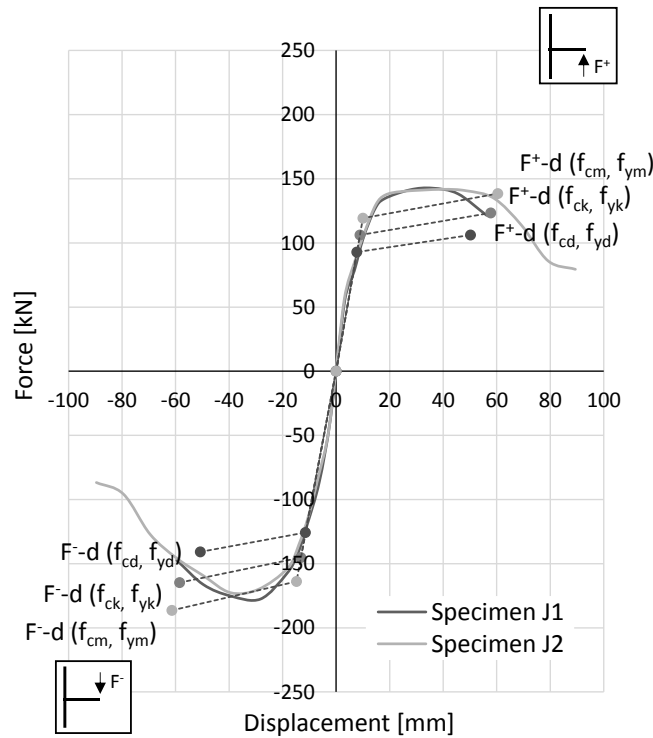
Fig. 13. Experimental force-displacement envelope curves of specimen J1 and J2, and relative predicting yield and ultimate values calculated using design, characteristic, and mean strengths.

It is observed that, both specimen J1 and J2, under the upward force, attain strength values which are larger than the calculated ultimate flexural strength, with a difference of +3% for J1 and +2.4% for J2. Hence it can be said that this load condition produces flexural failure of the beam (see Fig. 12).

Contrariwise, under the downward force, the beam does not achieve the ultimate flexural strength calculated using the mean compressive strength and strain values. This different behavior is due to the different amount of reinforcement at the top and at the bottom of the beam. Where the tensile reinforcement amount is lower, at the bottom of the beam, the upward force produces flexural failure, while, where the tensile reinforcement amount is greater, at the top, no flexural failure occurs under the downward force, but joint shear failure occurs, as it is demonstrated in the following.

2.5.2. Joint shear strength

The envelope of the joint shear force acting on the specimens, plotted in Fig. 14, is obtained from the expression of Paulay and Priestley [27]

$$V_{jh} = M_b \left[\frac{1}{z_b} - \frac{\dfrac{l_b}{l_{bn}}}{l_c + l_c'} \right] \tag{39}$$

where M_b is the beam moment at the column interface, resulting from the force applied by the actuator at the beam end, l_b is the distance from the applied load to the column axis, l_{bn} is the distance from the applied load to the beam-column interface, $l_c + l_c'$ is the distance between upper and downer column inflection points. As it can be seen in Fig. 4b, where the moment pattern for downward force acting on the beam is shown, this distance is equal to 1192+1008 = 2200 mm.
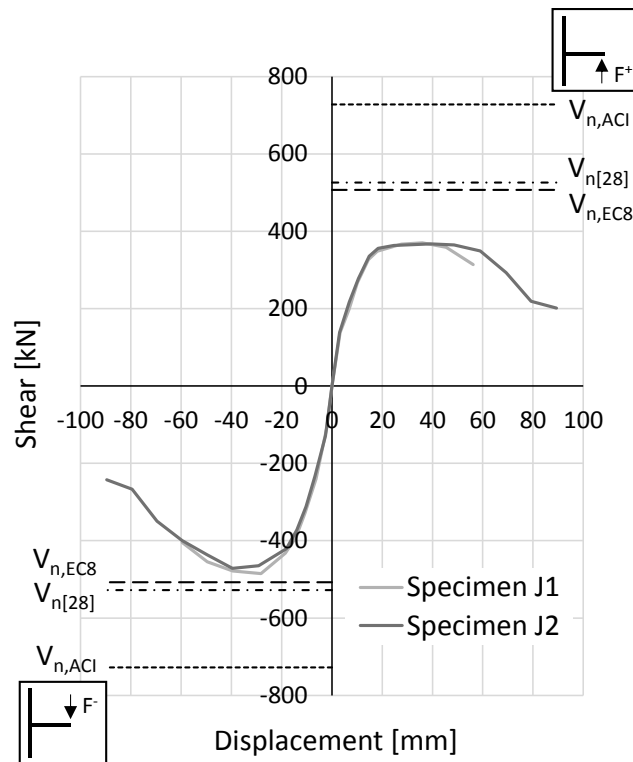
Fig. 14. Experimental shear-displacement envelope curves of specimen J1 and J2 and joint shear strength values obtained with the formulae of Eurocode 8 [2], ACI Code [4], and Pauletta et al [28].

Since the negative load envelopes of both sub-assemblages in Fig. 14 attain values of strength near to the shear strengths predicted by EC8 and [28], it can be said that joint shear failure occurs under downward maximum force. For upward forces, the maximum attained shear force is equal to +370.2 kN (J1) and +367.7 kN (J2), over 30% lower than

shear strength predicted by [28]. Hence, it can be surmised that, in this case, a failure mode different from shear failure has occurred.

To make a comparison, the joint shear strength of the specimens is evaluated using the formulae of Eurocode 8 (Eq. (29)), the ACI Code (Eq. (30)) and Pauletta et al. (Eq. (31)). The resulting values, obtained with the material's mean strength values for both concrete and steel, listed in Table 6, are reported in Fig. 14. It results that the joint shear strength evaluated with the expression of Pauletta et al. [28] is very close to that evaluated using the formula provided by Eurocode 8, and they well approximate the maximum force resisted by the specimens, while the corresponding joint capacity obtained by the ACI Code is unconservative, being this formula applicable to the joint with the minimum shear reinforcement provided. It should be noted that the potential plastic hinge completely develops in the beam under upward forces, and the joint shear does not increase further (horizontal pattern of the shear curve in Fig. 14); conversely, under downward forces, due to the absence of the required ties inside the joint core ($2\Phi 8$), the complete development of the beam plastic hinge is preceded by the joint shear failure (peak of the shear curve, which almost coincides with the shear strength value by EC8 and [28] in Fig. 14). Hence it can be said that, in the presence of a plausible construction error, a brittle collapse is likely to occur, even if the joint has been designed for high ductile behavior.

Since the expression of Pauletta et al. [28] well approximates the experimental results, the shear strength (Eq. (25)) of the same joint as specimens J1 and J2, but provided with all the Code-specified ties, is calculated. The strength results equal to 704.1 kN. By comparing this value with test results of specimens J1 and J2 (Fig. 13), it is observed that the joint in the presence of the Code-required ties would allow the complete development of the beam plastic hinges, avoiding shear failure. Therefore, it can be said that the respect of the Code requirements assures a beam-column joint behavior in accordance with capacity design principles.

2.5.3. Joint shear stress-strain behavior

The evolution of joint shear stress-strain cycles of specimens J1 and J2 is reported in Fig. 15, from the 1st step (4 mm) to the 7th step (40 mm).

Joint shear stress is obtained from the expression [27]

$$v_{jh} = \frac{V_{jh}}{b_j h_j} \tag{40}$$

where V_{jh} is given by Eq. (33), b_j= 450 mm (Eq. (2)) and $h_j=h_c$=300 mm. The shear strain of the joint core is calculated through the measurements of the joint transducers P1, P2, P3, P4 and P5 shown in Fig. 5. In particular, the horizontal component of the displacement of points at the intersection of transducers P1, P2 and P5 and P2, P3 and P5 are calculated by means of the measurements of these transducers using trigonometric functions. Then the average of this two horizontal displacements is considered and divided by the height of the joint core, to obtain the shear strain.
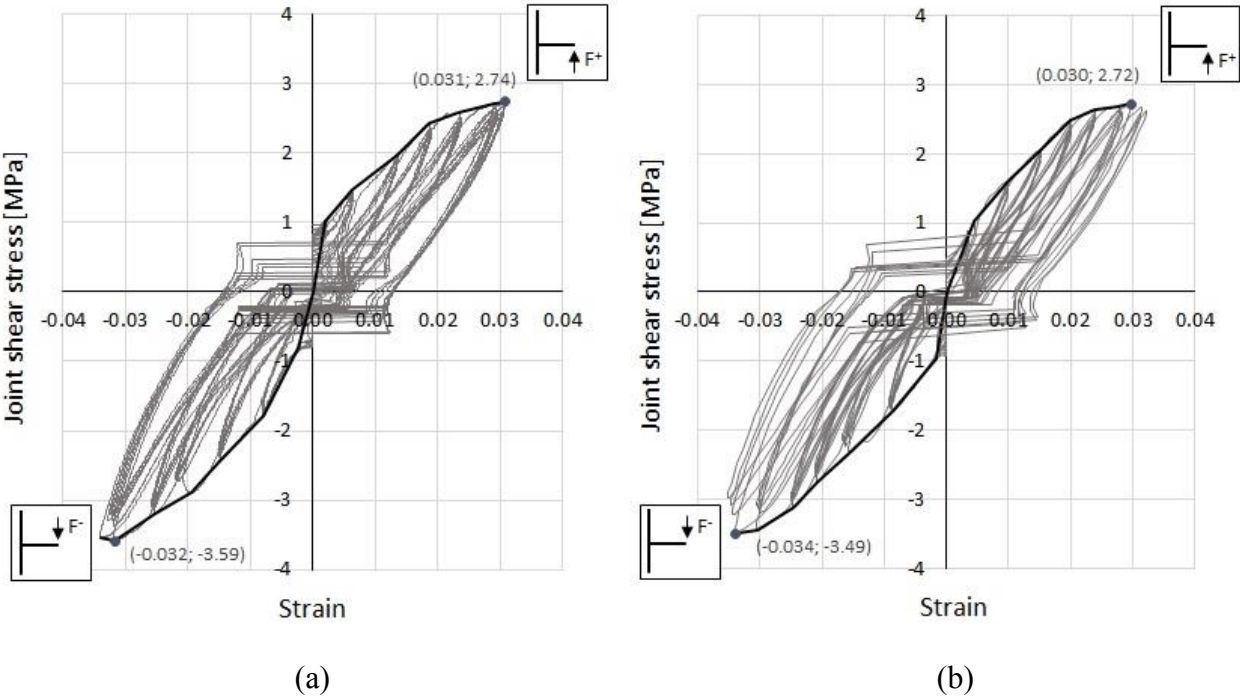
Fig. 15. Joint shear stress-strain diagrams: (a) load cycles of specimen J1; (b) load cycles of specimen J2.

As plotted in Fig. 15, for upward forces, the maximum attained shear stress is equal to +2.74 MPa and +2.72 MPa, for specimens J1 and J2, respectively. For downward forces, it is equal to -3.59 MPa and -3.49 MPa, respectively. Hence, the shear stress is higher in the last case and this confirms what already observed previously, namely that, for downward forces, shear failure occurs.

For both specimens in Fig. 15, it is observed the presence of horizontal branches of the cycles. This occurs after a certain imposed drift value, when diagonal cracks in the joint core have already formed. The horizontal pattern develops when the already formed

36

cracks close or re-open. For closing and re-opening already formed cracks it is not necessary a force increase, in fact the force remains almost constant (horizontal pattern).

2.5.4. Beam section moment-rotation behavior

In Fig. 16 the cyclic moment-rotation diagrams of the beam section at the interface with the column and the corresponding envelope curves are plotted for both specimens, up to the 7th load step (40 mm). The beam bending moment is obtained by imposing the rotational equilibrium of the beam subjected to the vertical force with respect to the beam-column interface, similarly to what was done in Eqs. (6) and (7). The rotation is calculated through the measurements of transducers I1, I2, I3 and I4 shown in Fig. 5.

(a)   (b)
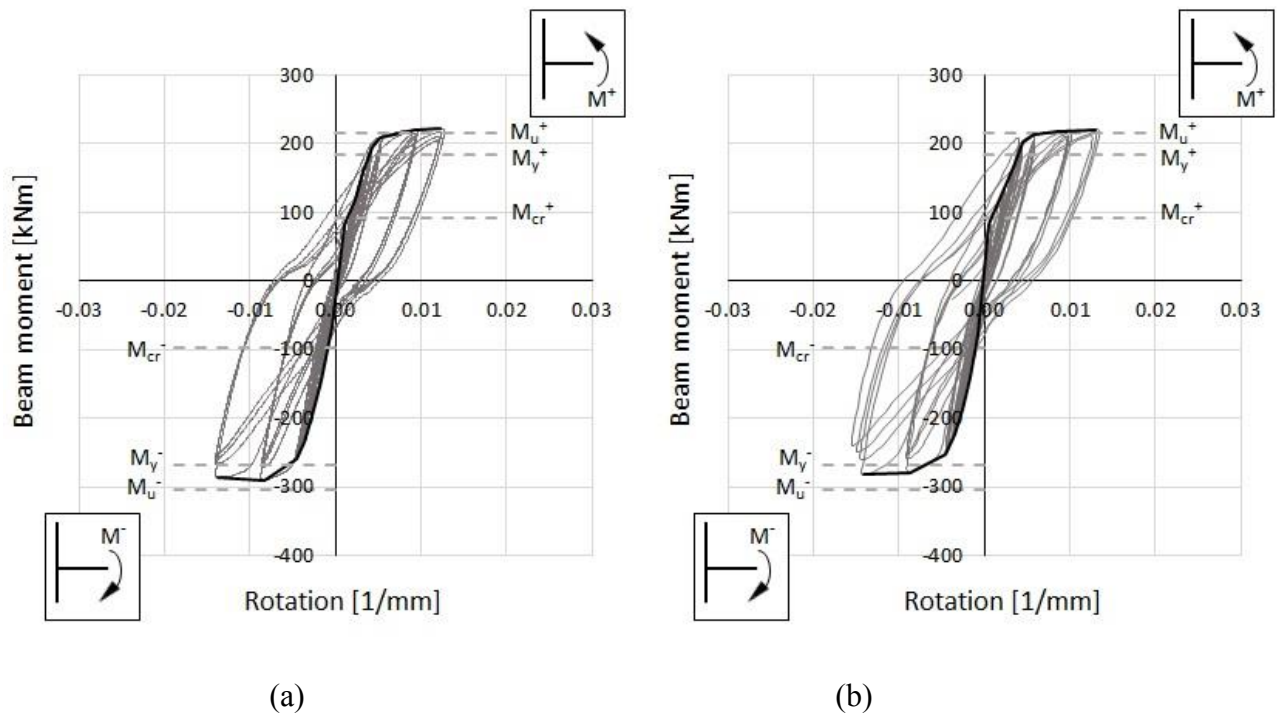
Fig. 16. Beam section moment-rotation diagrams: (a) load cycles of specimen J1; (b) load cycles of specimen J2.

The predicted values of the cracking, yield and ultimate moments, obtained with the materials' mean strengths, are reported in Fig. 16 for comparison. From the figure it can be observed that the envelope curves are very similar, as the specimens J1 and J2 are identical, and both of them show an approximate linear behavior from the first cycles to the onset of beam bars' yielding. Then a pseudo-plastic behavior occurs.

2.5.5. Strength loss

In Fig. 13 the two envelope curves that consider only the first loading cycle for each step have been built for both specimens. Being specimens J1 and J2 identical, the shape of the envelope curves is very similar.

As shown in Fig. 13 the peak load was attained at about 40 mm displacement step for both positive and negative half cycles, except for specimen J1, which attained the negative peak load at 30 mm displacement step. After the achievement of the peak load, by comparing the strength loss for both the specimens at 60 mm step, which was the maximum displacement for specimen J1, this specimen lost the 17% of strength in the negative half cycle, and specimen J2 lost the 16%. In the positive half cycle, specimen J1 lost 15% of strength while specimen J2 only 5%.

Specimen J2 was subjected to further loading cycles up to 90 mm applied displacement. For this specimen, the most significant loss of strength, equal to almost the 20%, occurred after the beam bottom bars failure, between 70 mm and 80 mm displacement steps. At the end of the test the joint presented a strength reduction of 44% and 50% for positive and negative cycles, respectively.

2.5.6. Stiffness degradation

The curves representing the degradation of the stiffness, calculated as secant between zero and the maximum force of the first cycle of each displacement step, are shown in Fig. 17 and Fig. 18 for downward and upward forces, respectively. There are no substantial differences between specimens' behavior.
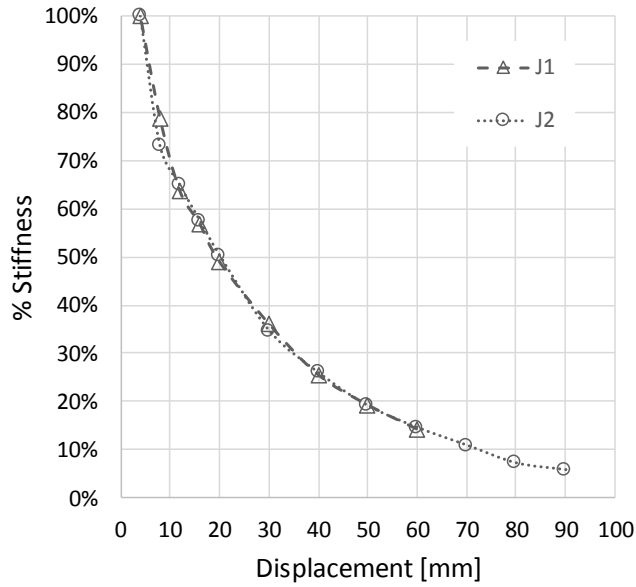
Fig. 17. Stiffness degradation during the tests for specimen J1 and J2 under downward forces.
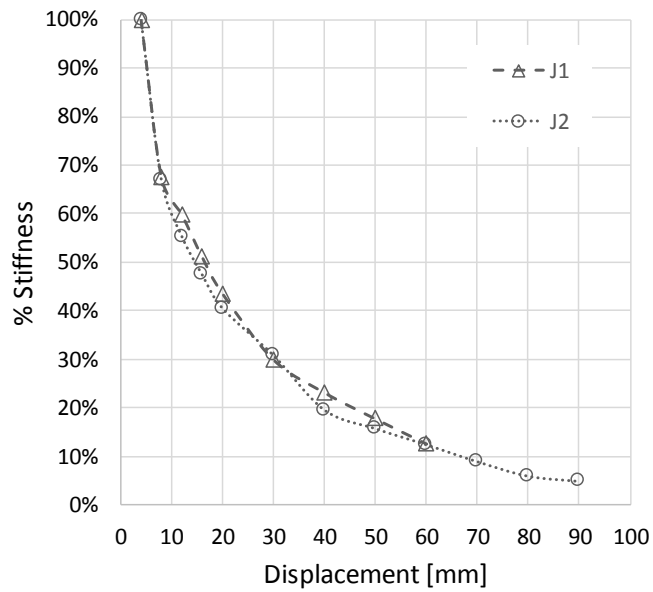
Fig. 18. Stiffness degradation during the tests for specimen J1 and J2 under upward forces.

The highest loss of stiffness is observed between 4 mm and 8 mm displacement steps, due to the start of crack development in the beam (predicted crack displacement in Table 4), then continued at a lower intensity up to the 30 mm displacement step, when the beam bars' yielding occurred and both the beam and the joint were visibly cracked. After the

30 mm displacement step the gradient of stiffness decrease is lower, because principal damage mechanisms have already occurred.

The specimens maintained on average a higher stiffness during the negative half cycles, compared to the positive half cycles, because of the different amount of reinforcing bars in the top and bottom beam. At the end of the 60 mm displacement step, specimen J1 retained only 14% of its original stiffness in the negative half cycle, and the 13% in the positive one; similarly, specimen J2 retained 15% and 12% in the negative and in the positive half cycles, respectively. The execution of the test on specimen J2 resulted, at the end of the 90 mm displacement step, in a residual stiffness of 6-7% of the original one, due to the complete collapse of the joint.

2.6. Conclusions

The two RC beam-column joints subjected to experimental tests, under cyclic reversal load, were designed according to the Italian Building Code (D.M. 14/01/08) [3] in high ductility class, omitting part of the horizontal joint reinforcement to simulate a plausible construction error.

From the tests it is observed that:

1) The values of calculated forces and displacements that best approximate specimens' behavior under reversal load are those obtained using the mean values of the material strengths and strains, as opposed to the design and the characteristic values.

2) Experimental force-displacement envelope curves reveal that, for upward applied forces, the beam flexural behavior, with a quite large yield range, is predominant in the development of the failure mechanisms. Conversely, for downward applied forces, the shape of the envelope curve indicates that the beam plastic hinge does not develop completely while shear behavior becomes predominant in leading the joint to the collapse. The different trend for negative and positive load cycles is justified by the disparate amount of top and bottom beam reinforcement.

3) In both specimens beam flexural failure was attained for positive half cycles, while joint shear failure occurred during half negative cycles, as evidenced by cracking patterns of both sub-assemblages.

4) Cracking patterns of both specimens show diagonal shear cracks in the joint panel and concrete crushing in the beam.

5) During the tests, both specimens reveal a strength loss after the first cycle of the same displacement step.

6) Both specimens exhibit essentially the same reduction in strength and stiffness, either for positive and negative applied force.

7) By observing the shear-displacement envelope curves, it can be seen that both joints reach the ultimate shear during the negative half load cycles, as was predicted. This is because the top beam bars transmit major horizontal shear forces to the joint panel, which, lacking the minimum necessary amount of horizontal reinforcement, cannot resist such forces.

8) Both the formulae of Pauletta et al. [28] and Eurocode 8 [2] for the evaluation of joint shear strength well approximate the capacity of the joint considered in these tests, while the ACI Code overestimates the shear strength of the specimens, since the formula is valid when the minimum shear reinforcement is provided. Hence it can be said that the expressions of Pauletta et al. and Eurocode 8 provide reliable predictions of joint shear strength for exterior joints.

9) In the presence of a plausible construction error, a brittle collapse is likely to occur, even if the joint has been designed for high ductile behavior. On the other hand, the respect of the Code shear reinforcement requirements [3] would allow the complete development of the beam plastic hinges, avoiding shear failure, as demonstrated by the comparison with formula of Pauletta et al. [28].

10) The proposed experimentation is a novelty in the literature. Even if there are experimental tests on beam-column joints designed for DCH, which consider executive problems for steel congestion in the joint core, none of them is similar to the case considered in this study, in which the realization of the specimens simulates a possible construction error. Hence other tests should be performed to make the conclusions presented herein more general.

3. Semi-empirical model for shear strength of RC interior beam-column joints subjected to cyclic loads

The main feature of seismic design of beam-column joints in ductile frames is to ensure the complete development of plastic hinges of adjacent elements (ordinarily the beams) and the dissipation of seismic energy, while preventing the occurrence of brittle failure mechanisms during earthquake shaking.

As mentioned in Chapter 1, the codes' provisions to design interior beam-column joints are not always the same, as they consider the development of different resisting mechanism. However, both Eurocode 8 [2] and ACI Building Code [1] require the confinement of concrete diagonal strut, by continuing column horizontal hoops also in the joint core.

Several authors proposed empirical and mathematical models to evaluate joint shear strength, taking into account the contributions of the concrete, the passing bars within the joint panel and the geometrical and mechanical characteristics of the elements. Kim and LaFave [7] introduced a parametrical simplified formula for joints with horizontal reinforcement, referring to the Bayesian estimation method. Wang et al. [8] proposed a model which included the nominal tensile strength of an idealized plane stressed concrete, the influence of the axial load of the column and the contributions of both the horizontal stirrups and the intermediate vertical bars in the joint core. Kassem [9] proposed an explicit formula by summing the different contributions given by the diagonal concrete strut, the joint stirrups and the column intermediate bars. In other cases, the shear strength calculation is based on an iterative procedure, like those reported by Hwang and Lee [14] or Wong and Kuang [17]. Despite all the proposals present in the literature, the resulting values of the joint shear strengths are not always accurate, due to difficulties in accounting for all the mechanisms involved in the behavior of ductile frames' joints.

In this study, a strut-and-tie model is proposed to determine the shear strength of interior joints; it represents an evolution of the models provided by Park and Mosalam [30] and Pauletta et al. [28] for exterior joints without and with shear reinforcement, respectively. In order to identify the forces acting in the joint core and on the cross sections of the adjacent elements, a plane frame joint is considered for simplicity.

The proposed shear strength model considers an approximate constitutive relationship for concrete softening response under plane stress state, based on Hwang and Lee's model [22], eliminating the need for an iterative procedure. Furthermore, the proposed model

considers the contributions of three inclined concrete compression struts, horizontal stirrups, and intermediate vertical bars crossing the joint core. The inclination of the concrete struts takes into account the axial load transferred to the joint by the upper column. All contributions are obtained on the basis of mechanical considerations and are multiplied by coefficients, which are derived from a collection of 69 test data found in the literature. The experimental results considered in this study concern interior RC beam-column joints that collapsed due to shear only, under the application of reversal cyclic forces. The collection of test data incorporates also 9 beam-column units without horizontal stirrups.

The accuracy and consistency of the prediction model are evaluated by means of comparison with predictions of the shear strength model proposed by Kim and LaFave [7], the model of Wang et al. [8], and the formula by Kassem [9] on 28 test data, different from the group of tests used for the calibration of the coefficients.

This study proposes also a design formula, whose predictions are compared to the design and nominal shear strengths obtained from the expressions of Eurocode 8 [2] and ACI Building Code [1], respectively.

3.1. Model basis

The forces transferred to a typical cruciform interior beam-column joint by the adjacent beams and columns under seismic load conditions are the shear actions and the tensile and compressive forces induced by flexure and axial actions, as shown in Fig. 19(a).
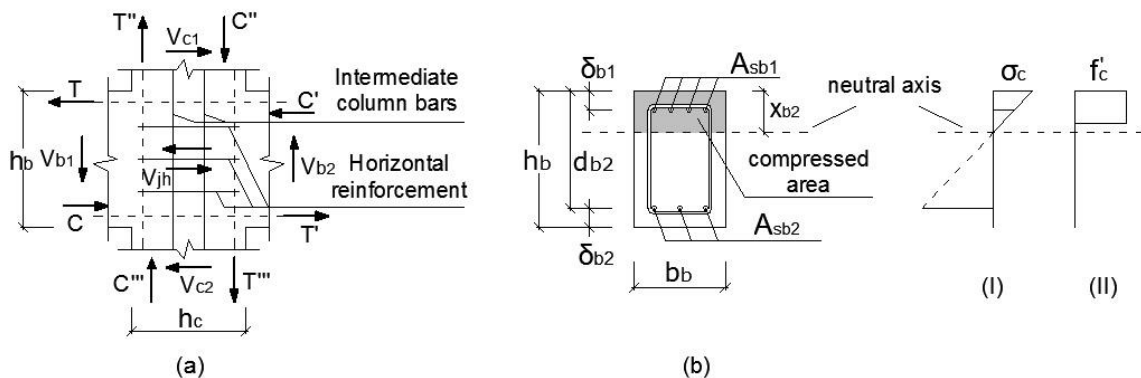
Fig. 19. (a) External actions on the interior beam-column joint core in seismic conditions; (b) right beam section: I linear stress distribution, II stress-block distribution.

The horizontal shear force acting in the joint core, V_{jh}, can be computed as follows

$$V_{\text{jh}} = T + C' - V_{c1} \tag{41}$$

where T is the tensile force in the top beam longitudinal bars, C' is the compression force in the beam section on the opposite side of the joint and V_{c1} the horizontal shear force acting in the column above the joint.

Therefore

$$T = A_{\text{sb1}} f_{\text{b1}}, \tag{42}$$

where A_{sb1} and f_{b1} are the transverse area and the tensile stress in the beam top reinforcement respectively, $C' = C'_s + C'_c$, with C'_s the compression force in the top beam longitudinal bars (on the opposite side of the joint) and C'_c the compression force acting on the concrete in the beam section.

Applying the horizontal equilibrium equation to the beam cross section gives $C' = T'$, where

$$T' = A_{sb2} f_{b2} \tag{43}$$

with A_{sb2} and f_{b2} the transverse area and the tensile stress in the beam bottom reinforcement, respectively.

Thus the value of C'_s can be calculated as difference between T' and C'_c as follows

$$C'_s = T' - C'_c \tag{44}$$

By adopting, in the beam cross section, a linear stress distribution (Fig. 19 (b)I) or a stress block (Fig. 19 (b)II) distribution, C'_c can be computed by means of the following expressions, respectively

$$C'_c = \frac{1}{2} \cdot \sigma_c x_{b2} \, b_b \tag{45}$$

$$C'_c = 0.8 \cdot x_{\text{b2}} b_{\text{b}} f'_{\text{c}} \tag{46}$$

where σ_c is the maximum concrete compression stress in the beam cross section for the linear distribution, x_{b2} is the neutral axis depth, and b_b is the beam width (Fig. 19 (b)). The value of x_{b2} can be computed from the horizontal equilibrium of the beam internal forces.

3.2. Joint shear strength

The horizontal shear nominal strength of interior RC beam-column joints V_n is obtained by adding two resisting contributions associated with two coexisting mechanisms of shear transfer [30]

$$V_n = V_{hc} + V_{hs} \tag{47}$$

where V_{hc} is the resisting contribution of concrete, provided by the principal strut ST1 ($V_{hc,ST1}$) and two side inclined struts ST2 and ST3 ($V_{hc,ST2-3}$) shown in Fig. 20(a), which can be expressed as follows

$$V_{hc} = V_{hc,ST1} + V_{hc,ST2-3} \tag{48}$$

and V_{hs} is the resisting contribution given by the truss mechanism, induced by the horizontal stirrups and the vertical reinforcement of the joint core (Fig. 19).

Hence, the sum of contributions shown in Fig. 20(a) and Fig. 21 give the total shear strength of the interior beam-column joint.

It has to be observed that the difference introduced in the model for interior joints respect to the model for exterior ones [28] is the presence of three concrete struts instead of two (Fig. 20(b)).

In the exterior joint in Fig. 20(b) the strut ST2 arises from the transfer to the joint core of a fraction of the beam top reinforcement tensile force, by means of bond. Contrariwise, it is assumed that the bond stresses transferred by the beam bottom reinforcement are negligible, because this reinforcement is subjected to a compressive lower intensity force.

In the interior joint in Fig. 20(a), the strut ST2 arises similarly to exterior joints, but also strut ST3 is present due to the transfer of bond stresses from the beam bottom reinforcement, which, in the region relevant to strut ST3, is subjected to a high tensile force inducing not negligible bond stresses.
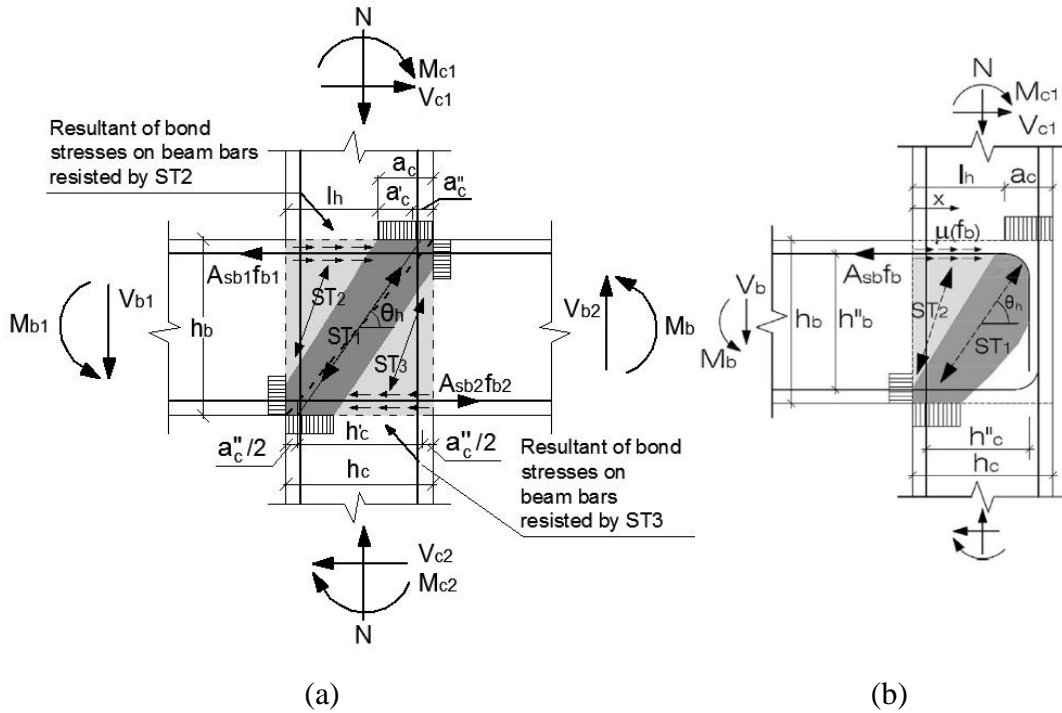
Fig. 20. The concrete struts: (a) three in interior joints; (b) two in exterior ones [28].
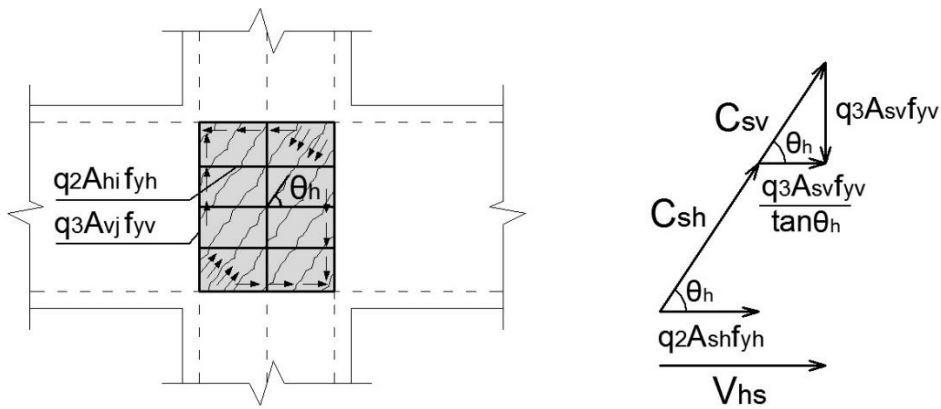
Fig. 21. Truss mechanism contributions.

In the proposed model it is assumed that joint shear failure is caused by the crushing of the main strut ST1, confined by any horizontal stirrup and vertical reinforcement in the joint core. The development of the inclined strut is marked by the onset of inclined cracks within the joint panel. Cases of failure due to bond deterioration inside the joint are not considered in this research.

The proposed model assumes that a fraction β, with $0 \leq \beta \leq 1$, of the total horizontal force $T + C'_s$ (Fig. 20(a)) transferred from the top beam longitudinal reinforcement to the

concrete, by means of bond, is supported by the inclined struts ST2-3, and that the remaining rate $(1 - \beta) \cdot (T + C_s')$ is transferred to the two trusses induced in the joint core by steel vertical and horizontal (stirrups) joint reinforcement (Fig. 21).

Thus, the rate of V_{jh} transferred to the truss mechanism only by bond, $V_{jh,s}$, can be expressed as follows [27]

$$V_{jh,s} = (1 - \beta) \cdot (T + C_s') \tag{49}$$

The residual rate of V_{jh} transferred to the concrete inclined struts, $V_{jh,c}$, can be derived from Eq. (1)

$$V_{jh,c} = \beta(T + C_s') + C_c' - V_{c1} \tag{50}$$

At joint failure the horizontal shear force in the joint core equals the joint strength

$$V_{jh} = V_n \tag{51}$$

3.2.1. Contribution of strut mechanisms to joint shear strength Vhc

Park and Mosalam's model [30] considers exterior beam-column joints without both stirrups inside the joint core and vertical intermediate column bars crossing it, and it assumes that the horizontal resisting mechanisms that develop in the joint core is given by two inclined and parallel concrete struts, ST1 and ST2. More specifically, ST1 is the strut that is activated when the 90-degree hooked beam reinforcement anchored inside the joint is subjected to tensile stresses, hence it transfers diagonal compressive stresses inside the joint core, and ST2 is the strut arising from the transfer to the joint core of a fraction of the beam reinforcement tensile force, by means of bond. For the development of these mechanisms, bond failure of the beam reinforcement anchorage have to be avoided.

With reference to Fig. 20(a), in the proposed model it is assumed that ST1 is the strut developed by beam and column flexural compression zones and a fraction of the beam longitudinal bars force, transferred by bond along the bar portion contained within the dark shaded region in Fig. 20(a). The inclined strut ST2, assumed to be parallel to ST1,

is developed by bond forces transferred to the joint core by the beam top bars along the clear shaded region in Fig. 20(a) (length l_h). The strut ST3, parallel to ST1 and ST2, forms in the other side of the joint region due to the bond forces transferred to the joint core by the beam bottom bars. The three struts' configuration is inverted at the inversion of the acting seismic forces.

3.2.1.1. Shear strength contribution $V_{hc,ST1}$

The contribution to joint shear strength of the main concrete strut ST1 ($V_{hc,ST1}$) is evaluated considering that the depth of the strut is equal to the depth of the column flexural compression zone a_c (Fig. 20(a)), whose value can be approximated by [27]

$$a_c = \left(0.25 + 0.85 \frac{N}{A_g f_c'} \right) h_c \tag{52}$$

where N is the compression force in the column above the joint, f_c' is the cylindrical compressive strength of concrete and A_g (Fig. 22) is the area of the whole column cross section.
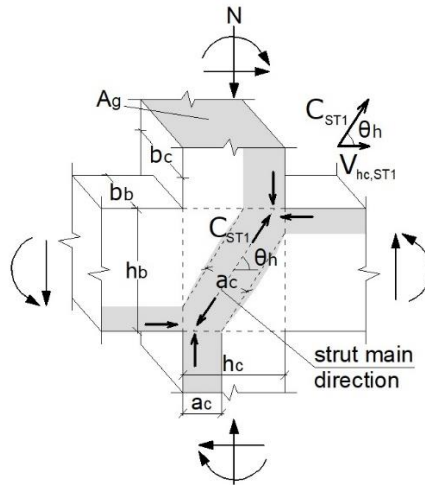
Fig. 22. Inclined strut ST1 mechanism contribution.

By decomposing a_c into its two components (Fig. 20(a))

$$a_c' = 0.25 \, h_c \tag{53}$$

which is independent from the column axial load N, and

48

$$a''_c = 0.85 \frac{N}{A_g f'_c} h_c \qquad (54)$$

which, instead, is function of N, Eq. (33) can be written as follows

$$a_c = a'_c + a''_c \qquad (55)$$

The inclination angle θ_h of the inclined struts ST1, ST2 and ST3 is defined by

$$\theta_h = \tan^{-1}\left(\frac{h_b}{h'_c}\right) \qquad (56)$$

where it is assumed that, when $N = 0$, $h'_c = h_c$, while, when $N > 0$, a reorientation of the strut ST1 arises due to the presence of the additional length rate a''_c in a_c. This reorientation occurs so that the end of the strut is centered on half the length a''_c (Fig. 20(a)), hence h'_c is given by the following equation (Fig. 20(a))

$$h'_c = h_c - a''_c \qquad (57)$$

The width b_j of the inclined strut ST1 is expressed [2] as (Fig. 22)

$$b_j = \begin{cases} \min(b_c, b_b + 0.5h_c) & \text{for } b_b < b_c \\ \min(b_b, b_c + 0.5h_c) & \text{for } b_b \geq b_c \end{cases} \qquad (58)$$

Naming $C_{ST1,max}$ the maximum compression force (parallel to the strut ST1) that the strut ST1 can sustain, in accordance with the strut-and-tie model, the horizontal shear strength of strut ST1 can be expressed as follows

$$V_{hc,sT1,max} = C_{ST1,max} \cdot \cos\theta_h \qquad (59)$$

where θ_h, defined by Eq. (34), is the inclination angle of the strut ST1 with respect to the horizontal direction.

The cross-sectional area of the inclined main concrete strut ST1 is considered [22] equal to $a_c \cdot b_j$ (Fig. 22), and its principal axis of inertia are assumed respectively parallel and

orthogonal to the direction of its inclination.

In the presence of the transverse tensile strain ε_r, the maximum compression stress (<0) that may develop in the strut principal direction is given by [22]

$$\sigma_{d,max} = -\zeta \cdot f'_c \tag{60}$$

where

$$\zeta = \frac{5.8}{\sqrt{f'_c}} \frac{1}{\sqrt{1 + 400\varepsilon_r}} \leq \frac{0.9}{\sqrt{1 + 400\varepsilon_r}} \tag{61}$$

Hence, the maximum compression force $C_{ST1,max}$, acting in the main concrete strut, is

$$C_{ST1,max} = -\sigma_{d,max}\, a_c\, b_j \tag{62}$$

Eq. (61) is verified if $5.8/\sqrt{f'_c}\,[\text{MPa}] \leq 0.9$, that is $f'_c \geq 42$ MPa, and, in this case, ζ assumes the value given by the left member of the inequality. Otherwise, ζ is equal to the right member of the inequality.

To gain the expression of ε_r to be used in Eq. (61) the constitutive law of tensile concrete can be considered linear with constant slope up to the ultimate tensile strength and, within this range, it can be assumed that the tensile Young's modulus is equal to that in compression. It results that ε_r can be expressed as $\varepsilon_r = \sigma_t/E_c$, where σ_t is the transverse stress in the concrete strut ST1 at joint failure.

The inclined concrete strut ST1 is subjected to a biaxial tension-compression stress state, which is unknown, because the maximum compressive and tensile stresses at failure, $\sigma_{d,max}$ and σ_t, are not known a priori.

It is known that concrete tensile strength in a biaxial tension-compression regime is lower than that under uniaxial regime. For this reason, the maximum value of tensile stress $\sigma_{t,lim}$ can be assumed equal to the limit value f_{ct} of concrete tensile strength and, for a safe computation, Eq. (60) can be expressed as $\sigma_{d,lim} = \sigma_{d,max|\varepsilon_r = f_{ct}/E_c}$.

To hold a single expression for $\sigma_{d,lim}$, the following approximation [31]-[32] depending on f'_c is used

$$\sigma_{d,lim}^* = -\chi\, f_c' \tag{63}$$

where χ is a non-dimensional interpolating function ([31]-[32]), also depending only on f_c', expressed as

$$\chi = 0.74 \cdot \left(\frac{f_c'}{105}\right)^3 - 1.28 \cdot \left(\frac{f_c'}{105}\right)^2 + 0.22 \cdot \left(\frac{f_c'}{105}\right) + 0.87 \tag{64}$$

with the limit range for the cylindrical compressive strength of $10 \le f_c' \le 105$ MPa. This equation is valid in general independently from the type of RC member [32].

Consequently, the approximating limiting value of the main concrete strut's shear contribution $V_{hc,ST1,lim}^*$ is obtained by substituting Eq. (62) in Eq. (59), and it is given by

$$V_{hc,ST1,lim}^* = \chi\, f_c' \cdot a_c \cdot b_j \cdot \cos\theta_h \tag{65}$$

Since $V_{hc,ST1,lim}^*$ is obtained by approximating $V_{hc,sT1,max}$ and the compression stress in the strut ST1 at joint failure will be lower or eventually equal to the maximum compression concrete strength $\sigma_{d,lim}^*$, it follows that the horizontal shear strength contribution of strut ST1 $V_{hc,ST1}$ (Fig. 22) can be expressed as follows

$$V_{hc,ST1} = q_1 \cdot \chi\, f_c' \cdot a_c \cdot b_j \cdot \cos\theta_h \tag{66}$$

where q_1 is a positive factor $(0 \le q_1 \le 1)$, whose value is derived on the basis of experimental results.

3.2.1.2. Shear strength contribution $V_{hc,ST2}$

The ST2 strut contribution to the horizontal joint shear strength, as noted above, is developed by bond forces transferred to the joint core by the beam top bars along the clear shaded region in Fig. 20(a).

When joint shear failure occurs, the horizontal contribution of the concrete strut ST2 to the joint shear strength can be expressed as

$$V_{hc,ST2} = \beta \sum_{i=0}^{s} n_{b1,i} \cdot \pi \cdot \Phi_{b1,i} \int_0^{l_h} \mu(f_{b1}) \, dx \tag{67}$$

where s is the number of different bar diameters present at the beam top; $\mu(f_b)$ represents the local bond stress of beam reinforcement, which, in real conditions, varies with the distance from the beam-column interface, and it is a function of the tensile stress acting in the beam top bars, f_{b1}; $n_{b1,i}$ is the number of top beam longitudinal bars (in tension) with corresponding diameter $\Phi_{b1,i}$; and l_h is the depth of the concrete strut ST2, which derives from

$$l_h = h_c - a_c \tag{68}$$

The ST3 strut contribution to the horizontal joint shear strength has an expression similar to Eq. (67), that is

$$V_{hc,ST3} = \beta \sum_{i=0}^{t} n_{b2,i} \cdot \pi \cdot \Phi_{b2,i} \int_0^{l_h} \mu(f_{b2}) \, dx \tag{69}$$

where t is the number of different bar diameters present at the beam bottom.

Since the variable bond stress distribution is unknown and would be too burdensome to handle, it is possible, referring to expressions available in the literature ([33]-[35]), to assume an approximate uniform value of bond stress, $\bar{\tau}$, along the joint portion l_h, both at the top and at the bottom of the beam, that is

$$\mu(f_{b1}) = \mu(f_{b2}) = \bar{\tau} \tag{70}$$

By substituting Eq. (70) in Eq. (67) and in Eq. (69) and, subsequently, simplifying them by introducing the average diameters Φ_{b1} and Φ_{b2} of the top and bottom beam longitudinal bars, respectively, the sum of the contribution of the side inclined struts ST2 and ST3 can be written as follows

$$V_{hc,ST2-3} = \beta (n_{b1}\Phi_{b1} + n_{b2}\Phi_{b2})\pi \, l_h \bar{\tau} \tag{71}$$

where n_{b1} and n_{b2} are the number of the top and bottom beam longitudinal bars, respectively, with corresponding average diameters Φ_{b1} and Φ_{b2}, calculated on the basis

52

of the top and bottom beam reinforcements A_{sb1} and A_{sb2}, and the fraction factor β is determined on the basis of experimental results.

3.2.2. Reinforcement contribution to joint shear strength Vhs

Beam-column joints can be reinforced by m levels of n-leg horizontal stirrups and p intermediate vertical column bars. The i-th stirrup level has cross-sectional area A_{hi} ($i = 1, \ldots, m$), while the j-the vertical bar has cross-sectional area A_{vj} ($j = 1, \ldots, p$). For the steel reinforcement contribution to joint shear strength, only the horizontal stirrups and vertical bars within the effective joint area $h_c \cdot b_j$ are considered in this model.

When both horizontal stirrups and vertical joint reinforcement bars are present, two strut-and-tie mechanisms (one due to the stirrups and one due to the vertical bars) form within the joint core, that work independently each other and contribute by super-position (Fig. 21) to the overall truss shear strength [22].

It is assumed herein (Fig. 21) that in the truss mechanisms the inclined compression resultants C_{sh} and C_{sv}, related to the horizontal stirrups and vertical reinforcement, respectively, are parallel to the three inclined concrete struts ST1, ST2 and ST3, and, for this reason, their contributions are added each other.

Russo et al. [28], [31]- [32] observed that, for exterior joints, corbels and deep beams, not all the horizontal reinforcements undergo to yielding in the condition of shear failure: the mid-height bars reach the yield strength f_{yh}, while other levels may be subjected to lower stresses. Similarly, the vertical bars probably reach the yield strength f_{yv} in the central region, whereas they achieve lower tensions elsewhere. This observation is considered valid also for the horizontal stirrups and vertical intermediate bars of interior beam-column joints.

Hence, the mean stress in the horizontal stirrups can be expressed as $q_2 f_{yh}$, with $0 < q_2 < 1$, and the mean stress in the vertical bars as $q_3 f_{yv}$, with $0 < q_3 < 1$. As a consequence, the horizontal force provided by the stirrups results $q_2 A_{sh} f_{yh}$, and the vertical force provided by the intermediate column bars is equal to $q_3 A_{sv} f_{yv}$ (Fig. 21), with

$$
\begin{aligned}
A_{sh} &= \sum_{i=0}^{m} A_{hi} \\
A_{sv} &= \sum_{i=0}^{p} A_{vi}
\end{aligned}
\tag{72}
$$

Thus, the contribution to shear strength, V_{hs}, provide by steel reinforcements, is equal to the vector sum (Fig. 21) of the horizontal force provided by the horizontal stirrups, $q_2 A_{sh} f_{yh}$, and the horizontal component of the resultant of compression forces acting in the inclined struts in the truss mechanism induced by the intermediate column bars, $q_3 A_{vj} f_{yv}/\tan\theta_h$

$$V_{hs} = q_2 A_{sh} f_{yh} + q_3 A_{sv} f_{yv}/\tan\theta_h \tag{73}$$

In the case of beam-column connections without vertical reinforcement, the shear strength contribution V_{hs} is given only by the horizontal stirrups contribution

$$V_{hs} = q_2 A_{sh} f_{yh} \tag{74}$$

3.2.3. Shear strength expression

The nominal shear strength formula for interior RC beam-column joints is obtained by introducing Eqs. (66), (71), (48) and (73) in Eq. (47)

$$V_n = 4\beta \left(\frac{A_{sb1}}{\Phi_{b1}} + \frac{A_{sb2}}{\Phi_{b2}}\right) l_h \bar{\tau} + q_1 \chi f_c' a_c b_j \cos\theta_h + q_2 A_{sh} f_{yh} + q_3 \frac{A_{sv} f_{yv}}{\tan\theta_h} \tag{75}$$

where χ and θ_h are respectively expressed by Eqs. (32) and (34), while β, $\bar{\tau}$ q_1, q_2 and q_3 are unknown coefficients, which can be calibrated on the basis of tests' data processing.

In the first term of Eq. (75) it is more convenient to have a unique coefficient to be calibrated, hence it is assumed $\beta\bar{\tau} = q_0$ and Eq. (75) becomes

$$V_n = 4 q_0 \left(\frac{A_{sb1}}{\Phi_{b1}} + \frac{A_{sb2}}{\Phi_{b2}}\right) l_h + q_1 \chi f_c' a_c b_j \cos\theta_h + q_2 A_{sh} f_{yh} + q_3 \frac{A_{sv} f_{yv}}{\tan\theta_h} \tag{76}$$

To determine the parameters q_0, q_1, q_2 and q_3, 69 test units have been selected from 25 investigations ([36]-[60]). The original labels of the selected test units are reported in Table B1 and Table B2, at the second column. All the considered specimens were cyclically loaded.

In selecting the test data, only interior beam-column joints that exhibited shear failure and not flexural or bond failure were considered.

A set of geometrical and mechanical properties of the specimens are involved to evaluate the joint shear strength with Eq. (75), and the validity ranges resulting from the processing of the collected data are reported in the list below:

- $19.3 \text{ MPa} \leq f_c' \leq 98.8 \text{ MPa}$;
- $36.9 \text{ deg} \leq \theta_h \leq 66.7 \text{ deg}$;
- $0 \text{ mm}^2 \leq A_{sh} \leq 3879.6 \text{ mm}^2$;
- $0 \text{ mm}^2 \leq A_{sv} \leq 6036.5 \text{ mm}^2$;
- $0 \text{ mm}^2 \leq \frac{A_{sv}}{\tan\theta_h} \leq 4011 \text{ mm}^2$;
- $235.4 \text{ MPa} \leq f_{yb1} \leq 1456 \text{ MPa}$;
- $235.4 \text{ MPa} \leq f_{yb2} \leq 1456 \text{ MPa}$;
- $235.4 \text{ MPa} \leq f_{yh} \leq 1456 \text{ MPa}$;
- $325 \text{ MPa} \leq f_{yv} \leq 1456 \text{ MPa}$;
- $0 \leq \frac{N}{A_g f_c'} \leq 0.48$;
- Percentage of top flexural reinforcement in the beam: $0.54\% \leq \rho_{sb1} \leq 3.59\%$;
- Percentage of bottom flexural reinforcement in the beam: $0.46\% \leq \rho_{sb2} \leq 2.79\%$.

The coefficient q_1 in Eq. (75) is collected as a common factor, hence Eq. (75) becomes

$$V_n = q_1 \left[4a_1 \left(\frac{A_{sb1}}{\Phi_{b1}} + \frac{A_{sb2}}{\Phi_{b2}} \right) l_h + \chi f_c' a_c b_j \cos\theta_h + a_2 A_{sh} f_{yh} + a_3 \frac{A_{sv} f_{yv}}{\tan\theta_h} \right] \tag{77}$$

where $a_1 = q_0/q_1$, $a_2 = q_2/q_1$, and $a_3 = q_3/q_1$.

The coefficient q_1 is determined herein by imposing that the average (AVG) of the ratios between the experimental shear strength values and the nominal shear strength computed with Eq. (75), $V_{jh,test}/V_n$, is equal to 1.0. This constrain enforces the accuracy of the proposed expression for shear strength.

The coefficients, a_1, a_2, and a_3 are determined by imposing that coefficient of variation (COV) of the ratios $V_{jh,test}/V_n$ is minimum. This constrain minimizes the scattering of the predicted results.

The values $q_0=1.32$, $q_1=0.80$, $q_2=0.14$ and $q_3=0.22$ have been determined accordingly, hence Eq. (75) becomes

$$V_{\mathrm{n}} = 5.28\left(\frac{A_{\mathrm{sb1}}}{\Phi_{\mathrm{b1}}} + \frac{A_{\mathrm{sb2}}}{\Phi_{\mathrm{b2}}}\right)l_{\mathrm{h}} + 0.80\chi\, f_{\mathrm{c}}' a_{\mathrm{c}} b_{\mathrm{j}}\cos\theta_{\mathrm{h}} + 0.14 A_{\mathrm{sh}} f_{\mathrm{yh}} + 0.22\frac{A_{\mathrm{sv}} f_{\mathrm{yv}}}{\tan\theta_{\mathrm{h}}} \quad (78)$$

For the 69 interior joints tested, Eq. (78) provides a COV value of 0.139. In Fig. 23 the ratios $V_{\mathrm{jh,test}}/V_{\mathrm{n}}$ versus $V_{\mathrm{jh,test}}$ values for the 69 specimens are reported. It can be observed the low scattering of the predictions.

By using Eq. (78) it is also possible to plot the percentage of the contributions offered by the different resisting mechanisms related to the specific specimen, by sorting them in ascending order of the concrete struts' contribution to the total horizontal shear strength (Fig. 23).
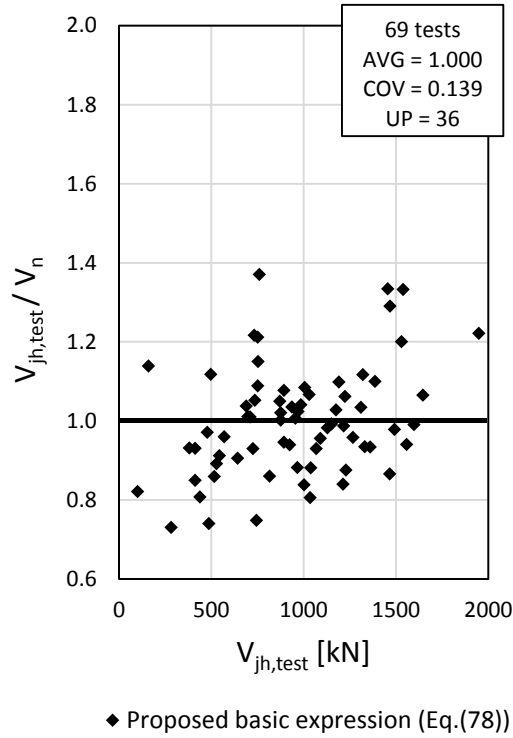
Fig. 23. $V_{jh,test}/V_n$ ratios versus $V_{jh,test}$ values.

56
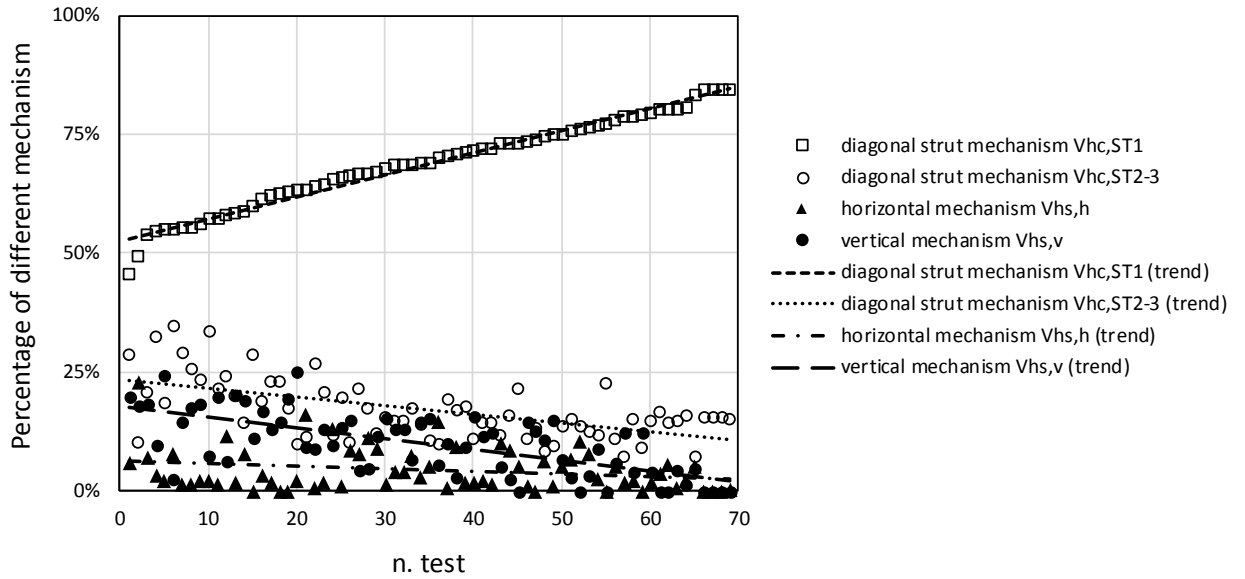
Fig. 24. Ratios of force distribution among the resisting mechanisms.

On the basis of Fig. 24, with the support of Table B1 and Table B2, the following observations can be made.

- The concrete struts' shear strength contribution is always greater than those offered by the joint horizontal stirrups and vertical intermediate reinforcement. The ST1 strut contribution is the greatest and ranges from 46% to 85 % of the total shear strength. The contributions of ST2-3 struts is minor and ranges from 7% to 35%. It can be observed than an increase in the ST1 contribution involves a decrease in the ST2-3 contributions. The minimum percentage of shear force carried by the three strut mechanisms is equal to 59% and is achieved in specimen J-3 [51], which has a horizontal joint reinforcement ratio $\rho_h = \frac{A_{sh}}{h_b b_j}$ equal to 2.16%, just a little less than the maximum ρ_h, which is equal to 2.31%. The corresponding percentage of vertical joint reinforcement effective in resisting horizontal shear forces is $\rho_v = \frac{A_{sv}}{h_c b_j tan\theta_h}$ equal to 1.07%, quite lower than the maximum ρ_v, which is equal to 2.66%.

  For specimens J-MO and J-HO [39], with no vertical joint reinforcement and with identical yield strength of horizontal stirrups, it is observed that a doubling of horizontal joint reinforcement ratio ρ_h (from 0.65% to 1.29%) results in an equivalent increase in the shear strength percentage carried by the horizontal stirrups (from 5.4% to 10.2%).

57

For specimens J-OH [39] and E0.0 [36], with no horizontal joint reinforcement and with similar yield strength of joint vertical intermediate reinforcement, it is observed that an increase in ρ_v of about 68% (from 0.80% to 1.34%) entails a 50% increase in the shear strength contribution provided by vertical joint reinforcement (from 13% to 20%). The gap between the two increments is probably due to the difference in the yield strength of 11% from specimens J-OH to E0.0.

It can be concluded that, in the proposed model, the three strut mechanisms provide a predominant contribution in carrying the joint shear forces, even in the presence of appreciable amounts of vertical and horizontal joint reinforcements.

- The maximum shear strength percentage resisted by the horizontal stirrups is equal to 23% and it is attained in specimen J-3 [51], which has a horizontal joint reinforcement ratio ρ_h equal to 2.16%, and tensile strength of this reinforcement equal to 1456 MPa. Specimen 1 [54] having the maximum value of ρ_h, equal to 2.31%, provides instead a shear strength contribution of 12%. In this case, however, the tensile strength of joint horizontal stirrups is equal to 320 MPa. By comparing the two specimens and the results obtained for them, it can be observed that, even though the two specimens have nearly the same values of ρ_h and horizontal stirrups with yield strengths that differ more than 4.5 times from each other, the ratio between the shear strength percentages carried by these reinforcements is not equal to 4.5. This behavior can be understood by considering that the concrete strength of specimen J-3 [51] is twice that of specimen 1 [54]. Thus, as it can be seen from Eq. (78), the contribution of the strut mechanisms to joint shear strength is greater for the first specimen, in spite of the contribution carried by the horizontal stirrups.

Hence, the percentage of shear strength provided by the horizontal stirrups does not depend only on the horizontal joint reinforcement ratio ρ_h, but also on the tensile strength of this reinforcement and the percentage of shear strength that can be carried by strut mechanisms, which is strictly related to the concrete compression strength.

- Specimens with identical geometrical and mechanical properties but different axial load values in the column exhibit different horizontal shear strength. In particular, the greater the compression force N on the column, the greater is the joint horizontal shear strength. The increase in the compression force acting in the

column induces an increase in θ_h, which leads to a decrease in the vertical joint reinforcement contribution to horizontal shear strength and a simultaneous increase in the concrete struts shear strength contribution. For specimens V [48] and VI [48] it is been observed that an increase in N of 1153% leads to an increase in θ_h of about 30%, which induces a simultaneous decrease in $cos\theta_h$ and increase in a_c, causing an increase in concrete struts contribution of 42% and a decrease in the vertical joint reinforcement contribution of about 39%. Overall, the total shear strength increases thanks to the increase in the column compressive force.

- In specimens I [48] and III [48], having identical geometrical and mechanical properties and the same compression force acting in the column, but different amounts of vertical joint reinforcement, an increase of 290% in vertical joint reinforcement induces an increase of 13% in the shear strength and only an increase of 1% in the shear force carried by strut mechanisms. Hence it can be concluded that the increase of A_{sv} increases the shear strength, but does not entail a variation in the concrete compression stresses.

3.3. Existing models

To assess the reliability of the proposed formula, a comparison between the values of joint shear strength obtained from Eq. (78) and those obtained from models of Kim and LaFave [7], Wang et al. [8] and Kassem [9] is performed.

3.3.1. Kim and LaFave

In their research Kim and LaFave introduced an empirical model [7] to evaluate shear strength of joints with horizontal reinforcement, using the Bayesian parameter estimation method.

From the evaluation of an experimental database of RC beam-column connections, the authors proposed the following simplified formula for RC joint shear strength, which includes six key parameters

$$V_{jh} = 1.31\alpha_t\beta_t\eta_t(JI)^{0.15}(BI)^{0.30}(f_c')^{0.75}A_{jh} \qquad (79)$$

where α_t is a parameter for qualifying the in-plane geometry (1.0 for interior joints), β_t is a parameter for qualifying the out-of-plane geometry (1.0 for in-plane sub-

assemblages), η_t describes joint eccentricity (1.0 for no eccentricity), JI is the joint transverse reinforcement index (JI $= (\rho_j \cdot f_{yj})/f_c'$) and BI the beam reinforcement index (BI $= (\rho_b \cdot f_{yb})/f_c'$).

3.3.2. Wang et al.

Wang et al. introduced a shear strength model [8], in which the reinforced concrete in the joint core is idealised as a homogeneous material in a plane stress state. The contribution of the joint shear reinforcement includes both the horizontal stirrups and the intermediate vertical bars of the column, and it is taken into account through the nominal tensile strength of the idealized concrete, $f_{t,n}$.

The critical shear force of the proposed model for interior beam-column joints is

$$V_{jh,max} = \frac{1 - \left(\sin^2 \alpha / f_{t,n} - 0.8 \cos^2 \alpha / f_c'\right)\sigma_y}{\left(1/f_{t,n} + 0.8/f_c'\right)\sin 2\alpha} b_j h_c \tag{80}$$

where

$$f_{t,n} = f_{tc} + \rho_{sh} f_{yh} \cos^2 \alpha + \rho_{sv} f_{yv} \sin^2 \alpha \tag{81}$$

with

$$f_{tc} = 0.556\sqrt{f_c'} \tag{82}$$

$$\alpha = \tan^{-1}(h_c/h_b) \tag{83}$$

$$\sigma_y = \frac{N}{b_c h_c} \tag{84}$$

3.3.3. Kassem

Kassem developed a mathematical method [9], built on the strut-and-tie model, to estimate the shear strength of reinforced concrete beam-column joints. The proposed model takes into account the shear stress contributions provided by the diagonal concrete strut and both horizontal stirrups and vertical intermediate column bars. The relevant explicit formula to evaluate the shear strength of interior joints is

$$V_{jh} = \left(0.26[\psi\cos(\phi)] + 0.44\left[\omega_h + 1.39\omega_b\left(\frac{b_b}{b_j}\right)\tan(\phi)\right]\right.$$
$$\left. + 0.07\left[\omega_v\left(\frac{b_c}{b_j}\right)\cot(\phi)\right]\right)f_c'b_ch_c \tag{85}$$

where

$$\psi = 0.6\left(1 - \frac{f_c'}{250}\right) \qquad (f_c' \text{ in MPa}) \tag{86}$$

$$\phi = \tan^{-1}(h_b/h_c) \tag{87}$$

$$\omega_h = (\rho_{jh} \cdot f_{yh})/f_c' \tag{88}$$

$$\omega_b = (\rho_b \cdot f_{yb})/f_c' \tag{89}$$

$$\omega_v = (\rho_c \cdot f_{yv})/f_c' \tag{90}$$

3.3.4. Model reliability

The shear strength values, V_n, of 28 collected interior RC beam-column joints (data listed in Table B3 and Table B4), different from those used for the coefficients' calibration, have been calculated applying the proposed formula (Eq. (78)), and the expressions of Kim and La Fave (Eq. (79)), Wang et al. (Eq.(80)) and Kassem (Eq. (85)). The author decided to compare different models on a set of data (28 specimens) different from that used for the calibration of the coefficients of the proposed formula (69 specimens), to demonstrate that the predictions of this formula are good in general, not only on the data set used for the calibration. The data set of 28 specimens can be considered adequately diversified and representative (see Table B3 and Table B4).

The computed values, V_n, are reported in Table B4 next to the experimental ones, $V_{jh,test}$. In the table there are reported also the ratios $V_{jh,test}/V_n$ and these ratios are plotted in Fig. 25, where the corresponding values of AVG, COV and UP (number of Unsafe Predictions) are specified.
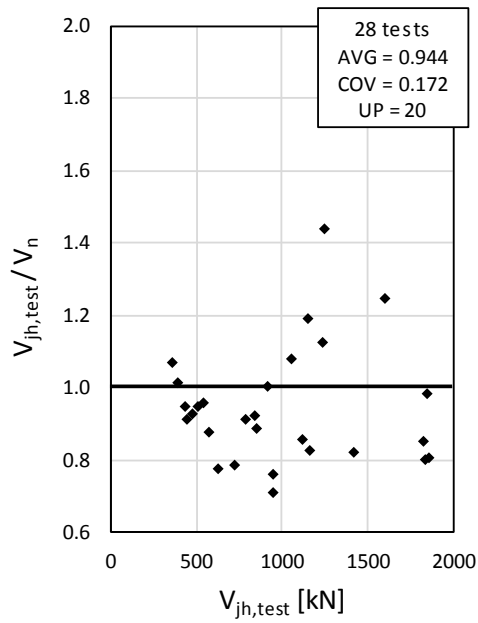
Fig. 25. Ratios $V_{jh,test}/V_n$ versus $V_{jh,test}$ values for 28 specimens calculated by means of (a) Kim and LaFave model, (b) Wang et al. model, (c) Kassem explicit formula and (d) proposed basic expression (Eq. (78)).

For these 28 tests, performed on beam-column connections with horizontal stirrups, the AVG and COV of $V_{jh,test}/V_n$ ratios result respectively equal to 0.944 and 0.172, for the model of Kim and LaFave, 1.082 and 0.181, for the procedure of Wang et al., 1.001 and

0.172, for the expression of Kassem, and 0.990 and 0.162, for the proposed formula (Eq. (78)).

A comparison has been performed also on 60+28=88 specimens (Tables B1-B4), considering also the specimens used for the calibration, apart 9 joints without horizontal reinforcement, for which it was not possible to use the model of Kim and La Fave. The ratios $V_{jh,test}/V_n$ are plotted in Fig. 26, where the corresponding values of AVG, COV and UP are specified.

◆ (a) Kim and LaFave model   ◆ (b) Wang et al. model
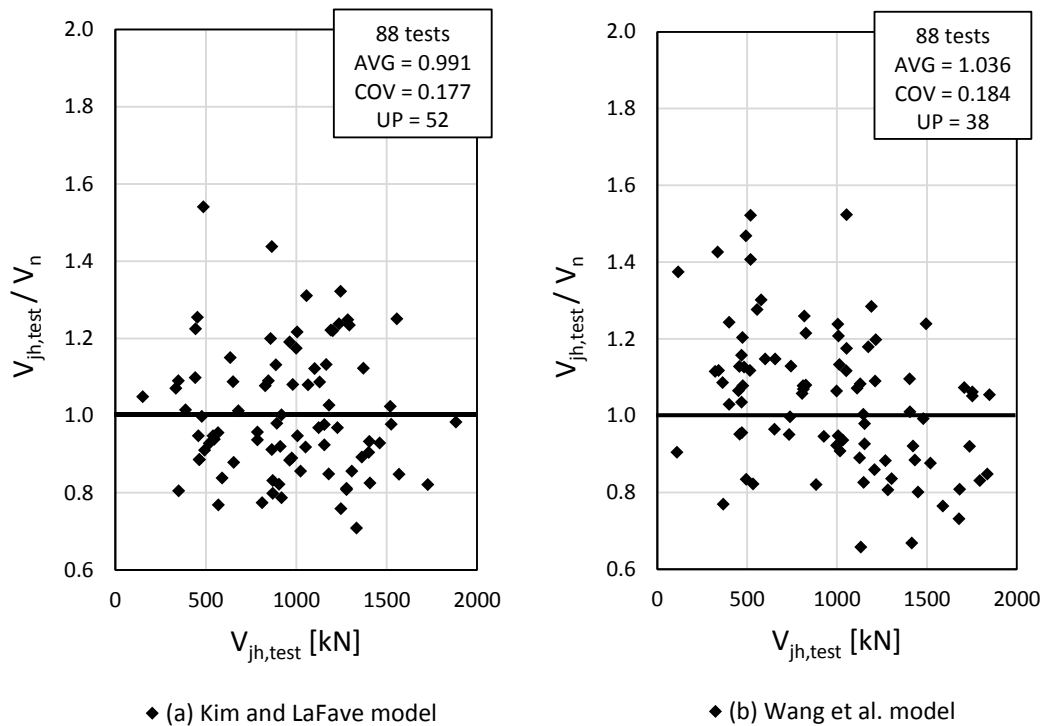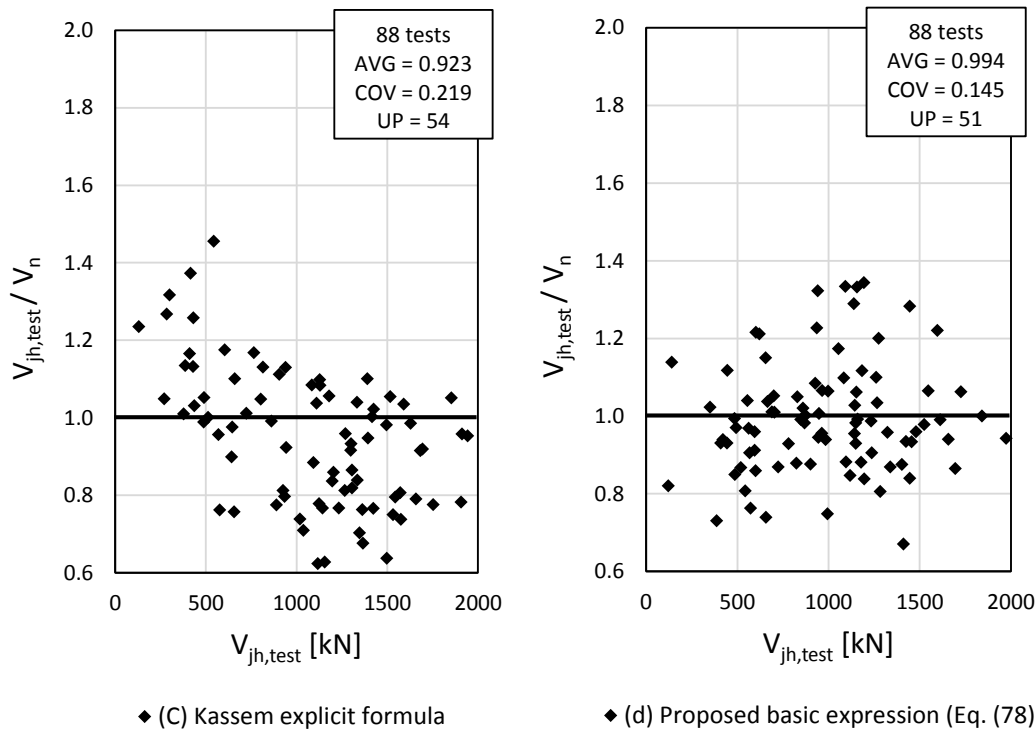
Fig. 26. Ratios $V_{jh,test}/V_n$ versus $V_{jh,test}$ values for 88 specimens calculated by means of (a) Kim and LaFave model, (b) Wang et al. model, (c) Kassem explicit formula and (d) proposed basic expression (Eq. (78)).

AVG and COV of $V_{jh,test}/V_n$ ratios result respectively equal to: 0.991 and 0.177, for the model of Kim and LaFave, 1.036 and 0.184, for the procedure of Wang et al., 0.923 and 0.219, for the expression of Kassem, and 0.994 and 0.145, for the proposed formula (Eq. (78)).

Since both in comparison with 28 specimens and 88 ones the proposed shear strength formula provides the lowest COV value, it can be said it is more consistent than the other considered formulae. Moreover, it is adequately accurate, since it provides AVG values very close to 1.

3.3.5. Value of the proposed strategy

From the comparison with other models, it emerges how the proposed shear strength formula (Eq. (78)) provides accurate and consistent predictions for a wide range of specimens, representative of joints of both new and existing RC buildings, and also considering specimens completely independent from those used for its calibration (see results for the data set of 28 specimens in Fig. 25).

With respect to the formula provided by Kim and LaFave [7], given by Eq. (79), the proposed formula well predicts also shear strength of joints without horizontal

reinforcement, while Eq. (79) is not usable in this case.

With respect to the formula of Wang et al. [8] (Eq. (80)), the advantage of the proposed formula is that it allows to separately calculate the contributions of the concrete struts and the truss mechanism, similarly to the formula proposed by Kassem [9] (Eq. (85)). However, differently from the last, the proposed formula takes into account also the influence of the column axial load.

The possibility to separately calculate the shear strength contributions enables to accurately evaluate, case by case, which, among these contributions, is the most prominent. This can be useful for further developments in the fields of buildings seismic assessment and retrofitting.

3.4. Design formula

The proposed shear strength formula (Eq. (78)) provides accurate and consistent predictions, as assessed through the comparison with other authors' formulae. However, since formula (78) presents an AVG equal to one, it is necessary to introduce a safety factor to employ it for design purposes.

It is possible to provide a design shear strength formula by multiplying Eq. (78) by a safety factor, without altering the COV value. The safety factor is determined on statistical basis here, so that there is a 95% probability that the predicted design shear strength is lower than the experimental one for the 69 test data used for the coefficients' calibration.

The proposed design formula derived is

$$
V_{n,d} = 0.80 \left[5.28 \left(\frac{A_{sb1}}{\Phi_{b1}} + \frac{A_{sb2}}{\Phi_{b2}} \right) l_h + 0.80 \chi \, f_c' a_c b_j \cos\theta_h + 0.14 A_{sh} f_{yh} + 0.22 \frac{A_{sv} f_{yv}}{\tan\theta_h} \right] \quad (91)
$$

which provides AVG=1.250.

To assess the reliability of this formula, a comparison with the formulae for interior joints provided by Eurocode 8 [2] and ACI 318-14 [1] is performed on 25 specimens, using the test data employed for the comparison with the existing models, apart 3 joints which do not satisfy both Codes requirements (Table B3 and Table B4).

3.4.1. Eurocode 8 [2]

In Eurocode 8 [2] the maximum horizontal shear force allowed in interior beam-column joints is

$$V_{jhd} = \eta f_{cd} b_j h_{jc} \sqrt{1 - \frac{\nu_d}{\eta}} \tag{92}$$

where $\eta = 0.6 \left(1 - \frac{f'_c}{250}\right)$, ν_d is the normalised axial force in the column above the joint and h_{jc} is the distance between the extreme layers of column reinforcement.

3.4.2. ACI Code 318-14 [1]

The nominal shear strength of interior beam-column joints in ACI Code 318-14 [1] is calculated accounting the compressive strength of the concrete and the geometry of the joint, through the following design formula

$$V_d = \phi V_n = \phi \cdot 0.083 \gamma \sqrt{f'_c} b_j h_c \tag{93}$$

where ϕ=0.85, γ is equal to 15 for joints confined by beams on two opposite faces, with beam widths at least three-quarters of the effective joint width, and $\gamma = 12$ for beam widths smaller than three-quarters of the effective joint width. The effective joint width b_j should not exceed the smallest of $(b_b + b_c)/2$, $b + 2x$ where x is the smaller distance from the beam vertical edges to the closest column vertical edges [1].

3.4.3. Comparison

All the 25 collected tests satisfy both ACI Code and Eurocode 8 requirements for beam-column connections and are considered in the comparison with both Codes (Fig. 27). In Eq. (78) the average value of concrete strength is used, i.e. $f'_c = f_{cm}$, while in Eq. (92), the design value, i.e. $f_{cd} = (f_{cm} - 8)/1.5$, and in Eq. (93), the specified one, i.e. $f'_c = f_{cm} - 8$, are used.

The computed shear strength values, V_d, are reported in Table B4 next to the experimental ones, $V_{jh,test}$. In the table there are reported also the ratios $V_{jh,test}/V_d$ and these ratios are plotted in Fig. 27

The ratios between the experimental results relevant the 25 collected interior joints and the results obtained by the application of the proposed design shear strength formula (Eq. (91)) give an AVG equal to 1.216 and a COV of 0.149. The Unsafe Predictions (UP) are 2.

For Eurocode 8 and ACI Code 318-148, the AVG and COV values of the $V_{jh,test}/V_d$ ratios and UP are respectively equal to 1.420, 0.501 and 7, and 1.439 0.216 and 2.
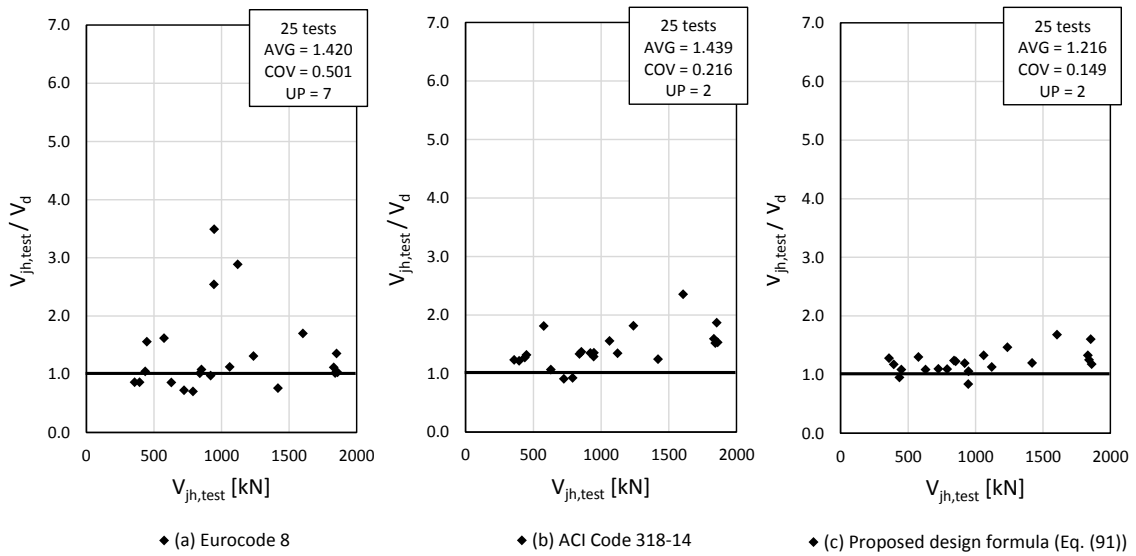
Fig. 27 Ratios $V_{jh,test}/V_d$ versus $V_{jh,test}$ values for 25 specimens calculated by means of (a) Eurocode 8, (b) ACI Code 318-14 and (c) proposed design formula (Eq. (91)).

From this comparison, it is apparent that the proposed design formula (Eq. (91)) gives appropriately safe predictions, since it leads only to 2 UP, without being excessively conservative (lowest AVG value in comparison to ACI Code and Eurocode 8). Furthermore, the proposed formula is the most consistent, since it provides the lowest COV.

A comparison has been made also on a set of 40+25=65 specimens, considering also the specimens used for the calibration (Tables B1-B4), apart 9 joints without horizontal reinforcement and 20 joints that did not satisfy both Codes requirements. The ratios $V_{jh,test}/V_d$ are plotted in Fig. 28, where the corresponding values of AVG, COV and UP are specified.
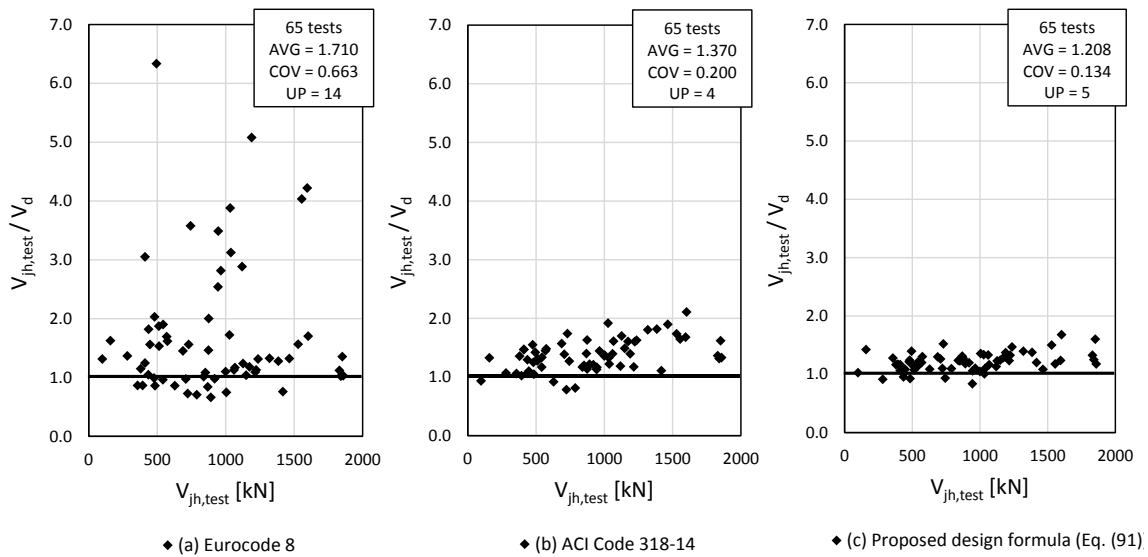
Fig. 28 Ratios $V_{jh,test}/V_d$ versus $V_{jh,test}$ values for 65 specimens calculated by means of (a) Eurocode 8, (b) ACI Code 318-14 and (c) proposed design formula (Eq. (91)).

The AVG and COV of $V_{jh,test}/V_n$ ratios and UP result respectively equal to: 1.710, 0.663 and 14 for Eurocode 8, 1.370, 0.200 and 4 for ACI Code and 1.208, 0.134 and 5 for the proposed design formula. These results confirm the considerations previously made for the comparison with the data set of 25 specimens.

It can be observed that the COV values gained by the formulae of the Codes are much larger than those obtained by the proposed design formula, because the Code formulations are simplified and contain less parameters than the proposed one. The latter, on the contrary, takes account of a greater number of mechanical phenomena and this makes the prediction more consistent.

As regards the unsafe predictions, it is clear that the proposed formula and ACI Code provide results safer than Eurocode 8.

3.5. Conclusions

On the basis of a mechanical analysis and the use of 69 previous experimental results, a new model for the shear strength prediction of interior RC beam-column joints under seismic loads has been obtained, and the following conclusions can be drawn:

1) The shear strength arises from the contribution of three inclined concrete struts and the contribution of horizontal stirrups and vertical reinforcement of the joint core. The model takes into account the column axial load influence on the inclination of the

concrete struts.

2) The sum of the three inclined concrete struts contributions constitute the main resisting mechanism.

3) The percentage of shear strength provided by the horizontal stirrups depends not only on the horizontal joint reinforcement ratio ρ_h, but also on the tensile strength of the stirrups and the percentage of shear strength that can be carried by the strut mechanisms, which is strictly related to the concrete compression strength.

4) An increase in the column axial compression load entails an increase in θ_h, which leads to a decrease in the vertical joint reinforcement contribution to horizontal shear strength and a simultaneous increase in the concrete strut shear strength contribution.

5) In interior RC beam-column joints, vertical bars are more effective than horizontal stirrups in providing shear strength.

6) In the experimental comparison with the formulae of Kim and LaFave, Wang et al. and Kassem, the proposed formula (Eq. (78)) gives the most consistent predictions, because it provides the the lowest COV value. Moreover, it is adequately accurate, since it provides AVG values very close to 1. Hence, it is possible to state that the proposed mechanical model well implements the actual mechanical behavior.

7) A design formula (Eq. (31)) is derived on the basis of a conservative criterion, by multiplying Eq. (78) by a safety factor. The experimental comparison, on a collection of 25 specimens, with the shear strength design formulae of Eurocode 8 and ACI Code 318-14 proves that the proposed design formula gives appropriately safe predictions, since it provides the lowest number of unsafe predictions, like ACI Code, without being excessively conservative, since it provides AVG values very close to 1. Furthermore, the proposed formula is the most consistent, since it provides the lowest COV value.

4. Study on experimental behavior of beam-column joints reinforced with smooth bars under cyclic actions

It is well known that Reinforced Concrete (RC) buildings under seismic actions are subjected to horizontal forces, which impose large deformations on the structure and lead the members' response into the post-elastic range [27].

In modern seismic codes, the design of RC frames is based on the principles of capacity design, which provide for the development of plastic hinges in specified regions of the structural elements, avoiding the occurrence of brittle failure mechanisms. Conventionally, the strong-column/weak-beam design approach is assumed, because it ensures the best ductile behavior of the structure, by developing plastic hinges at the ends of the beams.

In Italy, many existing RC buildings constructed before the mid-1970s present structural deficiencies, as they were designed to resist to gravity and windy loads only, in the absence of the prescriptions of modern seismic codes. In particular, the use of smooth reinforcing bars, inappropriate anchorage solutions and the lack of joint horizontal hoops are rather widespread. These structural deficiencies are also characteristic of buildings present in other seismic regions of the Mediterranean area.

The lack of transverse shear reinforcement in beam-column joint connections could cause brittle shear failure of the joints and the sudden collapse of the building [40]. Furthermore, in many resisting frames, the reinforcements' anchorage length is insufficient, especially in exterior joints [70]. Moreover, the use of smooth bars instead of deformed ones heavily influences the steel-concrete bond mechanism, due to the different bond-slip relationships [71], and could lead to slippage of the reinforcement. For instance, beam bars slippage in interior joints can produce additional lateral deformation of the structure with the potential onset of unexpected soft-storey failure mechanism, while, for exterior joints, beam bars slippage can lead to brittle local failure of the joint [72]. Finally, under seismic load conditions, the framing elements can transmit high stresses to the joint core, whose behavior is therefore highly influenced by the geometric and mechanical properties of the adjacent members. It follows that beam-column joints are critical elements in RC existing structures, because their behavior is governed by shear and bond-slip mechanisms, which may lead to brittle and sudden failures.

Hence, to design retrofitting of existing buildings, it is fundamental to study the seismic performance of beam-column joints especially in RC structures reinforced with smooth bars.

In recent years, many experimental tests have been conducted on beam-column joints reinforced with deformed bars [21], [24], [41], [58], [60], [66], and many empirical and mathematical models to predict these joints shear strength have been proposed [22], [28], [12], [15], [16]. However, only few experimental studies have been carried out on beam-column joints reinforced with smooth bars, even though many existing RC buildings have this kind of reinforcement.

This thesis reports the largest collection possible of experimental tests, available in the literature, on beam-column joints, both interior and exterior, reinforced with smooth bars. The corresponding test specimens represent typical joints of existing RC buildings designed before the mid-1970s. The investigations take into account several factors influencing the joint seismic response, including horizontal hoops amount, different reinforcement anchorage solutions, and column axial load. This research considers experimental test results of interior joints separately from those of exterior joints and looks for possible relationships between the different design assumptions and the final failure modes of the test units. The column axial load influence on the joint shear stress at failure is made explicit. Shear strength formulations present in the literature for joints with deformed bars are considered, to study their applicability for joints with smooth bars. These formulations are modified to take account of the very low bond stresses transferred by smooth bars.

This investigation constitutes a useful tool to better understand the seismic behavior of existing buildings with smooth bars, which has to be taken into account to design safe upgrade solutions.

4.1. Interior joints

4.1.1. Bond deterioration mechanism

The modern seismic design of RC structures ensures the development of plastic hinges in the beams, rather than in the columns, thereby avoiding soft-storey failure mechanism in the perspective of the strong-column/weak-beam approach. Under seismic load conditions, the beams (and the columns) framing into the joint are subjected to moments

in the same direction (Fig. 29), caused by the horizontal seismic forces. As a consequence of this, the longitudinal beam bars passing through the joint core are in tension on one side and in compression on the opposite side. Therefore, under severe cyclic loads, high bond stresses develop along the beam bars in the joint core and bond deterioration may occur, if the upper limit of bond strength is reached.
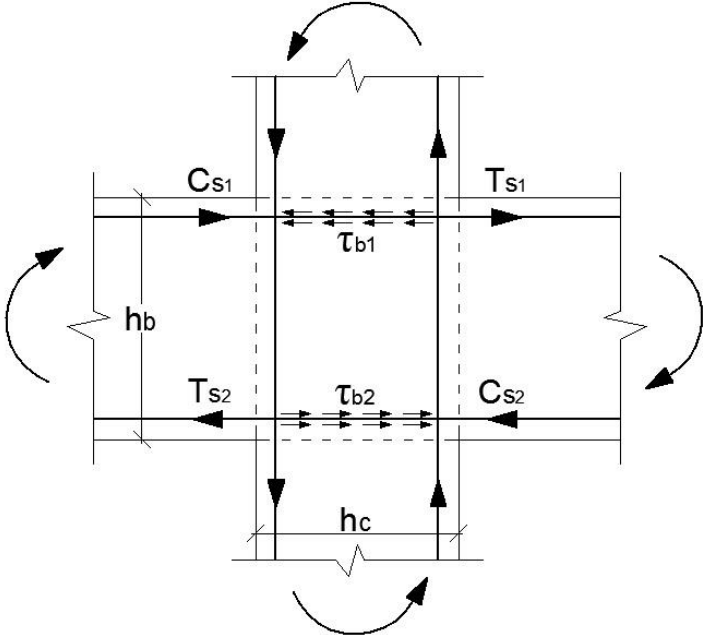
Fig. 29. Forces and stresses acting on the joint under seismic bending moments.

By assuming the bond stress τ_{b1} acting on the bars to be constant along the joint core, and considering, for simplicity, one single bar, the equilibrium between the tensile force at one side, T_{s1}, the compressive force at the opposite side, C_{s1}, and the bond stress on the beam top bar (Fig. 29) are related by the expression

$$C_{s1} + T_{s1} = \tau_{b1} \cdot d_b \pi \cdot h_c \qquad (94)$$

where d_b is the bar diameter and h_c is the column depth.

Since at the development of the plastic hinge the beam bar under tensile force yields at the column interface, by assuming an elastic-ideally plastic constitutive relationship for steel, the tensile and the compressive forces at the opposite sides of the joint can be computed as follows, respectively

$$T_{s1} = \frac{d_b^2}{4}\pi \cdot f_y \tag{95}$$

$$C_{s1} = \frac{d_b^2}{4}\pi \cdot f_s \tag{96}$$

where f_y and f_s are the yield strength and the compressive stress of the bar at the two sides, respectively. The compressive stress is assumed to be minor compared to the yield strength, since on the compression side the concrete also contributes to compressive strength. To avoid bond deterioration, the bond strength developed on the bar should be greater than the forces acting on the bar at the two sides of the joint, i.e. the sum of tension T_{s1} and compression C_{s1} (Fig. 29).

By substituting Eq. (95) and (96) in Eq. (94), this conditions results in

$$\tau_{b1} \cdot d_b \pi \cdot h_c \geq \frac{d_b^2}{4}\pi \cdot \left(f_y + f_s\right) \tag{97}$$

By simplifying Eq. (1), the limiting value of the ratio h_c/d_b can be obtained

$$\frac{h_c}{d_b} \geq \frac{f_y + f_s}{4\tau_{b1}} \tag{98}$$

In many Codes Eq. (98) represents the condition to be respected to avoid bond deterioration inside RC beam-column joints. Since this issue is of fundamental importance for the structures' strength under seismic actions, many researchers have devoted time to its study.

Among these researchers Hakuto et al. [73] carried out an in depth theoretical study on interior beam-column joints demonstrating the importance of having adequate ratios of longitudinal beam bars diameter, d_b, to column depth, h_c. In particular, they observed that, when bond deterioration occurs, the beam bars at the compression side slide and remain anchored to the side in tension. As a consequence, the penetration of the tensile stress through the bar and the transition of the bar on the compressed concrete side from compression to tension occurs. This phenomenon is all the more probable for large diameter bars, and shorter column depths. This is because large bar diameters and short column depths cause higher bond stresses concentrations. Furthermore, the phenomenon

becomes critical when the bars are smooth. Hakuto et al. also evaluated the reduction in flexural strength and available ductility of the beams, as a result of bond deterioration along the longitudinal bars passing through the joint. To calculate the flexural strength and the curvature ductility $\frac{\emptyset_u}{\emptyset_y}$, they assumed that plane sections remain plane under bending moments (Fig. 30), except for the strain in the reinforcement of the compression zone of the beam section ($\varepsilon_1 > 0$), whose compressive stress, after bond deterioration and bar slippage, becomes tension (f_1).
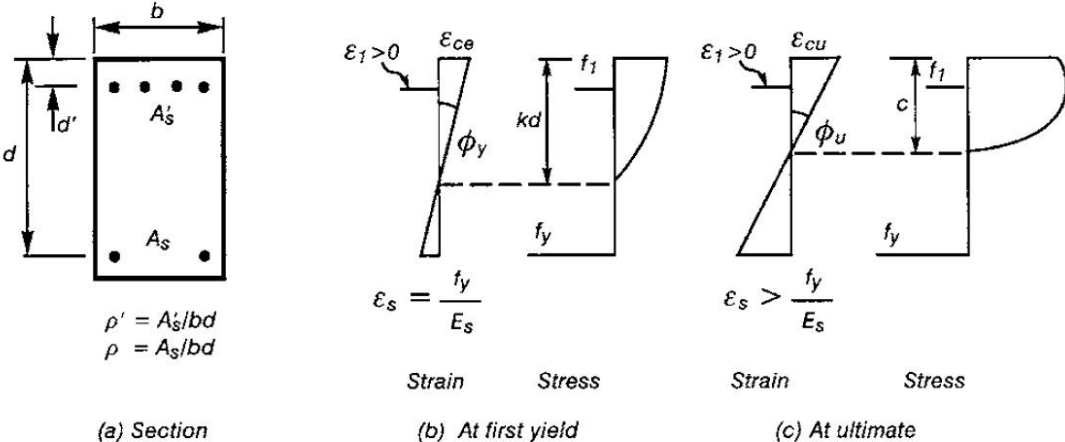
Fig. 30. (a) Doubly reinforced beam section at column interface; (b) at first yield; (c) at ultimate. [73]

In the case of perfect bond conditions, for positive bending moments (left side of Fig. 29), the compressed reinforcement could develop a curvature ductility factor of 18. As the bond deteriorates and the stress in the compression reinforcement switches from compression to tension, the available curvature ductility factor, when the tensile stress in that reinforcement reaches the yield strength is 5. This occurs just before the concrete, which remains under compression, crushes. Furthermore, Hakuto et al. compared the limiting values of longitudinal beam bar diameter to column depth ratio (d_b/h_c) permitted by seismic design standards NZS 3101:1995 [20]. They observed that the codes provide different maximum d_b/h_c ratios. These differences depend on how each code weights the advantages and disadvantages of considering a specific d_b/h_c limit. Indeed, it has to be considered that very small d_b/h_c ratios correspond to very small diameters of the reinforcing bars, or to large columns, which lead to design and construction difficulties. On the other hand, very large d_b/h_c values lead to strong bond degradation

74

and to the decrease of the global stiffness of the structure. In any case, Hakuto et al. suggested that a reduction in ductility of the beam plastic hinge should be considered when specifying the maximum permitted d_b/h_c value.

On the basis of all previous observations it can be said that the ratio of longitudinal beam bars diameter to column depth is fundamental in designing interior beam-column joints. This ratio can seriously compromise the global behavior of RC structures under seismic loads, by producing bond deterioration and the development of bar slippage brittle mechanisms. Many existing buildings do not provide the required value of this ratio, and this should be considered for the correct assessment of their seismic behavior, especially when smooth bars are present in the building.

4.1.2. Experimental investigations available in the literature

The main research findings about interior beam-column joints with smooth bars available in the literature are summarized below, in order to evaluate their behavior under seismic action.

Liu and Park [74]

Liu and Park investigated the seismic behavior of two RC interior beam-column joints with smooth bars having low transverse reinforcement amount in beams and columns and no shear reinforcement in the joint core, representing conditions of existing buildings designed according to pre-1970's codes. The two specimens, Unit 1 and Unit 2, were identical (Fig. 31) and had the same mechanical and geometric properties of Unit O1, belonging to another study conducted by Hakuto et al. [75], except for the use of smooth round bars for longitudinal reinforcement [73] instead of deformed bars [75]. These allowed a direct comparison between the behavior of the joints made with the two types of reinforcement.
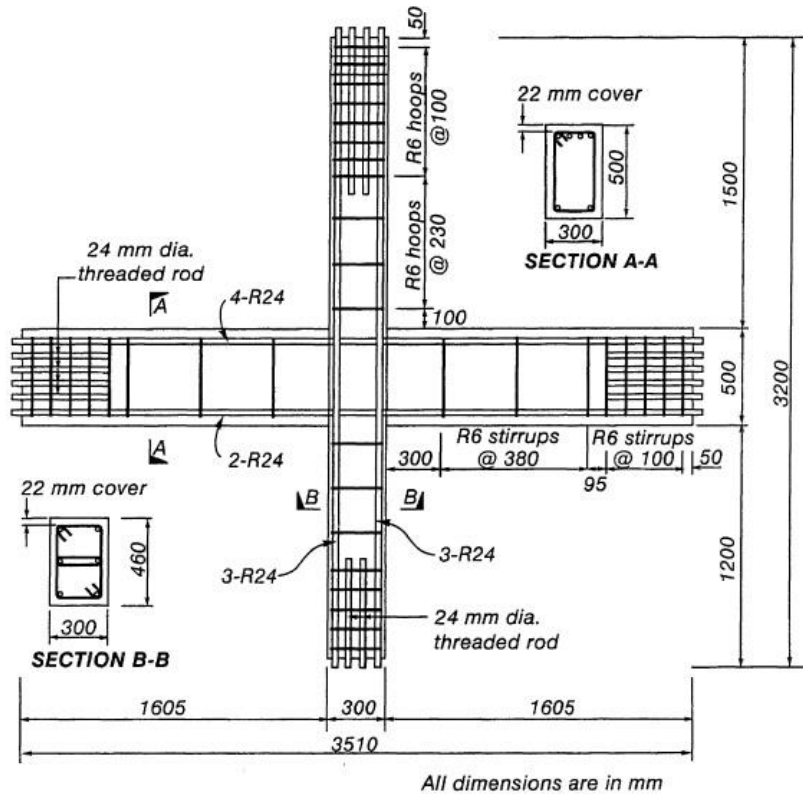
Fig. 31. Reinforcement details of Unit 1 and Unit 2 [74].

Unit 1 was tested under zero axial load, while Unit 2 was tested with a constant compression equal to $0.12 f_c' A_g$, where f_c' is the concrete cylinder compressive strength and A_g is the column section gross area [74].

Theoretical considerations on sub-assemblages strength, evaluated by the plane section theory, as well as the inadequate development length of the smooth bars within the joint core led the authors to expect significant bond degradation and longitudinal bars slippage. The theoretical strengths of the beams and columns were obtained with the hypothesis of perfect bond between steel and concrete. The development of the plastic hinges was expected in the columns for Unit 1, and in the beams for Unit 2. The storey shear, imposed at the column end, was calculated at the theoretical flexural strengths of the critical members and was equal to 80 kN for Unit 1 and 128 kN for Unit 2.

Liu and Park compared the experimental results of the two RC joints reinforced with smooth bars to that of the joints reinforced with deformed bars, in terms of bond deterioration. In particular, test results for Unit 1, with zero axial load, revealed that the damage was concentrated at the column-joint interface, with horizontal flexural cracks, as a result of bond deterioration and slippage of the column longitudinal bars that

76

increased the column fixed-end rotations. The authors observed that, for these bars, according to NZS 3101:1995 [20], the required h_b/d_c ratio was equal to 30.2, while the effective value was lower and equal to 20.8, where h_b is the beam height and d_c is the column bar diameter. Vertical cracks due to slippage of the longitudinal beam bars also occurred, at the beam-joint interface, but less pronounced than the horizontal cracks. According to NZS3101:1995 [20], the required h_c/d_b ratio for the beam longitudinal bars was 33, while the effective value was 12.5. Moreover, the tests revealed vertical cracks running through the columns and the joint core due to column bar buckling, as a result of the inadequate transverse reinforcement of the members. In fact, the stirrup spacing was equal to 230 mm and 380 mm in the columns and in the beams, respectively. There were no inclined tension cracks in the beams or in the columns, indicating that no more transverse reinforcement was needed for preventing shear cracks. The joint core, which was without stirrups, presented some minor diagonal cracks at the end of the test. The strains measured along the beam bars indicated that the slip of the bars through the joint induced the bars, which were theoretically under compression at one side of the joint, to be effectively in tension. As a result, the strains on the beam and column longitudinal reinforcement adjacent to the joint panel, as well as the flexural curvature, were higher. By comparing the theoretical strengths in terms of the storey shear to the actual strengths, it emerged that the formers were overestimated, due to the plane section theory assumption for the column flexural strength at the plastic hinge. The use of smooth bars led to a reduction in structural stiffness and flexural strength, with respect to the predicted values.

From the comparison of results of Units 1 and 2 with the results obtained by Hakuto [75] for the specimen O1 reinforced with deformed bars, Liu and Park concluded that the final failure of the sub-assemblages with smooth reinforcing bars [74] was governed by bond degradation and column bar buckling, rather than joint shear failure, and attributed the units' low structural stiffness and strength to slippage of the smooth bars. Conversely, the use of smooth round bars was found to improve the joint shear strength. At the theoretical flexural strengths of the columns, the nominal horizontal shear stresses were $0.5\sqrt{f_c'}$ for Unit 1, with smooth bars [74], and $0.61\sqrt{f_c'}$ Unit O1, with deformed bars [75]. As a consequence, Unit 1 [74] evinced less diagonal cracking and shear distortion in the joint core than Unit O1.

Test results on Unit 2 revealed that column axial compression enhanced the transmission of beam bar forces to the joint core by bond, and led to extensive diagonal shear cracking. As a consequence, the joint core deformation had a bigger contribution to the total storey drift, which was greater than that of Unit 1. Furthermore, the damage of Unit 2 spread to the regions near the joint, with wide flexural cracks in the beams. No diagonal tension crack occurred in the members adjacent to the joint for both Unit 1 and Unit 2, since the shear reinforcement in beams and columns was sufficient to provide adequate shear strength. On the other hand, the compressive axial load in the column of Unit 2, when combined with severe bond degradation, led to severe column bar buckling and extensive concrete spalling within the joint core and in the adjacent regions, due to the lack of joint transverse reinforcement. In the end, the presence of column axial compression on Unit 2 developed different cracking patterns and damages and enhanced column bar buckling, which caused the final failure of the sub-assemblage [74].

Pampanin et al. [72]

Pampanin et al. investigated the seismic vulnerability of RC beam-column joints of the typical Italian structures built from the 1950s through the 1970s, having smooth bars as longitudinal reinforcement and no joint transverse reinforcement. The sub-assemblages were not detailed to have ductile behavior. The study on interior joints considered two different beam bar configurations, one with continuous bars passing through the joint core (Fig. 32(a)) and the other with lap-slices and end hooks for the beam bars just outside the joint region (Fig. 32 (b)).

(a)   (b)
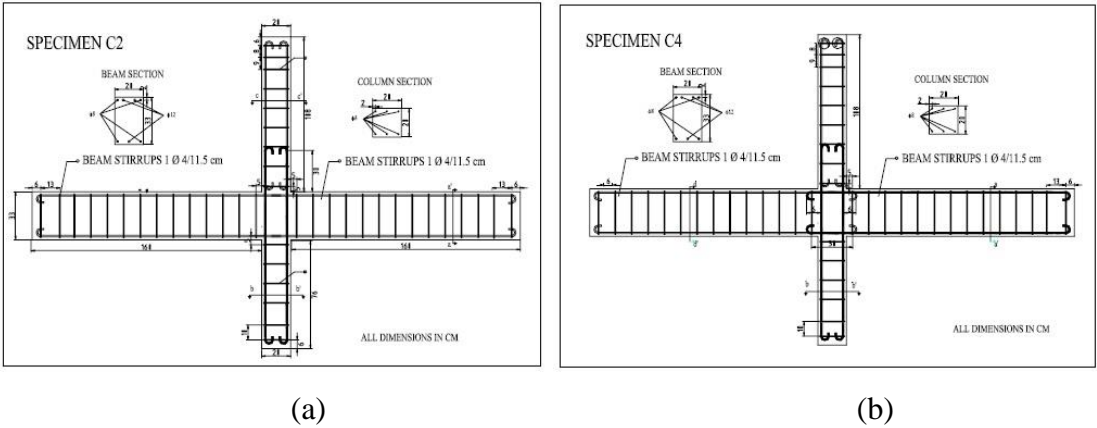
Fig. 32. Different beam bars configurations for interior joint sub-assemblages [72]: (a) continuous bars passing through the joint; (b) lap-slices with end hook anchorages outside the joint region.

In order to simulate the actual forces developed in a frame system during a seismic event, diversely from the other tests in the literature, in [72] the axial load applied on the upper column was varied as a function of the vertical load applied to the beams ends. At the local level, the brittle failure of the structural elements was expected. Particularly, for the considered joints, shear cracking was expected to occur first in the joint panel and, subsequently, the column hinging.

Instead, test results revealed that the interior joints developed a relevant resource of plastic deformation, even if they were designed without specific details for developing a ductile behavior. Actually, at early stages, flexural cracks occurred in the column and represented a sort of structural fuse for the joint core, which evinced no damage apart from the slippage of the column bars. From the comparison of the different anchorage solutions, it appeared that, at the local level, the higher deformability due to bar slippage did not result in decreased flexural strength. Anyway, the higher flexibility due to the ductile resource of interior joints, combined with the slippage of the column bars, led to flexural failure at the joint-column interface which resulted, at the global level, in an undesired soft-storey mechanism.

Braga et al. [77]

Braga et al. also investigated the failure mechanisms and their interactions for interior joints designed for gravity loads. They observed that the small section size of the columns and the inadequate longitudinal reinforcement in existing structures were the main causes of failure. In particular, these authors performed three experimental tests on interior joints reinforced with smooth bars: two specimens subjected to column axial load, C11-1 and C23-1, built in full scale and 2:3 scale, respectively, and specimen C23-2, built in 2:3 scale subjected to eccentric column load, to study the P-Δ effect. Failures were governed by the bond-slip of the columns longitudinal bars, with lumped yielding of the columns near to the joint-column interface (Fig. 33) and a consequent soft-storey failure mechanism.
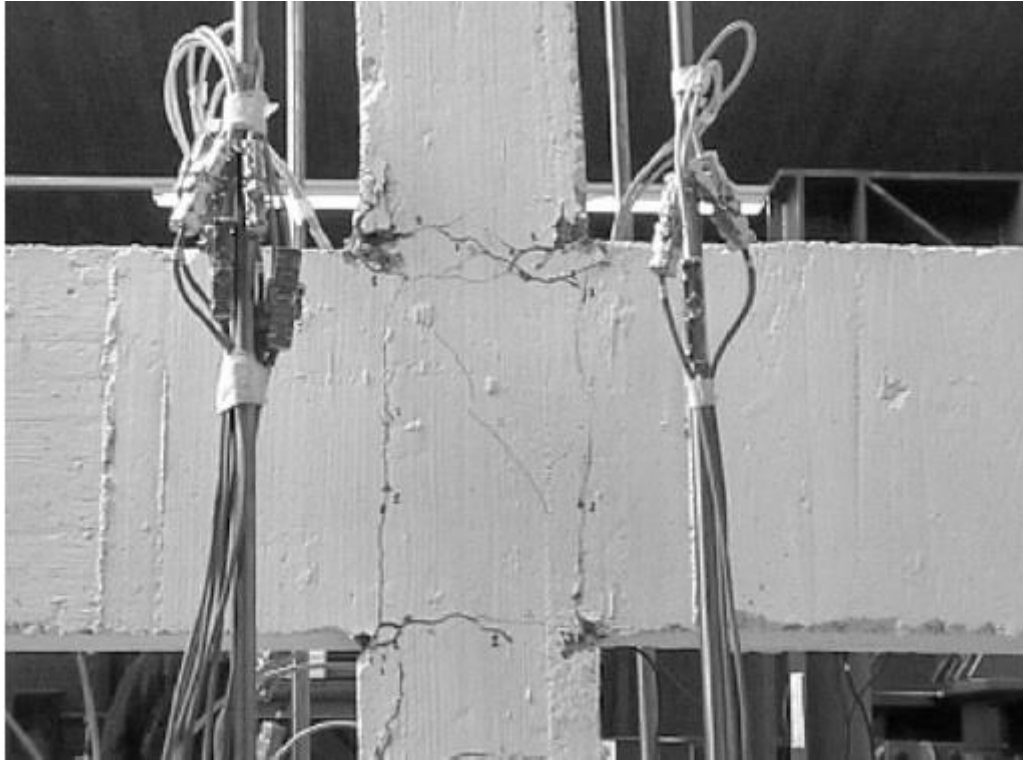
Fig. 33. Final damage pattern of specimen C23-1 [77].

However, by comparing behavior of columns with smooth bars whose specimens were subjected to flexure and axial load with the known behavior of the joints reinforced with deformed bars, they observed that the specimens with smooth bars show a reduced degradation of the cyclic response.

Afterwards, Braga et al. carried out an investigation [78] of the influence of bond loss of bars passing through the joint panel, and a series of experimental tests [77] on interior and exterior RC beam-column joints. They performed numerical analyses, considering different strength in compression of longitudinal bars, using a simplified model [79], which provides a stress-strain relationship that accounts for bond slippage. From the comparison, it appeared that the bond-slip of the beam and column longitudinal bars reduces the flexural strength of the sections, especially when the axial load is high. This phenomenon could promote flexural yielding of columns rather than beams, and modify the local failure mechanism of the structure.

Fernandes et al. [80]

Fernandes et al. carried out a comparative study on six full-scale RC interior joints (Fig. 34), representative of structures built in the mid-1970's, to assess the influence of bond properties, column axial load and amount of reinforcement on joint behavior.
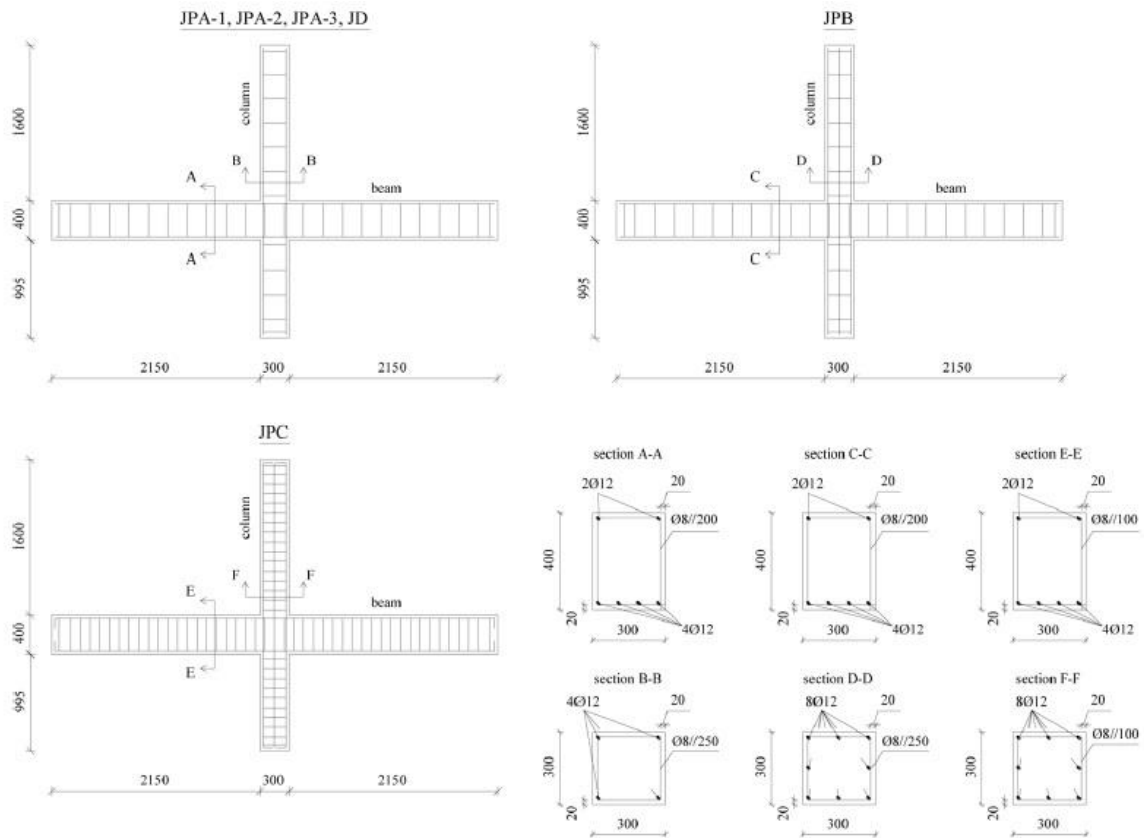
Fig. 34. Geometrical and reinforcing details of the specimens in [80]
(dimensions are in mm).

The investigation on the influence of bond properties focused on two specimens, without horizontal hoops in the joint: one reinforced with smooth bars, specimen JPA-1, and the other reinforced with deformed bars, specimen JD. Both specimens had normalized column axial load equal to 9.4%. In agreement with the other previously cited research works, the authors observed that the total energy dissipated by the specimen with deformed bars was higher than that of the specimen with smooth bars. Moreover, the specimens exhibited different damage modes, and their final cracking patterns well illustrated the influence of bond properties on the cyclic behavior of the joints. In particular, specimen JPA-1 with smooth bars showed flexural cracks concentrated at beam-joint and column-joint interfaces, and cracking in the joint core was negligible. Diversely, the joint with deformed JD bars exhibited spread damage, with cracks along the beam and column spans and cracking with concrete cover spalling in the joint core.

By examining the effects of the column axial load, the authors compared test results on specimen JPA-1, with normalized axial load of 9.4%, to that of specimen JPA-3, identical but loaded with column normalized axial load of 21.3%. The comparison revealed that the increase in the compression on the column, enhanced the lateral strength of the joint

and led to larger strength degradation, at maximum drift (4%), and larger energy dissipation. The damage was significant in the joint core, so that specimen JPA-3 exhibited diagonal cracking with concrete cover spalling and displayed larger energy dissipation and reached the conventional failure condition [80].

The influence of the steel reinforcement amount was also studied by Fernandes et al., under the normalized axial load of 21.3%. One unit, specimen JPB, was realized with a large amount of column longitudinal reinforcement; another unit, specimen JPC, with large amounts of column longitudinal bars and transverse reinforcement of both beam and column. The two sub-assemblages showed results very similar to each other, hence it appears that the large amount of transverse reinforcement did not make a significant contribution to specimen JPC's strength. The increase in the column longitudinal reinforcement led to minor damages in the columns, with flexural cracks concentrated at beam-joint interfaces and no damage in the joint region. Comparing the results of specimens JPB and JPC to that of specimen JPA-3, it is evidenced that increasing the amount of steel reinforcement results in marked decrease in energy dissipation.

Melo et al. [81]

Melo et al. studied the cyclic response of interior beam-column joints reinforced with smooth bars, by performing tests on six full-scale test units (Fig. 35), representative of RC structures built before the 1970s, without joint shear reinforcement, in the presence of applied column axial load equal to 450 kN. For comparison, an additional unit, specimen ID, with deformed reinforcing bars was built to investigate the bond influence on seismic response of beam-column joints. Moreover, the six specimens reinforced with smooth bars presented different geometric and mechanical properties, to investigate how the different reinforcement detailing of beams and columns, the presence of floor slabs and the concrete compressive strength might influence the global behavior and the failure mechanism of the sub-assemblages.

The experimental results evidenced that in units reinforced with smooth bars, the maximum strength of the joint increased with the concrete grade while, specimen ID, with deformed bars, developed the maximum strength, due to the greater steel grade of the reinforcement. All the tested joints developed shear failure mechanism, with diagonal cracks in the joint core followed by concrete spalling, except for specimen IPD, with lap-slices both in the beams and in the upper column, as shown in Fig. 35.
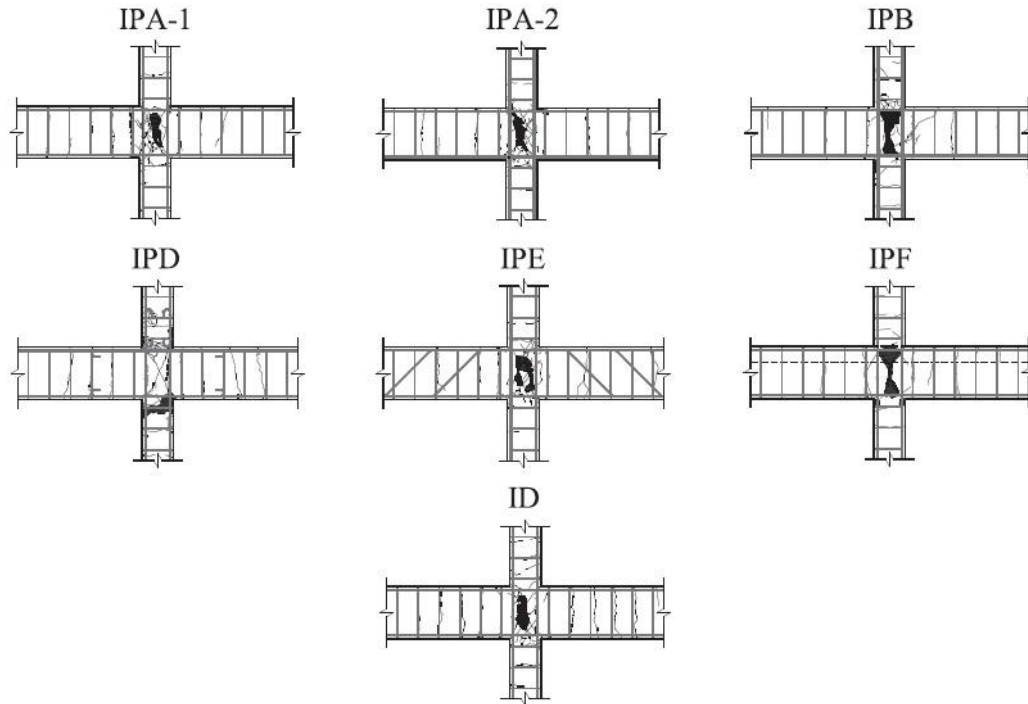
Fig. 35. Final damage patterns of the specimens in [81].

Specimen IPD presented larger damage at the inferior column-joint interface, with flexural cracks, concrete spalling and bars buckling. In fact, the overlapping of longitudinal beam bars in the joint region enhanced the shear strength of the joint and the flexural capacity of the beam-joint interface sections, thus affecting the failure mechanism of the unit, which did not exhibit joint shear failure.

As regards the influence of bond properties, the specimens with smooth bars developed concrete damage mainly in the joint core. The authors observed that shear failure occurred due to the lack of joint stirrups and the weak concrete confinement, and that failure was intensified by the slippage of the bars through the joint. The cracking pattern for specimen ID, with deformed reinforcing bars, was more distributed along the adjacent beams and columns.

Adibi et al. [82]

Adibi et al. studied the experimental behavior under cyclic load of one interior joint, specimen SC2, reinforced with smooth bars, and focused the attention on longitudinal bar slippage as the main failure mode. Moreover, they introduced a systematic procedure to predict the dominant failure mode of the joint, based on the dimensional properties, reinforcement details, and axial and shear load of the joint. From the experimental results,

the interior joint sub-assemblage SC2 with 7% constant axial load ratio, developed no diagonal cracks in the joint panel zone. At very small drift ratio (0.2%), vertical cracks occurred both at the left beam-joint interface and at a distance of 11 cm from the right beam-joint interface. Afterwards, at 1.35% drift ratio, several flexural cracks appeared on the beam. At the end of the test, corresponding to 2.7% drift ratio, some minor flexural cracks opened at the upper column-joint interface, but no serious damage occurred, as shown in Fig. 36, though the beams were stronger than the columns. The final damage pattern led the authors to state that the interior joint behavior was controlled by rocking, with beam bar slippage. Hence, the authors observed that specimen SC2 developed 81% of its full nominal flexural capacity, with a gradual strength deterioration and an increasing displacement in the cyclic response due to the presence of smooth reinforcing bars.

Fig. 36. Final cracking pattern of specimen SC2 at 2,7% drift ratio [82].

4.1.3. Discussion on interior joint behavior

On the basis of the previous collection of test results on interior beam-column joints reinforced with smooth bars, the following conclusions can be drawn.

First of all, joints with smooth bars subjected to cyclic loads generally do not exhibit shear failure, as do joints reinforced with deformed bars, but rather bond degradation and slippage of the longitudinal bars of beams and/or columns [74], [77], [80], [82]. Interior

joints reinforced with smooth bars exhibit conventional joint shear failure only when high axial load, in the range of 16%-27% of the section capacity, acts on the columns [80], [81]. This because high column axial loads improve bond strength between concrete and beam longitudinal bars in the joint core. This allows the transfer of greater forces from the bars, even though they are smooth, to the joint, leading to the development of joint shear cracking.

Bond degradation heavily affects the structural behavior resulting in lower structural stiffness and lower strength of the frame structure [75]. If this degradation affects the column bars, it produces flexural strength reduction, particularly in columns with small cross sections. This condition promotes the development of plastic hinges in the columns rather than in the beams, and leads to unexpected soft-storey failure [77].

Even by applying variable axial load on the columns, in order to simulate the real actions that occur in the presence of an earthquake, the slippage of the column smooth bars produces flexural failure at the joint interface, which leads to development of soft-storey failure in the structure [72]. Furthermore, the prediction of this failure is made inaccurate by the use of the plane section theory assumption for the sections reinforced with smooth bars, which leads to overestimation of the theoretical flexural strength of the columns at the plastic hinge region [74].

If bond degradation affects the beam bars, flexural cracks concentrated at the beam-column interface appear, while cracking of the joint core is negligible [80], [82]. In the presence of low axial loads on the columns, on the order of 7-9% of the section capacity, flexural cracks may contemporarily occur at the column-joint interface [80], [82].

The h_c/d_b ratio is a crucial parameter for predicting whether or not bond degradation will occur in the joint, because the degradation is all the more probable for large diameter bars and shorter column depths [73]. This is because large diameters and small column depths cause higher bond stress concentrations.

4.1.4. Influence on the cyclic response

To interpret the behavior of the collected specimens at varying of the column axial load, the shear stress τ acting in the joint core at failure is derived from the following equation and discussed

$$\tau = \frac{V_{jh,test}}{b_j h_c} \tag{99}$$

where $V_{jh,test}$ is the experimental shear strength value, h_c is the column depth and b_j is the effective joint width calculated as follows

$$b_j = \begin{cases} \min(b_c, b + 0.5h_c) & \text{for } b < b_c \\ \min(b, b_c + 0.5h_c) & \text{for } b \geq b_c \end{cases} \tag{100}$$

with b the beam width and b_c the column width.

Table 8 reports all the collected interior joints mechanical and geometrical properties, Table 9 reports the column axial load N, the shear force at failure $V_{jh,test}$, the τ values calculate by means of Eq. (6) and the failure mode (column (6)).

Table 8. Geometrical and mechanical properties of the collected interior beam-column joints

Author ref.	Specimen labels	b_b [mm]	h_b [mm]	b_c [mm]	h_c [mm]	b_j [mm]	A_{sb1} [mm²]	A_{sb2} [mm²]	A_{sh} [mm²]	f'_c [MPa]
[74]	Unit 1	300	500	460	300	450	1809	904	0	43.8
	Unit 2	300	500	460	300	450	1809	904	0	48.9
[72]	C2	200	330	200	200	200	327	214	0	23.9
[75]	JPA-1	300	400	300	300	300	226	452	0	27.8
	JPA-2	300	400	300	300	300	226	452	0	27.8
	JPA-3	300	400	300	300	300	226	452	0	27.8
	JPB	300	400	300	300	300	226	452	0	27.8
	JPC	300	400	300	300	300	226	452	0	27.8
[81]	IPA-1	300	500	300	300	300	452	452	0	21.5
	IPA-2	300	500	300	300	300	452	452	0	30.9
	IPB	300	500	300	300	300	452	452	0	24.5
	IPD	300	500	300	300	300	452	452	0	18.5
	IPE	300	500	300	300	300	452	226	0	21.2

Table 9. Forces and stresses acting in the collected interior beam-column joints and failure modes, where B = bond failure, CF = column flexural failure, JS = joint shear failure.

		(1)	(2)	(3)	(4)	(5)	(6)	(7)	(8)
Author ref.	Specimen labels	N	$V_{jh,test}$	τ	$\dfrac{\tau}{\sqrt{f'_c}}$	$\dfrac{N}{f'_c A_g}$	Failure mode	V_n	$\dfrac{V_{jh,test}}{V_n}$
		[kN]	[kN]	[MPa]				[kN]	[kN]
[74]	Unit 1	0	504	3.73	0.564	0.000	B	-	
	Unit 2	810	473	3.50	0.501	0.120	B	-	
[72]	C2	120	119	2.98	0.609	0.126	CF	-	
[75]	JPA-1	200	253	2.81	0.533	0.080	B	-	

86

	JPA-2	200	259	2.88	0.547	0.080	B	-	
	JPA-3	450	286	3.18	0.602	0.180	JS	369	0.78
	JPB	450	272	3.03	0.574	0.180	B	-	
	JPC	450	268	2.98	0.565	0.180	B	-	-
[81]	IPA-1	450	313	3.47	0.749	0.233	JS	261	1.20
	IPA-2	450	305	3.39	0.609	0.162	JS	334	0.91
	IPB	450	312	3.47	0.700	0.204	JS	286	1.09
	IPD	450	312	3.46	0.805	0.270	CF	-	
	IPE	450	221	2.45	0.532	0.236	JS	258	0.85
								AVG	0.966
								COV	0.180

In Fig. 37 the joint stress ratio $\tau/\sqrt{f_c'}$ (Table 9, column (4)) is plotted versus the axial load ratio $N/f_c'A_g$ (Table 9, column (5)), where f_c' is the concrete cylinder compressive strength and A_g is the column section gross area. The diagram also shows the joint failure modes, through the use of different symbols and reports a linear interpolation of the data.
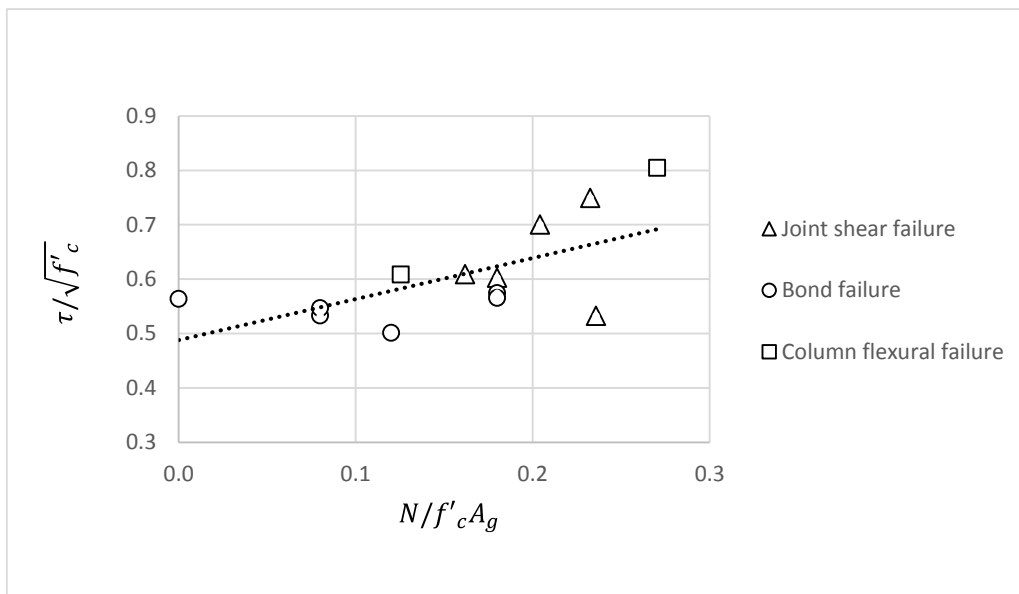
Fig. 37. $\tau/\sqrt{f_c'}$ versus $N/f_c'A_g$ ratios for interior joints with smooth bars.

On the basis of Fig. 37, it can be observed that, generally, an increase in the axial load ratio involves an increase in the joint stress ratio at failure. By considering the failure modes, it is observed that specimens exhibiting bond failure develop lower strength, as expected. For these test units, the increase in joint shear strength with the increase of axial load ratio is minimum. Whereas, specimens that exhibit joint shear failure and column flexural failure reach higher strengths. In these cases, an increase in the axial load ratio

results in an apparent increase in the joint shear strength. Hence, it can be said that the axial load is favorable to the joint strength.

4.1.5. Joint shear strength

To study the applicability of existing formulations for shear strength of joints with deformed bars to joints with smooth bars, the shear strength of the specimens, which exhibit shear failure, is calculated with Eq. (78).

In Eq. (78) joint shear strength is obtained by adding the contributions of three inclined concrete struts (first two terms of the equation) to the contributions of the truss mechanism of joint horizontal reinforcement and column intermediate bars (third and fourth terms, respectively). Regarding the three strut contributions, the second term of the equation represents the contribution due to the main concrete strut, which connects the beam and column compression regions. The first term of the equation represents the contributions due to two side struts, which arise thanks to the bond present in the beam bars outside the main concrete strut.

By considering the specimens reinforced with smooth bars, collected in section 4.1.2 and whose properties are reported in Table 8 and Table 9, it is expected that the bond forces transmitted from the bars to the concrete outside the compression region of the column are very low. As a consequence, the shear strength contributions due to the two side struts and the truss mechanism can be considered negligible. Hence, it is reasonable to consider only the main concrete strut contribute to joint shear strength, and the shear strength expression (Eq. (78)) reduces to

$$V_\mathrm{n} = 0.80\chi\, f_\mathrm{c}'a_\mathrm{c}b_\mathrm{j}\cos\theta_\mathrm{h} \tag{101}$$

where χ is equal to

$$\chi = 0.74 \cdot \left(\frac{f_c'}{105}\right)^3 - 1.28 \cdot \left(\frac{f_c'}{105}\right)^2 + 0.22 \cdot \left(\frac{f_c'}{105}\right) + 0.87, \tag{102}$$

b_j is the width of the diagonal strut, which in this case is the minimum value between the beam width, and the column width; a_c is the depth of the diagonal strut, whose value is approximated by

$$a_c = \left(0.25 + 0.85 \frac{N}{A_g f_c'}\right) h_c; \tag{103}$$

ϑ_h is the angle of inclination of the diagonal strut, defined as follows:

$$\theta_h = \tan^{-1}\left(\frac{h_b}{h_c'}\right) \tag{104}$$

with

$$h_c' = h_c \left(1 - 0.85 \frac{N}{A_g f_c'}\right) \tag{105}$$

By considering the ratios between the experimental shear strength values and the nominal shear strength calculated through Eq. (101), $V_{jh,test}/V_n$ (Table 9, column (8)) for specimens exhibiting joint shear failure, the average (AVG) of these ratios is equal to 0.97 and the coefficient of variation (COV) is 0.18.

On the basis of these values it can be said that, for the collected specimens, Eq. (101) is accurate (AVG close to 1) and consistent (COV close to 0) in the prediction of shear strength of interior beam-column joints with smooth bars.

4.2. Exterior joints

4.2.1. Shear failure mechanism

Differently from interior joints, the anchorage of longitudinal beam bars entering exterior joints is made by bending the bars' ends inside the joint core. When subjected to seismic actions, the forces of the members converging in the joint are transferred to the joint by a diagonal compression strut and a truss mechanism [27]. Modern seismic design recommends bending the beam longitudinal bars inside the joint core, because the bend permits the transfer of the tensile bar forces to the concrete compression strut [83]. RC buildings built before the mid-1970s presented anchorage details in exterior beam-column joints different from those provided by the modern seismic codes. Typically, beam bars' ends could be bent inside or outside the joint core with 90-degree hooks, or bent inside

the joint core with 180-degree hooks [72] and, in some cases, with straight bars and no hooks [70], [83]. Furthermore, older existing RC structures present substandard reinforcing details, like smooth bars and no horizontal hoops in the joint, which could lead to inadequate seismic response and different damage mechanisms, depending on the different anchorage solutions used for the beam bars (Fig. 38).

A number authors considered this issue and investigated the seismic behavior of exterior joints with different anchorage solutions and evaluated the influence of substandard reinforcing details.
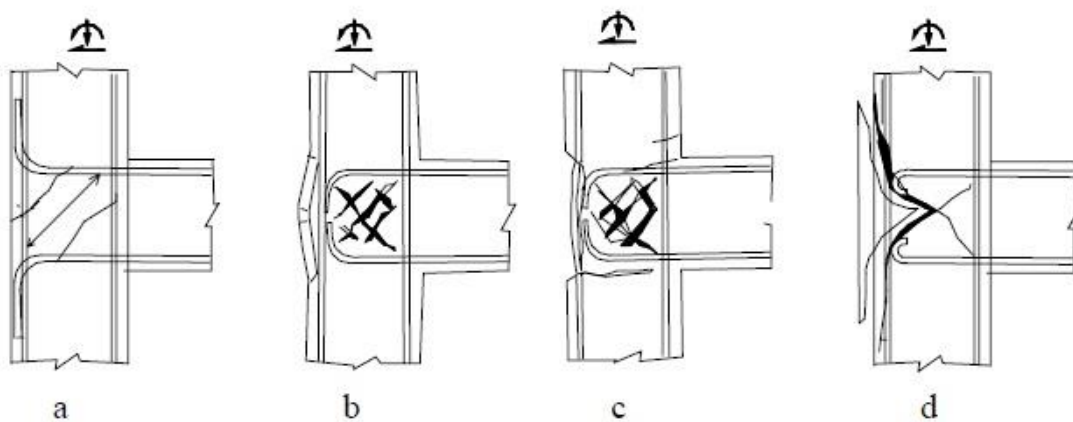
Fig. 38. Alternative damage mechanisms in exterior joints with: (a) beam bars bent out of the joint core; (b)-(c)beam bars bent into the joint core; (d) beam bars with 180-degree hook [72].

4.2.2. Experimental investigations available in the literature

The main experimental results collected in the literature on exterior beam-column joint reinforced with smooth bars are reported in the following.

Pampanin et al. [72]

Pampanin et al. investigated the seismic behavior of beam-column joints in RC buildings designed for gravity loads only. The authors reproduced with their specimens the typical structural deficiencies of Italian RC buildings constructed from the the 1950s through the 1970s and study the damage mechanisms of the joints in the absence of the capacity design principles. In particular, they tested one exterior beam-column joint, specimen T1, reinforced with smooth bars, no horizontal reinforcement in the joint core, and longitudinal beam bars with end hooks. Specimen T1 showed joint shear damage with

diagonal cracking, combined with slippage of beam longitudinal bars and high compressive force at hook ends, with a resulting concrete "wedge" mechanism (Fig. 39). The development of this hybrid failure mechanism, after initial joint diagonal cracking, led to an inefficient strut mechanism and the expulsion of the concrete "wedge" with sudden shear strength degradation at early stages. Hence, the lack of capacity design recommendations combined with the use of smooth reinforcing bars with hook ends revealed to be the source of brittle failure mechanisms, which inhibit additional sources of strength after the initial joint diagonal shear cracking.
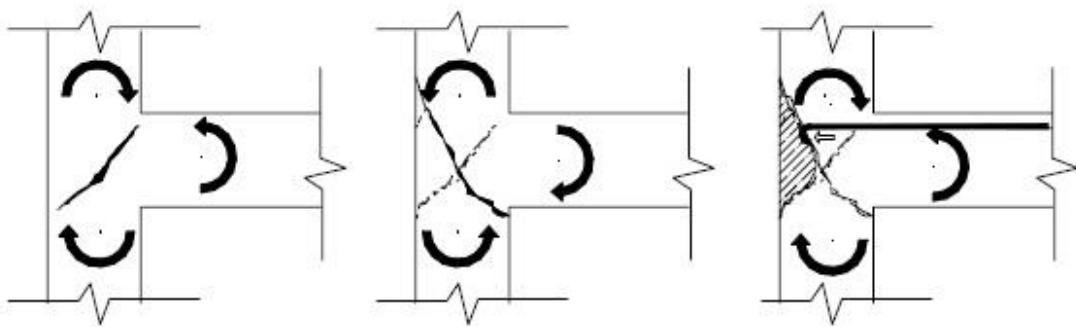
Fig. 39. Concrete "wedge" mechanism with hook-end beam bars [72].

Liu and Park [84]

Liu and Park [84] studied the seismic behavior of four exterior beam-column joints reinforced with smooth round bars, focusing their attention on the effects of different beam bars anchorage solutions and the influence of column axial load. Their specimens represented joints in existing RC frames designed before seismic codes, with inadequate amounts of joint shear reinforcement and beam and column stirrups.

The authors firstly observed the effects of two different anchorage solutions and the shear resisting mechanisms developed in specimens designed with them. For specimens EJ2 and EJ4, which had the beam bar anchorage bent into the joint core (Fig. 40) with the proper length according to New Zealand code [20], the authors reported that the contributions to joint shear strength are the diagonal compression strut and the truss mechanism, as postulated in [20].

Moreover, the authors demonstrated that, at the bend of the beam tensile bars, the strut mechanism exerts diagonal compressive forces in the concrete. These forces result in tension action at the beam bar anchorage, which tends to straighten, with consequent

spalling off of the column concrete cover (Fig. 40). Furthermore, bond degradation and slippage of smooth bars can further worsen this situation by increasing the tension action at the bend with premature concrete tension cracking failure along the beam bar anchorage. The authors stressed that only adequate joint horizontal shear reinforcement could prevent the opening of beam bar bends and effectively actuate the concrete strut mechanism, as in the case of exterior joints detailed with modern seismic codes' provisions.
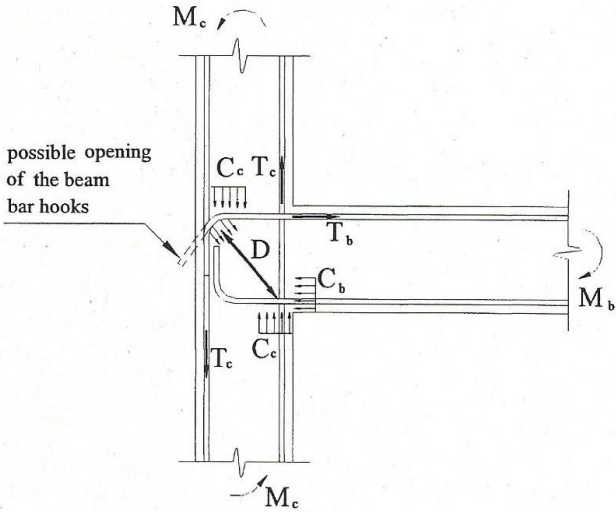
Fig. 40. Joint shear mechanism with beam bar anchorage bent into the joint core – specimens EJ2 and EJ4 [84].

For Units EJ1 and EJ3 with the beam bar anchorages bent out of the joint core (Fig. 41), like in typical RC structures in New Zealand built before the 1970s, which did not satisfy the modern code's [20] requirements, the authors observed an alternative joint shear resisting mechanism. In this case, the tensile force of the beam bars transferred within the bend could lead to concrete tension cracking in the columns, with consequent column bar buckling and beam bar bend opening (Fig. 41(a)). Furthermore, the use of smooth reinforcing bars caused bond degradation and bar slippage which enhance the tensile force at the bend, increasing the possibility of premature failure associated with the interaction of beam bar bends opening and column bar buckling.

The authors observed that the presence of extensive transverse reinforcement in the column region near the joint could prevent the premature concrete tension cracking failure and develop two inclined concrete compression struts, D and D1 in the joint core and in the column, respectively (Fig. 41 (b)), which contribute to the joint shear strength

mechanisms. On the basis of this observation, the authors stressed that only in this case would the seismic behavior of the whole frame be independent of joint shear reinforcement amount.

(a)   (b)
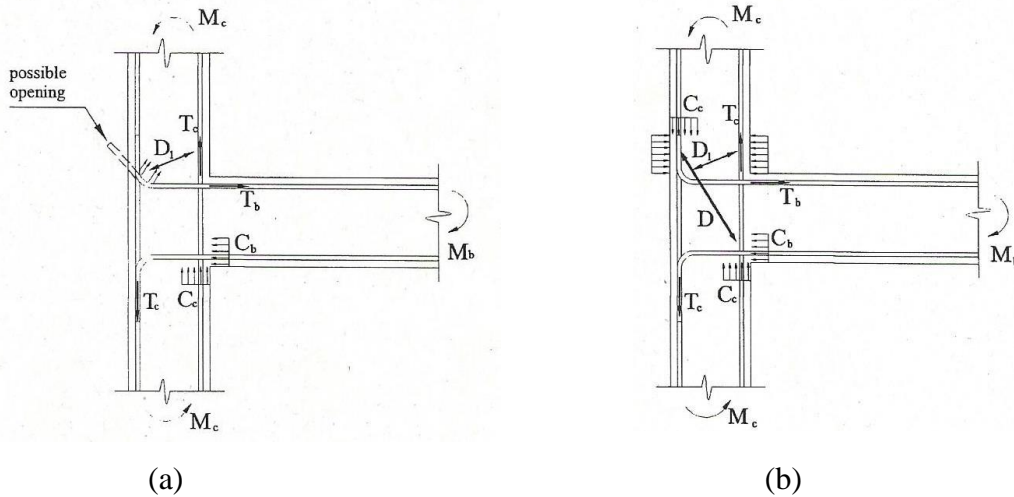
Fig. 41. Joint shear mechanism with beam bar anchorages bent out of the joint core
− specimens EJ1 and EJ3: (a) possible opening mechanism of beam bar bends;
(b) alternative joint force path in the presence of extensive column transverse
reinforcement [84].

By considering the effects of column axial load on joint behavior, test results on exterior joints with zero axial load, applied to Units EJ1 and EJ2, revealed that different beam bar anchorages significantly influenced the strength performance. Indeed, Units EJ1 and EJ2 reached 55% and 75% of theoretical shear strengths, respectively.

On the other hand, when a column axial load of $0.25 f_c' A_g$, was applied to specimens EJ3 and EJ4 , there was little difference between the performances of the joints with the two different anchorage details. As a matter of fact, the presence of the compressive load prevented premature tension cracking caused by the beam bar bends opening, and the attained joint shear strengths were about 85% and 95% of the theoretical values for specimen EJ3 and EJ4, respectively.

Besides greater strength, Unit EJ3 and EJ4 evinced greater stiffness, compared to that of specimens EJ1 and EJ2.

By comparing the experimental behavior of Unit EJ2 to that of Unit O6 tested by Hakuto et al. [75], identical to Unit EJ2 but reinforced with deformed bars, the authors assessed

that the use of smooth reinforcing bars increased premature concrete tension cracking failure along the beam bar anchorage. In particular, the flexibility of Unit EJ2 was twice that of Unit O6, and the joint shear strength was reduced by about 25%.

The authors observed that the assumption of plane sections is greatly violated, due to severe bond degradation for joints reinforced with smooth bars under seismic loads, and that conventional flexural theory overestimates the member flexural strength. Test results evince that the specimens were dominated by degrading flexural behavior of beams and columns due to bond failure of longitudinal reinforcement, rather than joint shear failure for all units.

Braga et al. [77]

As well as the study on interior joints, Braga et al. [77], investigated the experimental behavior of an exterior joint, labelled T23-1, designed for gravity only and subjected to cyclic lateral loads. Specimen T23-1 was built with low strength concrete, smooth reinforcing bars with 180-degree hooks and no shear reinforcement in the joint core, similarly to specimen T1 (Fig. 38(d)) investigated by Pampanin [72], except for the presence of inclined shear bars in the beam. During the test, the evolution of cracking patterns of specimen T23-1 (Fig. 42) exhibited two failure mechanisms: firstly flexural cracking in the beam, and afterwards shear cracking within the joint core, which acted as a structural fuse with respect to the other mechanisms, as it is more brittle.
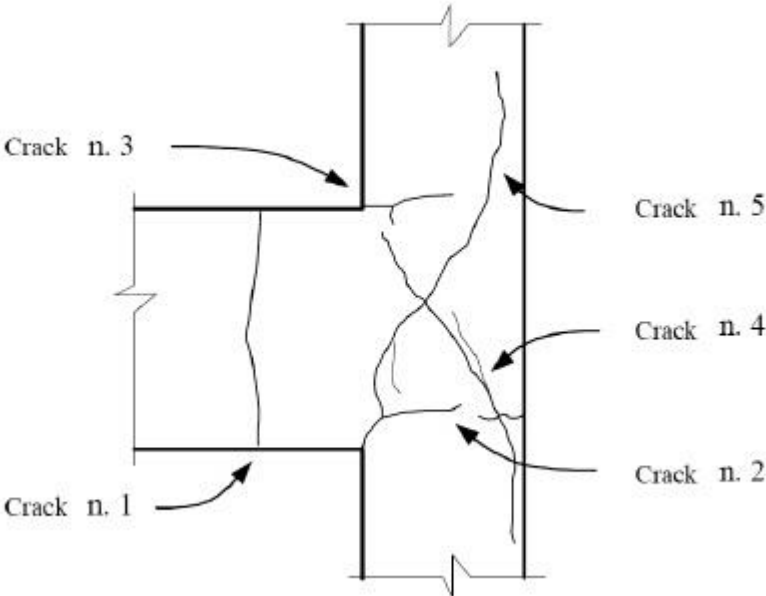
Fig. 42. Cracking pattern evolution of specimen T23-1 [77].

The opening of diagonal cracks, due to the overcoming of concrete tensile strength, and the reversal of the applied loads made the cracking spread in the columns.

Braga et al. observed that the inflection of the external column bars passing through the joint core, without any joint transverse reinforcement, caused the ejection of the concrete block on the right side of the two longer cracks in Fig. 42. The beam bar hooks did not show any slippage and remained in the internal concrete section, differently from specimen T1 of Pampanin (Fig. 39). Moreover, the authors considered that, compared to seismic behavior of joints with deformed bars, the bond deterioration with slippage of the smooth bars in exterior beam-column joints enhances the stability of the frame during the cycles, as the low bond between steel and concrete does not increase the joint panel damage.

Melo et al. [86]

Melo et al. carried out an experimental investigation on cyclic response of RC beam-column joints reinforced with smooth bars and investigated the effects of poor detailing in existing pre-70s buildings. In particular, they analyzed the cyclic behavior of five exterior joints reinforced with smooth bars, specimens TPA-1, TPA-2, TPB-1, TPB-2, and TPC, and one test unit reinforced with deformed bars, specimen TD. All the specimens had the same geometrical characteristics, without joint reinforcement, and specimens TPA-1 and TPA-2 were the control test units (Fig. 43).
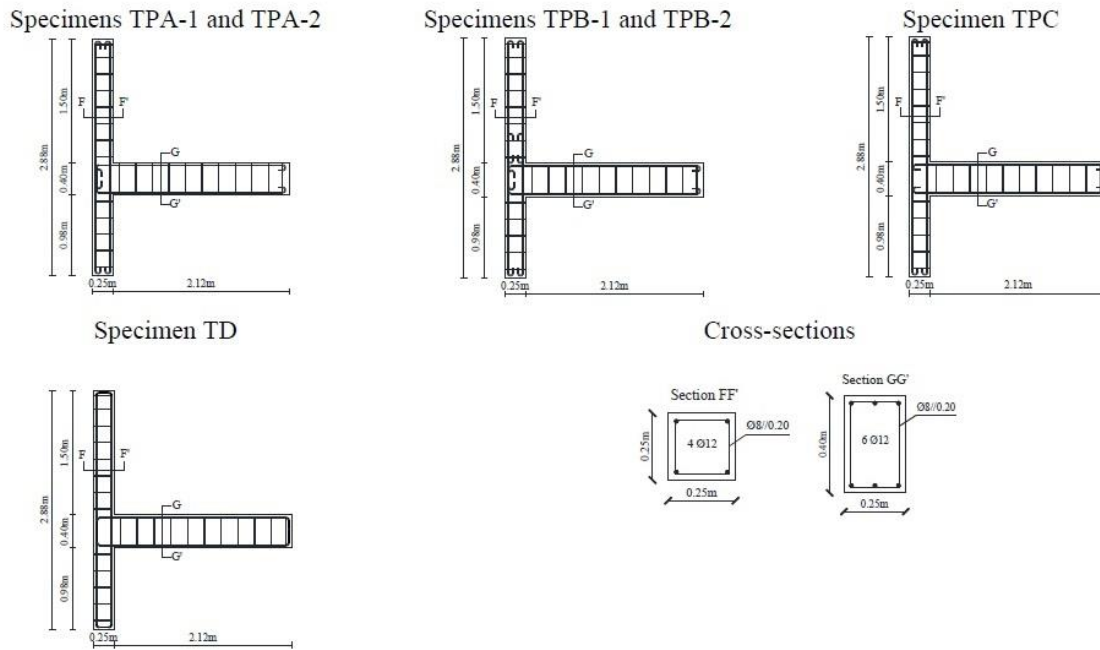
Fig. 43. Geometric characteristics and reinforcing detailing of exterior joint test units in [86].

Differently from the control units, specimens TPB-1 and TPB-2 had lap-splicing in the column, while specimen TPC had beam longitudinal bars bent in the joint with 180-degree hooks. Specimen TD was identical to TPA, but reinforced with deformed bars. Furthermore, to compare the different behavior of the units under monotonic and cyclic load, specimens TPA-1 and TPB-1 were tested under monotonic loading.

The test results revealed that the bond properties of reinforcement influenced the experimental behavior of the joints, as the specimens built with smooth bars evinced lower energy dissipation, stiffness and equivalent damping than the specimen with deformed bars, where the equivalent damping is calculated by considering the area enclosed by a hysteresis loop. Regarding lap-splicing, specimens TPB, having the splicing in the column, dissipated greater energy than did the control specimens, with damage concentrated at the column-joint interface (Fig. 45), without displaying cracking in the joint core, while all the other specimens showed diagonal shear cracking in the joint core. The force-displacement envelope curves of cycling tests on specimens TPA-2 and TPB-2 were similar to the monotonic curves of TPA-1 and TPB-1, respectively (Fig. 44) until the ultimate strength was reached.
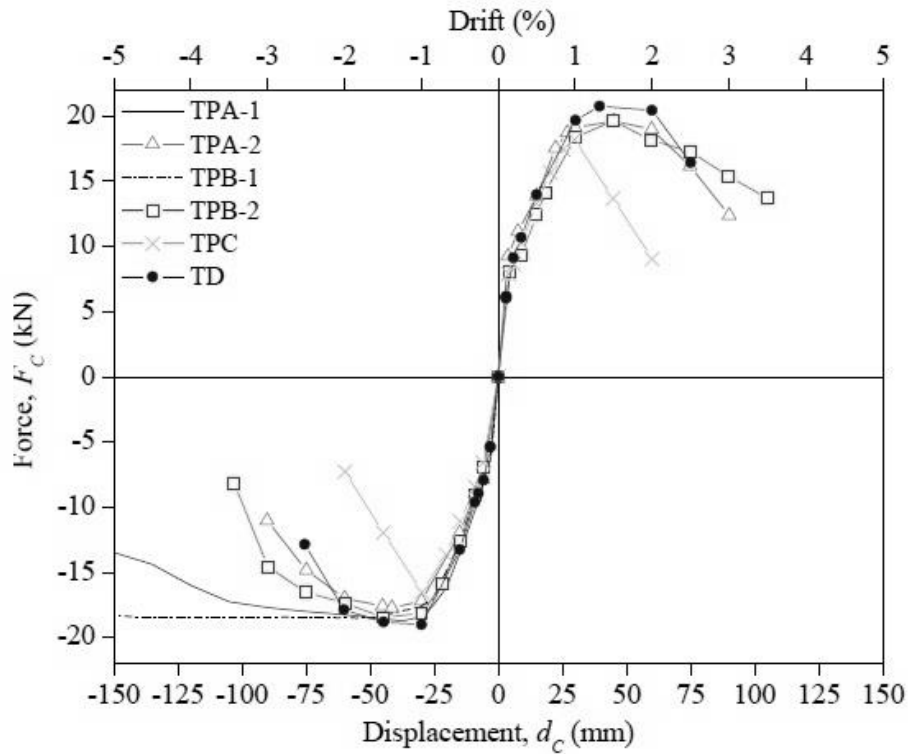
Fig. 44. Force-displacement envelope curves of exterior joints experimental results in [86].

Specimen TPC with 180-degree hooks displayed evident shear diagonal cracks, with a marked expulsion of the concrete from the joint core, while the control specimens exhibited spread damage in the joint core and concrete spalling on the exterior face of the joint (Fig. 45). As regards specimen TD, reinforced with deformed bars, it revealed severe diagonal cracking in the joint core, similarly to specimens TPA, and a strong expulsion of concrete at the joint's exterior face. Otherwise, specimen TD developed a larger number of flexural cracks along the beam compared to the specimens reinforced with smooth bars.
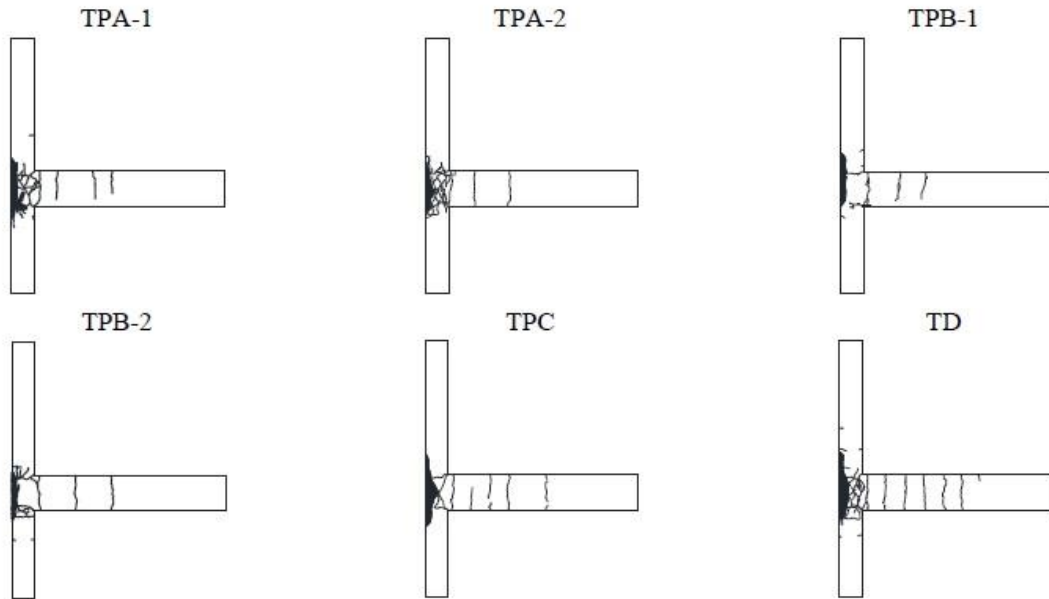
Fig. 45. Damage patterns of the specimens at the end of the test [86].

Moreover, the authors evaluated the cyclic behavior of interior joints with smooth round bars, presented previously [81], and they observed that in exterior joints the influence of bond properties was more significant, and that exterior joints evinced lower displacement ductility and larger equivalent dumping than interior joints.

Bedirhanoglu et al. [85]

Bedirhanoglu et al. also investigated the seismic behavior of exterior beam-column joints with smooth bars and low-strength concrete, to represent the joints of existing deficient RC buildings. They conducted tests series on exterior joints with 90-degree anchorages of the beam bars inside the joint core. Some of the specimens had the bent anchorages of top beam bars welded to the bent anchorages of bottom beam bars (Fig. 46), to investigate a potential rehabilitation technique. Furthermore, they varied several parameters of test units including the presence of column axial load and the amount of joint horizontal reinforcement.
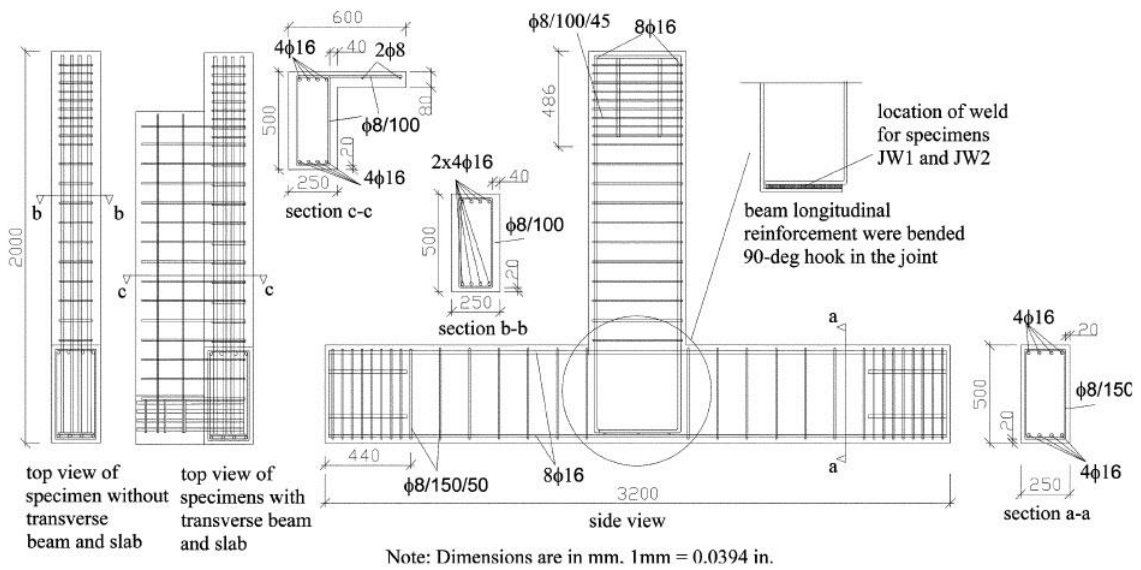
Fig. 46. Geometric and reinforcing details of the test units in [85].

The main observations on test results revealed that, under static load reversals, the capacity of specimens with 90-degree anchorages was limited by bond slip of beam reinforcement. Indeed the mean strength of specimens with welded bars was 35% higher than the mean strength of specimens with bent bars. Nevertheless, in all tested specimens, the beams and the columns did not reach their nominal strengths, and no specimen exhibited bond failure. All the specimens exhibited diagonal shear cracking in the joint core and the authors observed that, above 4% drift ratio, the joints with welded bars were more severely damaged than the others, due to the increase in shear forces induced by improved anchorage conditions. Regarding specimens with joint horizontal hoops, they exhibited thinner diagonal cracks in the joint core, improved load-carrying capacity, larger strains in beam bars, and better energy dissipation capacity. Moreover, by comparing the hysteresis curves of joint specimens subjected to column axial load to those of specimens with no axial load, the authors noticed a significant increase in the dissipated energy for the specimens with higher axial load.

Russo and Pauletta [70]

Russo and Pauletta carried out an experimental study on the seismic behavior of six RC exterior beam-column joints detailed accordingly with what was the construction practice of buildings in the 50s and 60s in Italy, i.e. with use of smooth bars, inadequate bar anchorages and no shear reinforcement in the joint core. Specifically, they tested four 2:3 scale units with beam bar anchorage length almost equal to the joint width (Fig. 47),

varying the amount of beam longitudinal and transverse reinforcement, and one full-scale specimen with beam bars ending with 180-degree hooks (Fig. 48).
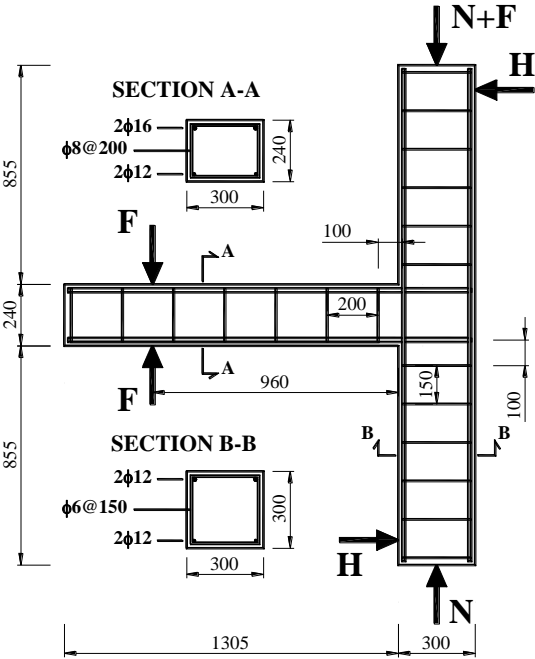
Fig. 47. Geometry and reinforcing details of a specimen with straight beam bars [70].
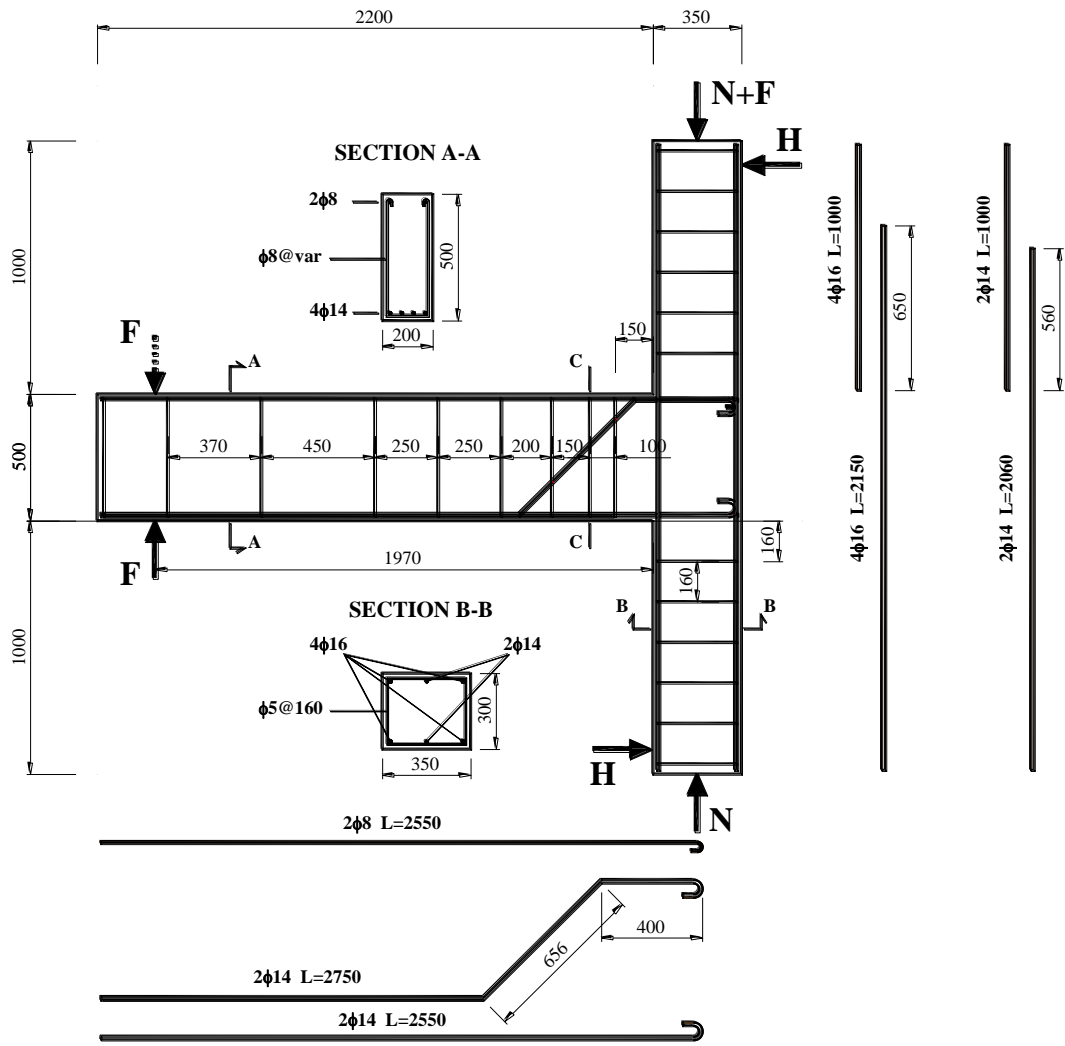
Fig. 48. Geometry and reinforcing details of a specimen with 180-degree hooks [70].

The test results revealed that, for the specimens with straight beam bar anchorages, bond failure occurred with corresponding severe strength and stiffness degradation, while in the joint with hooked beam bars anchorages, flexural failure of the beam occurred, and no slippage of the beam bars was observed. In all specimens, the forces applied to the beam were not high enough to generate joint shear failure, and no specimens exhibited joint diagonal cracking at the end of the test, despite the absence of joint transverse reinforcement. Shear failure did not occur even in the case of beam bars anchored with 180-degree hooks, due to the low amount of longitudinal reinforcement present in the beam.

De Risi and Verderame [87]

De Risi and Verderame carried out an experimental study on seismic performance of existing RC buildings with poor structural details, by testing four exterior beam-column joints with no horizontal hoops in the joint core and smooth bars as beams and columns longitudinal reinforcement. All four specimens had beam longitudinal reinforcement bent in the joint core with 180-degree hooks but differed in joint aspect ratio (h_b/h_c) and beam longitudinal reinforcement amount (Fig. 49), in order to evaluate the influence of these parameters on joint shear strength and deformability.
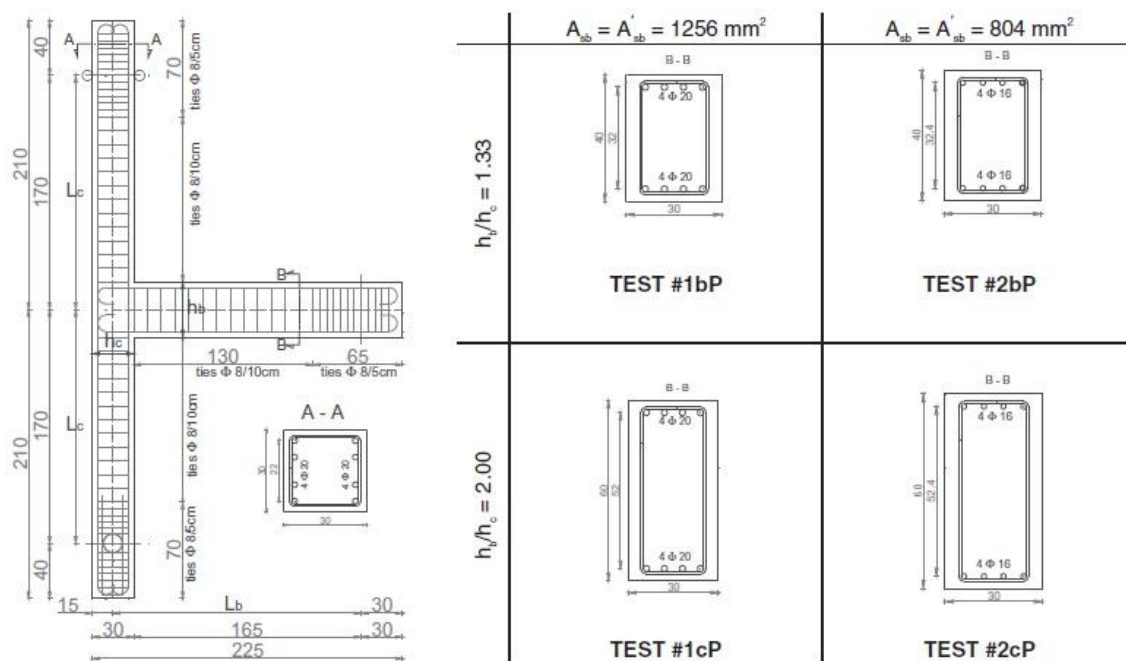
Fig. 49. Geometry (dimensions in cm) and reinforcing details of specimens in [87].

The test results showed that all the specimens experienced joint shear failure, with relevant concrete spalling at the exterior face of the joint. Similar to Pampanin [72], De Risi and Verderame associated the column cover spalling at the joint with the action of the beam hook anchorages. By considering the test units lateral load-drift responses, the authors observed that specimens with higher joint aspect ratio dissipated more energy than the others. As regards the deformability, the authors highlighted that, at ultimate load, higher joint aspect ratio reflected larger joint shear strain. Furthermore, the authors concluded that a greater amount of beam longitudinal reinforcement corresponds to higher joint shear strength, while higher joint aspect ratio corresponds to lower joint shear strength.

Cosgun et al. [88]

Cosgun et al. investigated the experimental behavior of exterior beam-column joints with smooth bars, low strength concrete and different anchorage details. In particular, they studied the effects of three different longitudinal beam bar anchorages in the joint core without joint horizontal reinforcement, namely Unit J2 (Fig. 50(a)) with 90-degree bent anchorages, Unit J3 (Fig. 50(b)) with 180-degree hooks, and Unit J4 (Fig. 51(a)) with straight bars. The reinforcement details of the reference specimen J1-REF (Fig. 51(b)) were designed according to the codes to avoid shear failure, expecting beam flexural failure at the cross-section. However, Unit J1-REF was built with smooth bars and low-strength concrete, too.

(a)   (b)
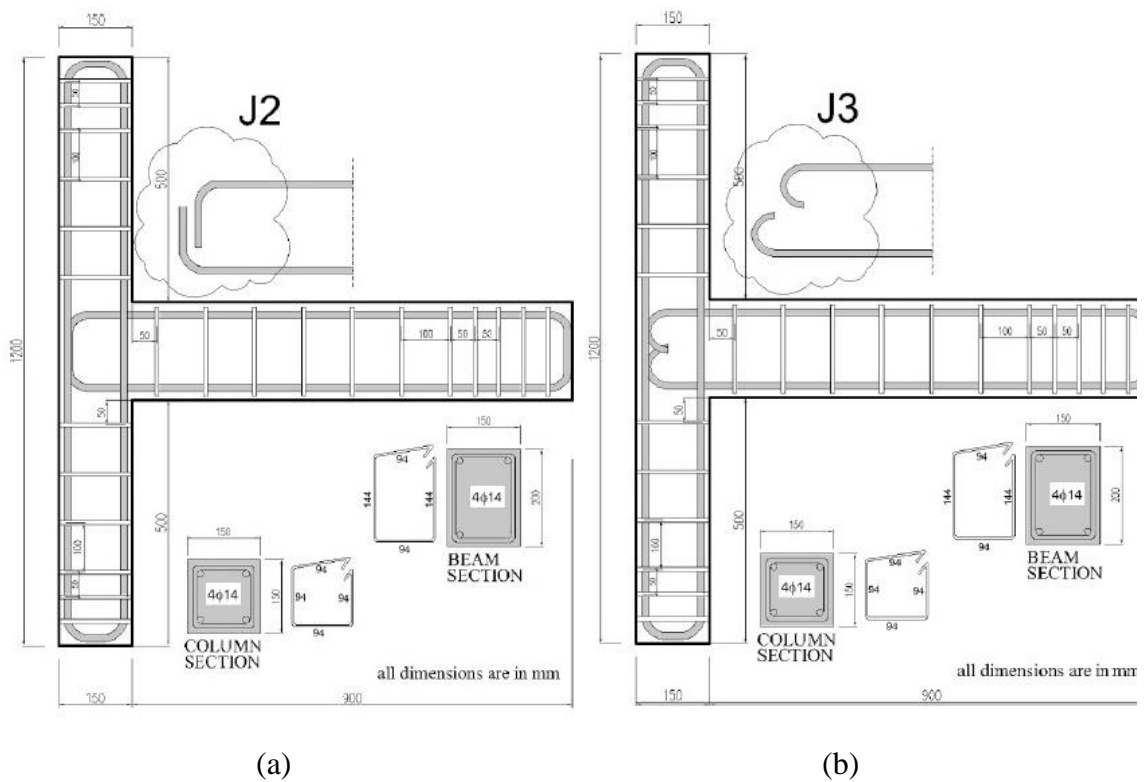
Fig. 50. Geometric characteristics and reinforcing details of spcecimens in [88]: (a) specimen J2; (b) specimen J3.
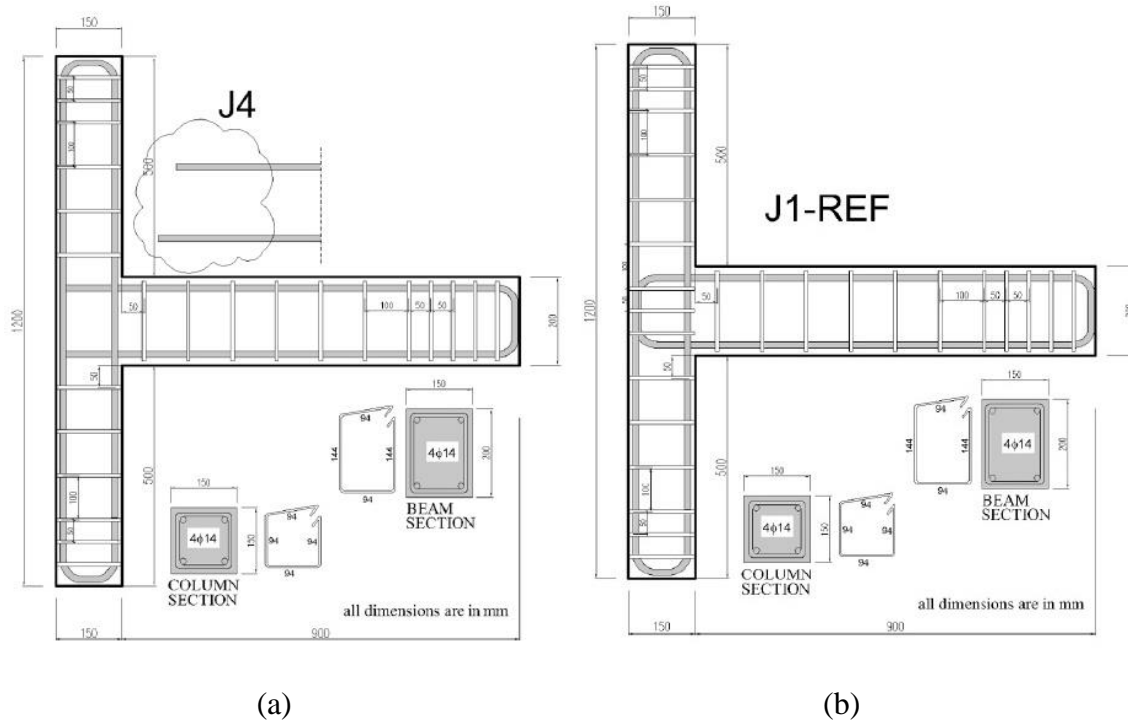
Fig. 51. Geometric characteristics and reinforcing details of spcecimens in [88]: (a) specimen J4; (b) specimen J1-REF.

The experimental results revealed that, except for specimen J1-REF, none of the specimens reached its beam flexural capacity, but failed with a reduction in beam section capacity of 31.8% (J2), 40.3% (J3), and 53.4% (J4). Cyclic behavior of specimens J2 and J3 was governed by the slip of beam longitudinal reinforcement and joint shear cracking, while specimen J4 was dominated only by beam bars slippage. Specimens J2, J3, and J4 reached the ultimate strength at 4% drift, while specimen J1-REF resisted up to 7% drift. Hence, the authors observed that anchorage details have significant influence on the joint seismic response, and that these design conditions of existing RC buildings, combined with the use of low-strength concrete and smooth round bars, can lead to considerable load-carrying capacity reduction, with the slip of beam longitudinal bars resulting in premature failure of the joints.

Adibi et al. [82]

Adibi et al. proposed a nonlinear model to simulate pre-and post-elastic behavior of RC beam-column joints, reinforced with smooth bars, whose failure was governed by bar slippage. In particular, to validate their model, they studied the experimental behavior of two nearly identical exterior joints, with the only difference being column axial ratio, which was 7% for Unit SC1 and 15% for Unit SC1-1. The joint sub-assemblages reflected

the typical deficiencies of non-seismically designed RC existing structures reinforced with smooth round bars, with no hoops in the joint core and inadequate anchorage conditions for longitudinal bars.

The final cracking pattern is shown in Fig. 52, where a deep vertical crack at the beam-joint interface developed in both the sub-assemblages, while the effect of higher axial load on specimen SC1-1 prevented the opening of diagonal shear cracks in the joint core, which did occur in specimen SC1. Nevertheless, the authors observed that bar slippage governed the cyclic behavior of both the test units.

(a)   (b)
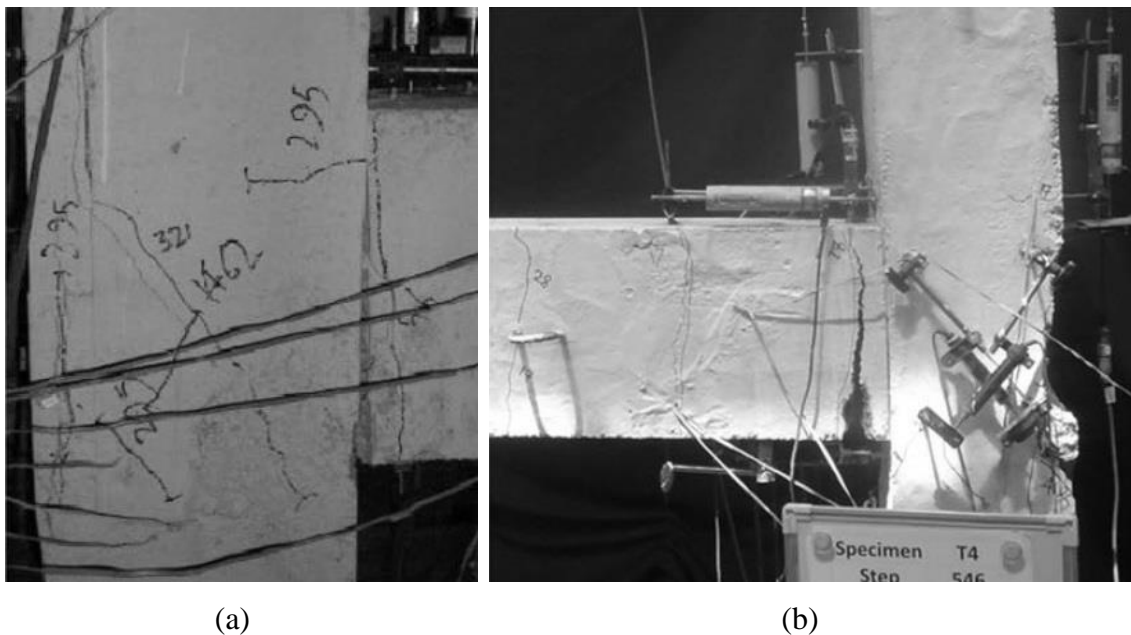
Fig. 52. Final damage pattern of the exterior joints at 2,7% drift ratio: (a) specimen SC1; (b) specimen SC1-1 [82].

By comparing this behavior, specimen SC1, with lower axial load, exhibited significant pinching effect and rapid strength degradation. The authors observed that the pinching effect could be attributed to the bond deterioration of beam bars and shear cracking in the joint core (Fig. 53(a)), while the strength loss could be due to the P-Δ effect. Compared to specimen SC1, Unit SC1-1 reached higher beam flexural capacity, even if not fully developed, as the column vertical load improved the beam bars' bond with concrete in the joint core and, at the same time, prevented the opening of shear diagonal cracks (Fig. 53 (b)).
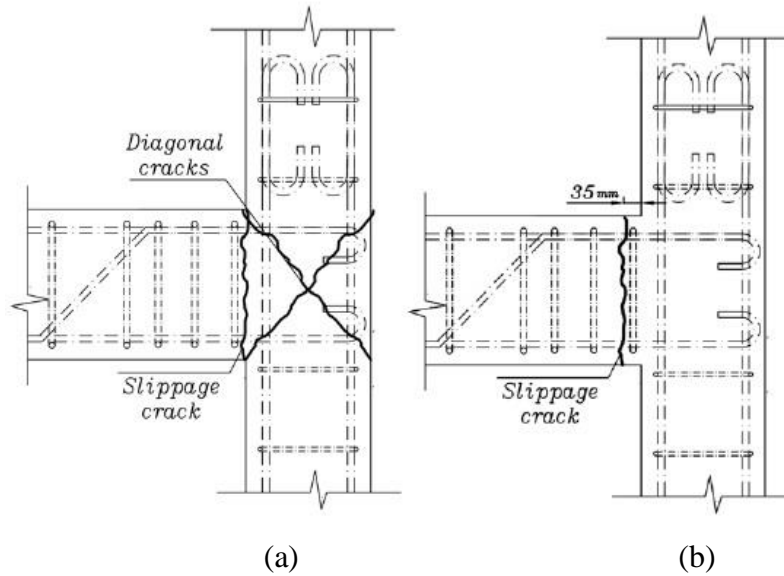
Fig. 53. Main developed cracks at the end of the tests: (a) specimen SC1; (b) specimen SC1-1 [82].

From the comparison of the final damage pattern (Fig. 53) of specimen SC1 with that of interior joint specimen SC2 [82], presented previously herein in section 2, and having the same axial load ratio as specimen SC1, the authors observed that the slippage crack at the beam-joint interface was wider in exterior joint SC1, about 5 mm width, than in interior joint SC2, about 2 mm width. Moreover, they asserted that interior joint damage pattern displayed more distributed cracks than did the exterior joint, and that specimen SC2 presented a gradual strength deterioration, with increasing displacement in cyclic response. Hence, it can be said that interior joint SC2 developed better hysteretic behavior and higher displacement ductility than exterior joint SC1.

4.2.3. Discussion on exterior joint behavior

On the basis of the results of experimental tests on exterior beam-column joints with smooth bars previously reported, the following conclusions can be drawn.

Compared to exterior beam-column joints reinforced with deformed bars, the exterior joints with smooth bars subjected to cyclic loads generally show lower energy dissipation capacity, stiffness and equivalent damping [86].

For joints with pain bars, exterior joints exhibit lower displacement ductility [82], [86] and larger equivalent damping than interior ones [86].

The seismic behavior of the specimens reinforced with smooth round bars is strongly influenced by the different anchorage solutions. A number of experimental campaigns [72], [77], [87], [88] revealed that the anchorage of beam longitudinal reinforcement with

106

180-degree hooks in the joint core does not ensure that bond slippage of smooth round bars is prevented. This anchorage solution contributes to joint damage by increasing shear diagonal cracking, with the formation of a concrete "wedge" and marked concrete spalling on the joint exterior face [72].

In many existing RC buildings, to hinder the slippage of smooth bars, the anchorage of beam bars is developed by 90-degree bents, which could be inside the joint core or, alternatively, outside. In the absence of joint transverse reinforcement, the bend inside the joint core subjected to tensile action tends to straighten and produce concrete spalling on the joint exterior face. Moreover, this anchorage solution could not prevent the beam bar bond deterioration, with consequent bar slippage [85], [88]. The bend outside of the joint also tends to straighten and produces concrete tension cracking in the columns and column bar buckling. However, if column hoops are present, these effects are prevented [84].

In the presence of straight beam bar anchorages, bond failure occurs with a corresponding severe strength and stiffness degradation [70].

In general, the difference between the response of exterior beam-column joints, with different anchorage arrangements, decreases with increasing column axial load [84]. In fact, the compressive load of the column, by enhancing beam bar bond with concrete in the joint core, permits the assemblies to reach higher flexural capacity before beam bar bond loss and, consequently, to develop ductile resisting mechanisms, with higher energy dissipation [85]. Furthermore, the bond forces transmitted from the beam bars to the concrete core increase the joint shear stress but, at the same time, contribute to the diagonal strut resisting mechanism. Since for exterior joints the bond forces on beam bars are transmitted to the concrete core only by one side, the contribution to the resisting mechanism prevails. These are probably the reasons why column axial load could prevent the opening of joint diagonal cracks [82] and soften the joint damage [84].

As regards joint horizontal reinforcement, the collected test results revealed that, in the absence of joint hoops, joint shear failure does not occur [70], [82], [88], but bond deterioration or beam flexural failure occurs. It has to be taken into account that, in the presence of severe bond deterioration, the assumption of plane sections is greatly violated and, as consequence, the conventional flexural theory overestimates the members' flexural strength [84].

Other parameters influencing the mechanical behavior of exterior beam-column joints reinforced with smooth bars are the joint aspect ratio and the beam longitudinal

reinforcement amount. The higher the joint aspect ratio, the greater the energy dissipation capacity, the greater the shear deformation of the joint, and the lower the shear strength. The greater the amount of longitudinal reinforcement of the beam, the greater the shear strength of the joint [87].

4.2.4. Influence on the cyclic response

In order to evaluate the influence of the column axial load on exterior joint behavior, the stress τ acting in the joint core at failure, is calculated from (Eq. (99)), also for exterior joints.

Table 10 and Table 11 report all the collected exterior joints mechanical and geometrical properties, as previously made for interior joints.

Table 10. Geometrical and mechanical properties of the collected exterior beam-column joints.

Author ref.	Specimen labels	b_b	h_b	b_c	h_c	b_j	A_{sb1}	A_{sb2}	A_{sh}	f'_c
		[mm]	[mm]	[mm]	[mm]	[mm]	[mm²]	[mm²]	[mm²]	[MPa]
[72]	T1	200	330	200	200	200	327	327	0	23.9
[84]	EJ1	300	500	460	460	460	1356	904	0	33.7
	EJ2	300	500	460	460	460	1356	904	0	29.2
	EJ3	300	500	460	460	460	1356	904	0	34.0
	EJ4	300	500	460	460	460	1356	904	0	36.5
[77]	T23-1	200	333	200	200	200	440	440	0	14.5
[86]	TPA-1	250	400	250	250	250	339	339	0	24.2
	TPA-2	250	400	250	250	250	339	339	0	25.8
	TPB-1	250	400	250	250	250	339	339	0	15.8
	TPB-2	250	400	250	250	250	339	339	0	27.3
	TPC	250	400	250	250	250	339	339	0	23.8
[85]	JO5	250	500	250	500	250	804	804	0	8.3
[70]	12 6	300	240	300	300	300	226	226	0	22.2
	12 8	300	240	300	300	300	226	226	0	22.2
	16 6	300	240	300	300	300	402	226	0	22.2
	16 8	300	240	300	300	300	402	226	0	22.2
	8 8 A	200	500	300	350	300	408	308	0	20.2
[87]	1bP	300	400	300	300	300	1256	1256	0	14.8
	2bP	300	400	300	300	300	804	804	0	14.8
	1cP	300	600	300	300	300	1256	1256	0	14.8
	2cP	300	600	300	300	300	804	804	0	14.8

Table 11. Forces and stresses acting in the collected exterior beam-column joints and failure modes, where B = bond failure, CF = column flexural failure, BF= beam flexural failure, JS = joint shear failure.

		(1)	(3)	(4)	(5)	(6)	(7)	(8)	(9)
Author ref.	Specimen labels	N	$V_{jh,test}$	τ	$\dfrac{\tau}{\sqrt{f'_c}}$	$\dfrac{N}{f'_c A_g}$	Failure mode	V_n	$\dfrac{V_{jh,test}}{V_n}$
		[kN]	[kN]	[MPa]				[kN]	[kN]
[72]	T1	100	54	1.344	0.275	0.105	JS	-	-
[84]	EJ1	0	209	0.987	0.170	0.000	B	-	-
	EJ2	0	263	1.243	0.230	0.000	B	-	-
	EJ3	1800	333	1.574	0.270	0.250	B	-	-
	EJ4	1800	384	1.812	0.300	0.233	B	-	-
[77]	T23-1	var	46	1.142	0.300	0.000	BF	-	-
[86]	TPA-1	200	119	1.897	0.386	0.132	JS	163	0.73
	TPA-2	200	118	1.884	0.371	0.124	JS	170	0.69
	TPB-1	200	119	1.901	0.478	0.203	CF	-	-
	TPB-2	200	118	1.882	0.360	0.117	CF	-	-
	TPC	200	119	1.906	0.391	0.134	JS	-	-
[85]	JO5	130	141	1.129	0.392	0.125	JS	154	0.92
[70]	12 6	300	46	0.515	0.109	0.150	B	-	-
	12 8	300	56	0.619	0.132	0.150	B	-	-
	16 6	300	117	1.300	0.276	0.150	B	-	-
	16 8	300	65	0.718	0.152	0.150	B	-	-
	8 8 A	300	122	1.161	0.258	0.142	B	-	-
[87]	1bP	133	265	2.942	0.766	0.100	JS	-	-
	2bP	133	239	2.652	0.690	0.100	JS	-	-
	1cP	133	221	2.459	0.640	0.100	JS	-	-
	2cP	133	238	2.646	0.689	0.100	JS	-	-

Fig. 54 shows the joint stress ratio $\tau/\sqrt{f'_c}$ plotted versus the axial load ratio $N/f'_c A_g$, where the different symbols distinguish the different failure modes. Specimen T23-1 [77] is excluded since the axial load varies with the force applied on the test units.
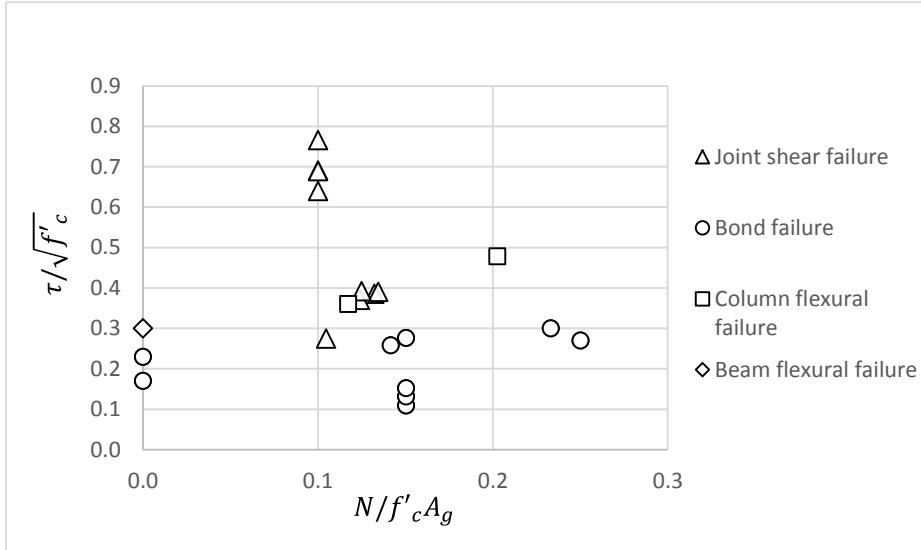
Fig. 54. $\tau/\sqrt{f_c'}$ versus $N/f_c'A_g$ ratios for exterior joints with smooth bars.

Differently from interior joints, no evident correlation is observed between $\tau/\sqrt{f_c'}$ and $N/f_c'A_g$ in Fig. 54. Only in the case of the specimens with bond failure developed, an increase in the axial load ratio involves on average a slight increase in the joint stress ratio at failure. Anyway, it can be observed that specimens which exhibited joint shear failure reach higher shear strength than the others, similarly to interior joints. Finally, it is observed that specimens which exhibited column flexural failure develop $\tau/\sqrt{f_c'}$ values that are on average lower than those obtained with joint shear failure and higher than those developed with bond failure. Hence, also for exterior joints, the lowest strength occurs in presence of bond failure.

4.2.5. Joint shear strength

In order to evaluate the possibility of using existing formulations for shear strength of joints with deformed bars for joints with smooth bars the shear strength of the collected specimens is calculated by means of the formula of Pauletta et al. [28], present in the literature

$$V_n = 0.71 \frac{\chi f_c' a_c b_j \cos \vartheta_h}{\alpha} + 0.56 A_h f_{yh} + 0.37 \frac{A_v f_{yv}}{\tan \vartheta_h} \tag{106}$$

Three shear strength contributions can be individuated in Eq. (106), which is valid in the case of joints with the beam bars bent at 90 degrees inside the joint. The first term

represents the contribution of the main diagonal concrete strut plus the contribution of a concrete side strut, which develops due to the bond present in the beam bars subjected to tension. The second and third terms represent the contributions of the horizontal joint reinforcement and the column intermediate bars, respectively.

Similarly to interior joints, also for exterior joints reinforced with smooth bars it is expected that the bond stresses transmitted by joint reinforcements outside the main concrete strut are low. As a consequence, the contributions developed by the joint reinforcement and column intermediate bars become negligible. Hence, Eq. (106) reduces to

$$V_n = 0.71 \, \frac{\chi f_c' a_c b_j \cos \vartheta_h}{\alpha} \tag{107}$$

where χ is expressed in Eq. (102). The coefficient α is obtained from the following expression

$$\alpha = \frac{2HL}{2HL - (2L + h_c) \cdot j_{db}} \cdot \left(1 - \frac{4k l_h \sqrt{f_c'}}{d_b \cdot f_{bi}}\right) \leq 1 \tag{108}$$

where H is the distance between the upper and lower columns' inflection points; L is the length from section of load application at the beam end to the column face; j_{db} is the beam cross section lever arm; l_h is the length of the column tensile region under combined compressive and bending stresses, calculated as $l_h = h_c - a_c$. Since $k\sqrt{f_c'}$ represents the bond stress average value along l_h, it is assumed that, in case of smooth bars, k is equal to zero at joint failure and the value of α becomes equal to 1, consequentially.

By considering all the collected exterior joints which exhibit joint shear failure, it is observed that the beam bars anchorage arrangements of the 180-degrees hooks and of the 90-degrees bend out of the joint, enact additional stresses which change the resisting mechanisms development. Hence, in these cases Eq. (106) is no longer valid. Accordingly, only 3 specimens, whose properties are reported in Tables 3 and 4, has been considered.

From Table 4 it is observed that the experimental shear strength $V_{jh,test}$ is always lower than the theoretical one V_n evaluated with Eq. (107). As a matter of fact, test results of specimen JO5 [85], revealed that the capacity of the joint is affected by the bond slip of

beam longitudinal reinforcement. Whereas, the anchorage arrangement of specimens TPA-1 and TPA-2 [86], shown in Fig. 43, presents not only 90-degree bent bars, but also 180-degree hooks at the end of the bends, in the joint region, which could interfere with the strut resisting mechanism. On the basis of these results, it can be said that, for the considered specimens, the strut resisting mechanism is not fully developed.

4.3. Conclusions

On the basis of the informations reported and commented previously, it is remarked that, to predict the possible behavior of beam-column joints reinforced with smooth bars under seismic load, the main influencing parameters have to be known as accurately as possible. These are the mechanical characteristics of the materials, the geometry of the joint and the converging elements, the bar anchorage arrangements, and the column axial load.

The principal observations on the behavior of joints with smooth bars subjected to cyclic loads, which can be draw from experimental findings considered in this study, are pointed out in the following.

As regards interior joints with smooth bars:

1. Joints generally do not exhibit shear failure, but rather bond degradation and slippage of the longitudinal bars of beams and/or columns.
2. Bond degradation along the beams bars is all the more probable, the larger the diameter of the bars, or the smaller the depth of the column.
3. If bond degradation affects the beam bars, flexural cracks concentrated at the beam-column interface appear, while cracking of the joint core is negligible, since shear action transferred to the joint is small.
4. If bond degradation affects the column bars, it promotes the development of plastic hinges in the columns, leading to soft-storey failure.
5. The use of the plane section theory assumption leads to overestimation of the theoretical flexural strength of the columns at the plastic hinge section.
6. Bond degradation results in lower stiffness and strength of the frame structure.
7. Joint shear failure occurs only when high axial load acts on the columns, because it allows transfer of higher bond stresses from the beam bars to the joint core.
8. The relationship between the joint horizontal stress ratio at failure and the column axial load ratio is directly proportional.

9. Specimens which exhibit joint shear failure developed higher shear stress ratio than the others.

10. It is reasonable consider only the strut resisting mechanism for the evaluation of joint strength, for the specimens which exhibit joint shear failure.

As regards exterior joints with smooth bars:

1. Compared to exterior joints with deformed bars, they generally show lower energy dissipation capacity, stiffness, and equivalent damping.

2. Compared to interior joints with smooth bars, they show lower displacement ductility and larger equivalent damping.

3. The higher the joint aspect ratios, the greater the energy dissipation capacity: the greater the joint shear strain and the lower the shear strength.

4. The greater the amount of longitudinal reinforcement of the beam, the greater the shear strength of the joint

5. Different anchorage arrangements strongly influence the behavior of the joints:

    a. Anchorage with 180-degree hooks contributes to joint damage by increasing shear diagonal cracking, with the formation of a concrete "wedge" and concrete spalling on the joint exterior face;

    b. Anchorage developed by 90-degree bends inside the joint core, in the absence of joint transverse reinforcement, tends to straighten and produces concrete spalling on the joint exterior face and may not prevent bar slippage;

    c. Anchorage developed by 90-degree bends outside the joint core, in the absence of column hoops, also tends to straighten and produces concrete tension cracking in the columns and column bars buckling;

    d. Straight anchorage produces bond failure with consequent severe strength and stiffness degradation.

6. In the absence of joint hoops, joint shear failure does not occur, but bond deterioration or beam flexural failure occur.

7. In the presence of severe bond deterioration, the conventional flexural theory overestimates the members' flexural strength.

8. Differently from interior joints, the presence of column axial load can lead to joint shear strength increase. This because, even there is an increase of the horizontal force transferred from the beam to the joint core due to the improved bond conditions, this increase is lower than that occurs in interior joins, since in exterior

113

joints there is only one beam framing into the joint. Overall then, column axial load helps mainly in preventing the opening of joint diagonal cracks and joint damage, and contributes to the diagonal strut resisting mechanism.

9. The compressive load on the column permits the beam to reach higher flexural capacity, allowing the development of ductile resisting mechanisms, with higher energy dissipation.

10. Similarly to interior joints, exterior joints which develop joint shear failure reach higher shear stress ratio than the others.

11. Different anchorage arrangements strongly influence joint shear strength and enact additional stresses which change the resisting mechanisms development.

12. Specimens which exhibit joint shear failure, however develop limited shear capacity due to the bond slip of smooth bars and the additional forces of particular anchorage solutions.

The observations above are helpful for understanding behavior of joints with smooth bars under seismic actions and can form the basis for upgrading these joints, when a retrofit intervention on an existing building is planned.

5. Conclusions

The seismic behavior of two identical full-scale RC exterior joints has been analyzed by testing in the Laboratory for Testing materials and Structures of the University of Udine. The joint properties were selected from a building designed under high ductility requirements, according to the Italian Building Code [3]. To investigate how a construction error could influence the joint behavior, the specimens were built without the required ties inside the joint panel. From the elaboration of the experimental results, it has been observed that, although the joint were designed for high ductility class, a 50% reduction of the horizontal reinforcement in the joint core and 25% in the column critical regions, led the specimens to shear failure, with diagonal concrete cracking in the joint core. In detail, for both joints, for upward applied forces, the beam flexural failure was observed, with yielding and rupture of the bottom bars and top concrete crushing near the joint. This revealed the development of a ductile mechanism failure. For downward applied forces, joint shear failure occurred, because the amount of top beam reinforcement was higher than the bottom one and the beam plastic hinge did not completely develop. In this case, the top beam bars transmitted higher horizontal stresses to the joint panel, which could not resist due to the lack of the minimum horizontal reinforcement required, and developed joint shear failure.

Shear strength obtained from the tests has been compared to that evaluated with the formulae provided for exterior joints by Eurocode 8 [2], ACI Code [4] and Pauletta et al [28]. It has been observed that both the expressions of Pauletta et al. [28] and Eurocode 8 [2] well approximate the experimental shear strength thus predicting the joint shear failure. Conversely, the formula provided by ACI Code [4] overestimates the joint shear capacity thus not predicting the shear failure, since it is valid only when the required joint reinforcement is arranged and the concrete confinement is fully developed.

A strut-and-tie model for the evaluation of RC interior beam-column joint shear strength has been proposed. On the basis of mechanical considerations, a direct formula for interior joint shear strength has been derived, by considering the resisting contributions of the concrete strut mechanism and the truss mechanism, developed by joint shear reinforcement and vertical intermediate column bars. In comparison to the model for exterior joints previously developed by Pauletta et al. [28], three inclined concrete struts has been considered instead of two and the influence of the upper column axial load on

the inclination of the struts has been taken into account. The shear strength proposed formula has been calibrated on the basis of 69 experimental tests present in the literature, by the introduction of numerical coefficients. From the comparison with other shear strength existing expressions, it can be said that the proposed formula gives the most consistent and accurate predictions. Moreover, a design shear strength formula has been proposed, with the introduction of a multiplying coefficient, and afterwards compared to the design formulae of Eurocode 8 [2] and ACI Code [4]. The comparison with the codes' formulae has revealed that the proposed design formula gives adequately safe predictions and it is the most consistent.

After the presented study on exterior and interior beam-column joints reinforced with deformed bars, the behavior of joints reinforced with smooth bars has been investigated. The largest number of tests on both interior and exterior beam-column joints reinforced with smooth bars, present in the literature, has been collected, to evaluate the effects of the main influencing parameters on joint seismic response. The investigation on interior joints with smooth bars has highlighted that they generally exhibit bond-slip failure, rather than shear failure, which however occurs when the column axial load is high. Concerning the exterior joints with smooth bars, it has been observed that the different anchorage arrangements strongly influence seismic behavior and joint shear strength, as they enact additional stresses into the joint core and modify the resisting mechanisms development. Differently from interior joints, column axial load improves exterior joints shear strength, by preventing the opening of diagonal cracks in the joint core and by increasing beam bars bond condition, which enhances beam flexural strength, with the development of ductile mechanisms and energy dissipation. Furthermore, it has been observed that this improvement in bond conditions increases joint shear stresses, but also contributes to the concrete strut resisting mechanism. Finally, to evaluate the applicability of shear strength expressions for joint reinforced with deformed bars to joints with smooth bars, the shear strength of the collected specimens which exhibit shear failure has been calculated with the shear strength formula proposed in this thesis, for interior joints, and with the formulation of Pauletta et al. [28], for exterior joints. For both interior and exterior joints, the shear strength expressions have been modified by conserving only the main concrete strut resisting contribution, to take account of the low bond transferred to the joint panel. It has been found that, the strut resisting contribution well predicts the shear strength of interior joints. For exterior joints, instead, the shear capacity provided

by the concrete strut is not completely developed because the arise of other mechanisms due to particular anchorage arrangements or to bond slip of the beam smooth bars.

Bibliography

[1] ACI Committee 318. Building code requirements for structural concrete (ACI 318-14) and commentary (ACI 318R-14). Farmington Hills; American Concrete Institute; 2014.

[2] UNI EN 1998-1. Eurocode 8: design of structures for earthquake resistance - Part 1: General rules, seismic actions and rules for buildings. CEN, Comité European de Normalisation; 2004.

[3] Ministero delle Infrastrutture. DM 14 gennaio 2008. Norme tecniche per le costruzioni; 2008 [in Italian].

[4] ACI Committee 352. Recommendations for design of beam-column connections in monolithic reinforced concrete structures. Farmington Hills; American Concrete Institute; 2002.

[5] Somma G, Pieretto A, Rossetto T, Grant DN. R.C. beam to column connection failure assessment and limit state design. Materials and Structures 2015; 48(4):1215-1231.

[6] Somma G. Shear strength of beam-column joints under seismic loading-Fiber effectiveness. 3rd International fib Congress and Exhibition, Incorporating the PCI Annual Convention and Bridge Conference 2010, United States 2010; Code 126173.

[7] Kim J, LaFave J. A simplified approach to joint shear behavior prediction of RC beam-column connections. Earthquake Spectra 2012; 28(3):1071-1096.

[8] Wang GL, Dai JG, Teng JG. Shear strength model for RC beam-column joints under seismic loading. Engineering Structures 2012; 40:350-360.

[9] Kassem W. Strut-and-tie modelling for the analysis and design of RC beam-column joints. Materials and Structures 2016; 49:3459-3476.

[10] Unal M, Burak B. Joint shear strength prediction for reinforced concrete beam-to-column connections. Structural Engineering and Mechanics 2012; 41(3):421-440.

[11] Russo G, Somma G, Angeli P, Mitri D. Contributi resistenti a taglio nei nodi interni soggetti ad azione sismica. In: XI National Congress "Seismic engineering in Italy". Genova, Italy; 2004: 25-29.

[12] Muhsen BA, Umemura H. New Model for Estimation of Shear Strength of Reinforced Concrete Beam Column Joints. Procedia Engineering 2011; 14:2151-2159.

[13] Attaalla SA. General Analytical Model for Nominal Shear Stress of Type 2 Normal- and High-Strength Concrete Beam-Column Joints. ACI Struct J 2004; 10(1):65-75.

[14] Hwang SJ, Lee HJ. Analytical model for predicting shear strengths of interior reinforced concrete beam–column joints for seismic resistance. ACI Struct J 2000; 97(1):35-44.

[15] Massone LM, Orrego GN. Analytical model for shear strength estimation of reinforced concrete beam-column joints. Engineering Structures 2018; 173:681-692.

[16] Pan Z, Guner S, Vecchio FJ. Modeling of interior beam-column joints for nonlinear analysis of reinforced concrete frames. Engineering Structures 2017; 142:182-191.

[17] Wong HF, Kuang JS. Predicting shear strength of RC interior beam-column joints by modified rotating-angle softened-truss model. Computers and Structures 2014; 133:12-17.

[18] Uma SR and Jain SK. Seismic design of beam-column joints in RC moment resisting frames - Review of codes. Structural Engineering and Mechanics 23(5), pp. 579–597; 2006.

[19] ACI Committee 318. Building code requirements for structural concrete (ACI 318M-02) and commentary (318M-02). Farmington Hills; American Concrete Institute; 2002.

[20] NZS 3101. "Concrete structures standard, Part 1 and 2, Code and commentary on the design of concrete structures". New Zealand Standard, New Zealand, 1995.

[21] Hwang SJ, Lee HJ, Liao TF, Wang KC, Tsai HH. Role of hoops on shear strength of reinforced concrete beam-column joints. ACI Structural Journal, 102(3), pp. 445–453; 2005

[22] Hwang SJ, Lee HJ. Analytical model for predicting shear strengths of exterior reinforced concrete beam–column joints for seismic resistance. ACI Struct J 1999; 96(5):846-857.

[23] Ehsani MR, Wight JK. Exterior reinforced concrete beam-to-column connections subjected to earthquake-type loading. ACI Structural Journal 82(4), pp. 492–499; 1985.

[24] Kotsovou G and Mouzakis H. Seismic design of RC external beam-column joints. Bulletin of Earthquake Engineering, 10(2), pp. 645–677; 2012.

[25] UNI EN 1992-1-1:2005. Eurocode 2: Design of concrete structures - Part 1: General rules and rules for buildings. CEN, Comité European de Normalisation; 2004.

[26] Cosenza E, Maddaloni G, Magliulo G, Pecce M, Ramasco R. Progetto Antisismico di Edifici in Cemento Armato. Pavia. IUSS Press, 2005.

[27] Paulay T, Priestley MJN. Seismic design of reinforced concrete and masonry buildings. New York: John Wiley and Sons; 1992.

[28] Pauletta M, Di Luca D, Russo G. Exterior beam-column joints – Shear strength model and design formula. Engineering Structures 2015;94:70-81.

[29] Consiglio Superiore dei Lavori Pubblici. Circolare 2 febbraio 2009, n. 617 - Istruzioni per l'applicazione delle "Nuove norme tecniche per le costruzioni" di cui al D.M. 14 gennaio 2008; 2008 [in Italian].

[30] Park S, Mosalam KM. Analytical model for predicting shear strength of unreinforced exterior beam-column joints. ACI Struct J 2012; 109(2):149-159.

[31] Russo G, Venir R, Pauletta M. Reinforced concrete deep beams – shear strength model and design formula. ACI Struct J 2005; 102(3):429-437.

[32] Russo G, Venir R, Pauletta M, Somma G. Reinforced concrete corbels – shear strength model and design formula. ACI Struct J 2006; 103(1):3-10.

[33] Russo G, Pauletta M. A simple method for evaluating the maximum slip of anchorages. Mater Struct 2006; 39:533–546. http://dx.doi.org/10.1617/s11527-006-9092-1.

[34] Russo G, Pauletta M, Mitri D. Solution for bond distribution in asymmetric R.C. structural members. Engineering Structures 2009; 31(3):633-641.

[35] Piccinin R, Cattaneo S, Biolzi L. Breakout capacity of headed anchors in confined concrete: Experimental evidence. ACI Structural Journal 2013; 110(3):469-479.

[36] Au FTK, Huang K, Pam HJ. Diagonally-reinforced beam-column joints reinforced under cyclic loading, Proceedings Of The Institution Of Civil Engineers: Structures And Buildings 2005; 158(1):21-40.

[37] Birss GR. The elastic behaviour of earthquake resistant reinforced concrete beam-column joints. Research Report No. 78-13. Department of Civil Engineering, University of Canterbury, Christchurch, New Zealand; 1978.

[38] Fujii S, Morita S. Comparison between interior and exterior RC beam-column joint behavior. In: Jirsa JO, editor. Design of beam-column joints for seismic resistance, SP-123, American Concrete Institute, Farmington Hills, Mich. 1991; 145-165.

[39] Goto Y, Joh O. An experimental study of shear failure mechanism of RC interior beam-column joints. In: 11th World Conference on Earthquake Engineering, Acapulco Mexico; 1996; 1194.

[40] Hakuto S, Park R, Tanaka H. Seismic load tests on interior and exterior beam-column joints with substandard reinforcing details. ACI Struct J 2000; 97(1):11-25.

[41] Joh O, Goto Y, Shibata T. Behavior of Reinforced Concrete Beam-Column Joints with Eccentricity. In: Design of beam-column joints for seismic resistance, SP-123, American Concrete Institute, Detroit (MI), 1991; 317-357.

[42] Kamimura T, Takeda S, Tochio AM. Influence of joint reinforcement on strength and deformation of interior beam-column subassemblages. In: Proceedings of the 12th world conference on earthquake engineering. Auckland, New Zealand; 2000.

[43] Kitayama K, Lee S, Otani S, Aoyama H. Behavior of high-strength R/C beam–column joints. In: Proceedings of the 10th world conference on earthquake engineering. Rotterdam, Holland, 1992; 3151–3156.

[44] Kitayama K, Otani S, Aoyama H. Development of design criteria for RC interior beam column joints. Design of beam-column joints for seismic resistance, SP-123, American Concrete Institute, Farmington Hills, Mich. 1991; 97-123.

[45] Kusuhara F, Azukawa K, Shiohara H, Otani S. Tests of reinforced concrete interior beam-column joint subassemblage with eccentric beams. In: Proceedings of the 13th world conference on earthquake engineering. Vancouver, Canada; 2004.

[46] Lee WT, Chiou YJ, Shih MH. Reinforced concrete beam–column joint strengthened with carbon fiber reinforced polymer. Composite Structures 2010; 92:48-60.

[47] Li B, Tran C. Seismic behavior of reinforced concrete beam-column joints with vertically distributed reinforcement. ACI Struct J 2009; 106(6):790-799.

[48] Meinheit DF, Jirsa JO. The shear strength of reinforced concrete beam-column joints. CESRL Report No. 77-1, University of Texas at Austin, 1977.

[49] Noguchi H, Kashiwazaki T. Experimental studies on shear performances of RC interior beam-column joints with high-strength materials. In: Proceedings of the 10th world conference on earthquake engineering. Rotterdam, Holland, 1992; 3163-3168.

[50] Noguchi H, Kurusu K. Correlation of bond and shear in RC beam-column connections subjected to seismic forces. In: Proceedings of the 9th world conference on earthquake engineering. Tokyo-Kyoto, Japan, 1988; 597-602.

[51] Oka K, Shiohara H. Tests of high strength concrete interior beam-column-joint subassemblages. In: Proceedings of the 10th world conference on earthquake engineering. Rotterdam, 1992; 3211-3217.

[52] Owada Y. Three dimensional behaviors of reinforced concrete beam–column joint under seismic load. In: Proceedings of the 12th world conference on earthquake engineering. Aukland, New Zealand, 2000.

[53] Owada Y. Seismic behavior of beam-column joint of reinforced concrete exterior

frame under varying axial load. In: Proceedings of the 10th world conference on earthquake engineering. Rotterdam, Holland, 1992; 3181–3184.

[54] Park R, Milburn JR. Comparison of recent New Zealand and United States seismic design provisions for reinforced concrete beam-column joints and tests results from four units designed according to the New Zealand code. Bull New Zealand Nat Soc Earthq Eng 1983; 16(1):3-24.

[55] Park R, Gaerty L, Stevenson EC. Tests on an interior reinforced concrete beam-column joint. Bull New Zealand Nat Soc Earthq Eng 1981; 14(2):81-92.

[56] Pessiki SP, Conley CH, Gergely P, White RN. Seismic behavior of lightly-reinforced concrete column and beam-column joint de.tails: Report No. NCEER-90-0014. State University of New York, Buffalo, 1990

[57] Shiohara H, Zaid S, Otani S. Test of innovative reinforcing detail for R/C interior beam-column connections subjected to seismic action. In: Proceedings of the Third International Conference on Concrete under Severe Conditions, University of British Columbia, Vancouver, Canada, 2001; 1:739-746.

[58] Supaviriyakit T, Pimanmas A. Comparative performance of sub-standard interior reinforced concrete beam–column connection with various joint reinforcing details. Materials and Structures 2008; 41:543-557.

[59] Wang Y-C, Hsu K. Shear strength of RC jacketed interior beam-column joints. ACI Struct J 2009; 106(2):222-232.

[60] Yang H, Zhao W, Zhu Z, Fu J. Seismic behavior comparison of reinforced concrete interior beam-column joints based on different loading methods. Engineering Structures 2018; 166:31-45.

[61] Abrams DP. Scale relations for reinforced concrete beam-column joints. ACI Struct J 1987; 84(6):502-12.

[62] Durrani AJ, Wight JK. Behavior of interior beam-to-column connections under earthquake-type loading. ACI J 1985; 82(3):343-349.

[63] Hwang HJ, Eom TS, Park HG. Design considerations for interior RC beam-column joint with additional bars. Engineering Structures 2015; 98:1-13.

[64] Hwang HJ, Park HG, Choi WS, Chung L, Kim JK. Cyclic Loading Test for Beam-Column Connections with 600 MPa (87 ksi) Beam Flexural Reinforcing Bars. ACI Struct J 2014; 111(4):913-24.

[65] Joh O, Goto Y. Beam-column joint behavior after beam yielding in r/c ductile frames. In: Proceedings of the 12th world conference on earthquake engineering. Auckland,

New Zealand; 2000.

[66] Lee JY, Kim JY, Oh GJ. Strength deterioration of reinforced concrete beam-column joints subjected to cyclic loading. Engineering Structures 2009; 31:2070-2085.

[67] Leon RT. Shear strength and hysteretic behavior of interior beam-column joints. ACI Struct J 1990; 87(1):3-11.

[68] Morita S, Kitayama K, Koyama A, Hosono T. Effects of beam bar bond and column axial load on shear strength in reinforced concrete interior beam-column joints. Transaction of the Japan Concrete Institute 1999; 21:453-460.

[69] Otani S, Kitayama K, Aoyama H. Beam bar bond requirements for interior beam-column connections. In: Proceedings, International Symposium on Fundamental Theory of Reinforced Concrete and Prestressed Concrete, Nanjing Institute of Technology, China, 1986.

[70] Russo G, Pauletta M. Seismic Behavior of Exterior Beam-Column Connections with Plain Bars and Effects of Upgrade. ACI Structural Journal 2012; 109(2):225-233.

[71] Somma G, Vit M, Frappa G, Pauletta M, Pitacco I, Russo G. A new cracking model for concrete ties reinforced with bars having different diameters and bond laws. Engineering Structures 235,112026; 2021.

[72] Pampanin S, GM Calvi and M Moratti. Seismic behaviour of RC beam-column joints designed for gravity loads, 12th ECEE, London, Paper No. 726; 2002.

[73] Hakuto S, Park R and Tanaka H. Effect of deterioration of bond of beam bars passing through interior beam-column joints of flexural strength and ductility. ACI Structural Journal, 96 (5), pp. 858-864; 1999.

[74] Liu A and Park R. Seismic load tests on two concrete interior beam-column joints reinforced by plain round bars designed to pre-1970s seismic codes. Bull NZ Soc Earthq Eng, 31 (3), pp. 164-176; 1998.

[75] Hakuto S Park R and Tanaka H. Retrofitting of reinforced concrete moment-resisting frames. Research Report 95-4, Department of Civil Engineering, University of Canterbury, New Zealand; 1995.

[76] Liu A. Seismic assessment and retrofit of pre-1970s reinforced concrete frame structures. PhD Thesis. University of Canterbury, New Zealand; 2001.

[77] Braga F, Gigliotti R, Laterza M. R/C existing structures with smooth reinforcing bars: experimental behaviour of beam-column joints subjected to cyclic lateral loads. The Open Construction & Building Technology Journal, 3(1), pp. 52-67; 2009.

[78] Braga F, Gigliotti R, Laterza M, D'Amato M, Suman R. Modeling of longitudinal

passing bars within the joint panel in poor anchorage condition. ANIDIS, L'ingegneria sismica in Italia. Padova; 2013.

[79] Braga F, Gigliotti R, Laterza M, D'Amato M, Kunnath S. Modified steel bar model incorporating bond-slip for seismic assessment of concrete structures. Journal of Earthquake Engineering, ASCE, 138(11), pp. 1342-1350; 2012.

[80] Fernandes C, Melo J, Varum H and Costa A. Cyclic behavior of substandard reinforced concrete beam-column joints with plain bars. ACI Structural Journal, 110 (1), pp. 137-147; 2013.

[81] Melo J, Varum H and Rossetto T. Cyclic behavior of interior beam-column joints reinforced with plain bars, Earthquake Engineering and Structural Dynamics, 44, pp. 1351-1371; 2015.

[82] Adibi M, Marefat M, Allahvirdizadeh R. Nonlinear modeling of cyclic response of RC beam-column joints reinforced by plain bars. Bull Earthquake Eng, 16, pp. 5529-5556; 2018.

[83] Park R. A summary of results of simulated seismic load tests on reinforced concrete beam-column joints, beams and columns with substandard reinforcing details. Journal of Earthquake Engineering, 6 (2), pp. 147-174; 2002

[84] Liu A, Park R. Seismic behaviour and retrofit of pre-1970's as-built exterior beam-column joints reinforced by plain round bars. Bulletin of the New Zealand Society for Earthquake Engineering, 34(1), pp. 68-81; 2001.

[85] Bedirhanoglu I, Ilki A, Pujol S, Kumbasar N. Behavior of deficient joints with plain bars and low-strength concrete. ACI Structural Journal, 107(3), pp. 300-310; 2010.

[86] Melo J, Varum H, Rossetto T, Costa A. Cyclic response of RC beam-column joints reinforced with plain bars: an experimental testing campaign. 15th WCEE, World Conference on Earthquake Engineering, Paper 4799; 2012.

[87] De Risi MT, Verderame GM. Experimental assessment and numerical modelling of exterior non-conforming beam-column joints with plain bars. Engineering Structures, 150, pp. 115-134; 2017.

[88] Cosgun C, Turk AM, Mangir A Cosgun T. Experimental behaviour and failure of beam-column joints with plain bars, low-strength concrete and different anchorage details. Engineering Failure Analysis, 109, 104247; 2020

Appendix A – Joint Shear Capacity

A detailed presentation of the manner in which the shear capacity is calculated for each of the methods investigated is reported in the following for the considered joint.

A1. Eurocode 8 [2]

Eurocode 8 [2] provides the following formula to calculate the horizontal shear force in exterior beam-column joints,

$$
V_{jhd} = \min \begin{cases} 0.8 \cdot \eta f_{cd} b_j h_{jc} \sqrt{1 - \dfrac{v_d}{\eta}} \\[2em] b_j h_{jc} \sqrt{\left(\dfrac{A_{sh} f_{ywd}}{b_j h_{jw}} + f_{ctd} \right) (f_{ctd} + v_d f_{cd})} \end{cases}
\tag{A.1}
$$

According to the geometric (Fig. 2) and mechanical (Table 2) characteristics of specimens J1 and J2, it results

$$
\begin{aligned}
b_j = \min(b_c, b + 0.5 h_c) &= \min(500 \text{ mm}, 300 \text{ mm} + 0.5 \cdot 300 \text{ mm}) \\
&= 450 \text{ mm}
\end{aligned}
\tag{A.2}
$$

$$
\eta = 0.6 \cdot \left(1 - \frac{f_{ck}}{250} \right) = 0.6 \cdot \left(1 - \frac{49.85}{250} \right) = 0.48
\tag{A.3}
$$

$$
v_d = \frac{N}{A_c f_{cd}} = \frac{327 \text{ kN}}{150000 \text{ mm}^2 \cdot 49.85 \text{ MPa}} \cdot 1000 = 0.044
\tag{A.4}
$$

$h_{jc} = 226$ mm, $A_{sh} = 603$ mm^2, $f_{ywd} = 527.7$ MPa, $f_{ctd} = 3.62$ MPa and $h_{jw} = 476$ mm.

Finally, the joint shear strength of specimens J1 and J2, calculated with the formula of Eurocode 8 [2] (Eq. (A.1)), is equal to

$$V_{n,EC8} \tag{A.5}$$

$$= \min \begin{cases} 0.8 \cdot 0.48 \cdot 49.85\ \text{MPa} \cdot 450\ \text{mm} \cdot 226\ \text{mm} \sqrt{1 - \dfrac{0.044}{0.48}} \\[2em] (450 \cdot 226)\ (\text{mm}^2)\sqrt{(1.49 + 3.62)(\text{MPa})(3.62 + 0.044 \cdot 49.85)(\text{MPa})} \end{cases}$$

$$= \min \begin{cases} 1855.4\ \text{kN} \\ 507.3\ \text{kN} \end{cases} = 507.3\ \text{kN}$$

as reported in Table 6.

A2. ACI Code 352R [4]

According to the ACI Code [4], joint shear capacity is given by

$$V_n = 0.083\gamma\sqrt{f_c'}\,b_j h_c \tag{A.6}$$

By considering the characteristics of test units J1 and J2 and the Code prescriptions, the terms of Eq. (A.6) are equal to

$$b_j \le \min \begin{cases} \dfrac{b_b + b_c}{2} = \dfrac{300 + 500}{2}\ \text{mm} = 400\ \text{mm} \\[1.5em] b_b + \sum \dfrac{mh_c}{2} = 300 + \sum \dfrac{0.3 \cdot 500\ \text{mm}}{2} = 375\ \text{mm} \\[1.5em] b_c = 500\ \text{mm} \end{cases} \tag{A.7}$$

$$= 375\ \text{mm}$$

$\gamma = 12$, $f_c' = 49.85$ MPa, and $h_c = 300$ mm.

By substituting these terms in Eq. (30), the resulting value of joint shear capacity, $V_{n,ACI}$, for specimens J1 and J2 is equal to

$$V_{n,ACI} = 0.083 \cdot 12 \cdot \sqrt{49.85\ \text{MPa}} \cdot 375\ \text{mm} \cdot 300\ \text{mm} = 727.8\ \text{kN} \tag{A.8}$$

as reported in Table 6.

It has to be underlined that this value of shear capacity is calculated by neglecting the ACI Code prescription, which provides for that the formula is applicable only to joint provided of the minimum shear reinforcement required.

A3. Pauletta et al. [28]

Pauletta et al. [28] proposed the following shear strength formula

$$V_{n[28]} = 0.71 \left[\frac{\chi f_c' a_c b_j \cos \vartheta_h}{\alpha} + 0.79 A_h f_{yh} + 0.52 \frac{A_v f_{yv}}{\tan \vartheta_h} \right] \tag{A.9}$$

The non-dimensional interpolating function χ is defined as

$$\chi = 0.74 \cdot \left(\frac{f_c'}{105} \right)^3 - 1.28 \cdot \left(\frac{f_c'}{105} \right)^2 + 0.22 \cdot \left(\frac{f_c'}{105} \right) + 0.87 \tag{A.10}$$

where $f_c' = 49.85$ MPa, hence, $\chi = 0.765$. A_h and A_v are the total areas of horizontal hoops and vertical intermediate column bars, equal to 603 mm² and 509 mm², respectively; f_{yh} and f_{yv} are the transverse reinforcement and the longitudinal column bars mean yield strengths, respectively, and they are both equal to 527.7 MPa; a_c is the depth of the column compression zone, equal to

$$\begin{aligned}
a_c &= \left(0.25 + 0.85 \frac{N}{A_g f_c'} \right) h_c \\
&= \left(0.25 + 0.85 \frac{327 \text{ kN}}{150000 \text{ mm}^2 \cdot 49.85 \text{ MPa}} \cdot 1000 \right) \cdot 300 \text{ mm} \\
&= 86.15 \text{ mm}
\end{aligned} \tag{A.11}$$

and ϑ_h is the angle of inclination of the diagonal strut

$$\theta_h = \tan^{-1} \left(\frac{h_b''}{h_c''} \right) = \tan^{-1} \left(\frac{476 \text{ mm}}{226 \text{ mm}} \right) = 64.6° \tag{A.12}$$

The width of the diagonal strut is defined as

$$b_j = \min(b, b_c) = \min(300 \text{ mm}, 500 \text{ mm}) = 300 \text{ mm} \tag{A.13}$$

The coefficient α in Eq. (A.9) is equal to

$$\alpha = \frac{2HL}{2HL - (2L + h_c) \cdot j_{db}} \cdot \left(1 - \frac{l_h \sqrt{f_c'}}{d_b \cdot f_{bi}}\right) \tag{A.14}$$

where $H = 2200$ mm, $L = 1600$ mm, $h_c = 300$ mm, $l_h = h_c - a_c = 213.9$ mm, $d_b = 17.4$ mm.

In Eq. (A.14) f_{bi} is the tensile stress in the longitudinal beam reinforcement at joint shear failure, defined as

$$f_{bi} = (0.63 \cdot \omega^{-0.21}) \cdot f_{yb} \tag{A.15}$$

where ω is the mechanical reinforcement ratio of the tensile longitudinal reinforcement, equal to

$$\omega = \frac{A_s'' \cdot f_{yb}}{b_b \cdot h_b \cdot f_c'} = \frac{1018 \text{ mm}^2 \cdot 527.7 \text{ MPa}}{(300 \cdot 550) \text{ mm}^2 \cdot 49.85 \text{ MPa}} = 0.065 \tag{A.16}$$

otherwise

$$\omega = \frac{A_s \cdot f_{yb}}{b_b \cdot h_b \cdot f_c'} = \frac{663 \text{ mm}^2 \cdot 527.7 \text{ MPa}}{(300 \cdot 550) \text{ mm}^2 \cdot 49.85 \text{ MPa}} = 0.043 \tag{A.17}$$

Hence, for downward forces f_{bi} is equal to 589.6 MPa, while for upward forces is equal to 645.2 MPa.

By substituting the values of f_{bi} in Eq. (A.14), it results that $\alpha > 1$, for both downward and upward forces. Since the value of this coefficient has to be ≤ 1, it assumes the value 1.

By substituting all the geometric and mechanical characteristics of specimens J1 and J2 to the terms of Eq. (A.9), it results that the shear strength is equal to

$$V_{n[28]} = 0.71 \left[\frac{0.765 \cdot 49.85 \text{ MPa} \cdot 86.15 \text{ mm} \cdot 300 \text{ mm} \cdot \cos 64.6°}{1} + 0.79 \right.$$

$$\left. \cdot \, 603 \text{ mm}^2 \cdot 527.7 \text{ MPa} + 0.52 \, \frac{509 \text{ mm}^2 \cdot 527.7 \text{ MPa}}{\tan 64.6°} \right] \qquad \text{(A.18)}$$

$$\cdot \frac{1}{1000} = 525.7 \text{ MPa}$$

as reported in Table 6.

Appendix B – Data Tables

Table B1. Geometrical properties and reinforcement areas of the 69 specimens used for the calibration of the coefficients q_0, q_1, q_2 and q_3 in the proposed formula (Eq. (78))

Author references	Specimen labels	b_b (mm)	h_b (mm)	b_c (mm)	h_c (mm)	δ_{b1} (mm)	δ_{b2} (mm)	δ_c (mm)	A_{sb1} (mm²)	A_{sb2} (mm²)	ϕ_1 (mm)	ϕ_2 (mm)	A_{sh} (mm²)	A_{sv} (mm²)
[36]	E0.0 [a]	250	300	300	300	28	28	28	804	804	16.0	16.0	0	1206
	E0.3 [a]	250	300	300	300	28	28	28	804	804	16.0	16.0	0	1206
	H0.0	250	300	300	300	28	28	28	804	804	16.0	16.0	1017	1206
	H0.3	250	300	300	300	28	28	28	804	804	16.0	16.0	1017	1206
[37]	B1	356	610	457	457	68	68	42	2512	2512	20.0	20.0	2026	452
	B2 [b]	356	610	457	457	68	68	42	2512	2512	20.0	20.0	531	452
[38]	A1	160	250	220	220	38	38	30	570	570	9.5	9.5	170	759
	A2	160	250	220	220	38	38	30	570	570	9.5	9.5	170	759
	A3	160	250	220	220	38	38	30	570	570	9.5	9.5	170	759
[39]	J-HH [b]	200	350	300	300	35	35	30	1519	1519	25.4	25.4	1357	1130
	J-HO [b]	200	350	300	300	35	35	30	1519	1519	25.4	25.4	1357	0
	J-OH [a]	200	350	300	300	35	35	30	1519	1519	25.4	25.4	0	1130
	J-MM [b]	200	350	300	300	35	35	30	1519	1519	25.4	25.4	678	565
	J-MO [b]	200	350	300	300	35	35	30	1519	1519	25.4	25.4	678	0
	J-LO [b]	200	350	300	300	35	35	30	1519	1519	25.4	25.4	28	0
[40]	O1 [a]	300	500	460	300	58	58	58	1809	904	24.0	24.0	0	0
[41]	JXO-B1	150	350	300	300	30	30	30	380	380	12.7	12.7	190	253
[42]	A-1	200	300	300	300	50	50	50	1163	1163	22.2	22.2	509	0
[43]	I3	200	300	300	300	55	40	40	1194	796	15.9	15.9	254	1194
	I5	200	300	300	300	53	53	40	762	381	12.7	12.7	285	1194
	I6	200	300	300	300	40	40	40	861	574	19.1	19.1	285	1194
[44]	B1	200	300	300	300	62	62	40	1016	1016	12.7	12.7	225	1194
	B3	200	300	300	300	62	62	40	856	856	9.5	9.5	592	762
	A1	200	300	300	300	62	40	40	1016	508	12.7	12.7	255	1194
[45]	JE-0	180	300	320	280	51	51	33	710	710	9.5	9.5	192	508
[46]	JI0	300	600	400	400	50	50	50	1519	1519	25.4	25.4	1013	1013
[47]	JA [b]	250	500	400	400	45	30	30	2065	1548	25.4	25.4	1936	1032
	JB [b]	250	500	400	400	45	30	30	2581	1936	19.1	19.1	2439	1032
	JC [b]	230	460	400	400	30	30	30	1548	1548	19.1	19.1	3067	2065
	JD [b]	230	460	400	400	30	30	30	1548	1548	19.1	19.1	3880	2065
[48]	I [b]	279	457	330	457	67	64	62	2457	1519	32.3	25.4	506	1548
	II	279	457	330	457	67	64	67	2457	1519	32.3	25.4	506	3276
	III [b]	279	457	330	457	67	64	69	2457	1519	32.3	25.4	506	6037
	IV [b]	406	457	457	330	67	64	65	2457	1519	32.3	25.4	1013	1266
	V	279	457	330	457	67	64	67	2457	1519	32.3	25.4	506	3276
	VI [b]	279	457	330	457	67	64	67	2457	1519	32.3	25.4	506	3276
	VII [b]	406	457	457	330	67	64	65	2457	1519	32.3	25.4	1013	1266
	XII [b]	279	457	330	457	67	64	67	2457	1519	32.3	25.4	2382	3276
	XIII	279	457	330	457	67	64	67	2457	1519	32.3	25.4	1519	3276
	XIV [b]	406	457	457	330	67	64	67	2457	1519	32.3	25.4	3038	1266

Author references	Specimen labels	b_b (mm)	h_b (mm)	b_c (mm)	h_c (mm)	δ_{b1} (mm)	δ_{b2} (mm)	δ_c (mm)	A_{sb1} (mm²)	A_{sb2} (mm²)	ϕ_1 (mm)	ϕ_2 (mm)	A_{sh} (mm²)	A_{sv} (mm²)
[49]	OKJ-1	200	300	300	300	48	41	40	1194	929	13.0	13.0	339	1061
	OKJ-4	200	300	300	300	48	41	40	1194	929	13.0	13.0	339	1061
[50]	NO.2	200	300	300	300	46	46	37	785	785	10.0	10.0	57	796
	NO.4	200	300	300	300	33	33	37	663	663	13.0	13.0	57	796
[51]	J-1	240	300	300	300	48	41	30	1143	889	12.7	12.7	283	1064
	J-3	240	300	300	300	50	50	30	1064	1064	13.0	13.0	1944	1064
	J-4	240	300	300	300	50	50	30	1266	1266	12.7	12.7	283	1064
	J-5	240	300	300	300	48	41	30	1143	889	12.7	12.7	283	1064
	J-6	240	300	300	300	48	41	30	1143	889	12.7	12.7	170	1064
	J-8	240	300	300	300	48	41	30	2583	2009	19.1	19.1	283	2296
	J-10	240	300	300	300	48	41	30	1143	889	12.7	12.7	283	1064
	J-11	240	300	300	300	48	41	30	2583	2009	19.1	19.1	283	2296
[52]	JO-1	150	150	150	150	20	20	20	381	381	13.0	13.0	113	252
[53]	J0C-1	120	150	150	150	22	22	22	214	214	9.5	9.5	79	0
[54]	1	229	457	305	406	56	56	42	1608	1608	16.0	16.0	3215	904
[55]	1	229	457	305	406	56	56	40	1608	1608	16.0	16.0	2010	628
[56]	1 [a]	356	610	406	406	62	62	64	2564	1282	28.6	28.6	0	0
	2 [a]	356	610	406	406	62	62	64	2564	1282	28.6	28.6	0	0
	3 [a]	356	610	406	406	62	62	60	2564	1282	28.6	28.6	0	0
	4 [b]	356	610	406	406	62	62	59	2564	1282	28.6	28.6	142	776
	5 [b]	356	610	406	406	62	62	59	2564	1282	28.6	28.6	427	776
[57]	S3	200	300	300	300	49	49	35	995	995	16.0	16.0	256	1148
[58]	J3B	175	300	200	350	52	39	30	678	452	12.0	12.0	628	904
[59]	Ho-JI1 [a]	300	400	400	400	40	40	40	1140	1140	19.1	19.1	0	1013
	Ko-JI1 [a]	300	500	300	300	50	50	35	2026	2026	25.4	25.4	0	1013
[60]	BL1	350	500	400	400	38	38	38	1407	1206	16.0	16.0	1809	402
	BL2 [b]	300	500	400	400	52	40	40	1884	1256	20.0	20.0	2035	628
	BL3	250	400	350	450	54	36	36	1608	804	16.0	16.0	1356	402
	BL4	300	500	400	400	47	38	38	1608	1005	16.0	16.0	2035	402

[a] Joints without horizontal hoops

[b] Joints that did not satisfy both ACI Code and EC8 requirements

Table B2. Mechanical properties, forces and results of the 69 specimens used for the calibration of the coefficients q_0, q_1, q_2 and q_3 in the proposed formula (Eq. (78))

Author references	Specimen labels	f'_c (MPa)	f_{yh} (MPa)	f_{yv} (MPa)	N (kN)	θ_h (deg)	$V_{hc,ST1}$ (%)	$V_{hc,ST2-3}$ (%)	$V_{hs,h}$ (%)	$V_{hs,v}$ (%)	V_n (kN)	$V_{jh,test}$ (kN)	$\dfrac{V_{jh,test}}{V_n}$	$\dfrac{V_{jh,test}}{V_{n,Kim}}$	$\dfrac{V_{jh,test}}{V_{n,Wang}}$	$\dfrac{V_{jh,test}}{V_{n,Kassem}}$	V_d (kN)	$\dfrac{V_{jh,test}}{V_d}$	$\dfrac{V_{jh,test}}{V_{d,EC8}}$	$\dfrac{V_{jh,test}}{V_{d,ACI}}$
[36]	E0.0[a]	43.1	460	513	0	45	63	17	0	20	689	750	1.09	-	-	-	551	1.36	-	-
	E0.3[a]	46.1	460	558	1080	52	79	9	0	12	947	815	0.86	-	-	-	758	1.08	-	-
	H0.0	50.6	460	595	0	45	59	14	8	19	828	869	1.05	0.89	1.07	0.92	662	1.31	0.84	1.40
	H0.3	45.1	460	518	1080	52	75	8	6	11	994	744	0.75	0.82	0.66	0.80	795	0.94	3.58	1.27
[37]	B1	27.9	346	427	311	54	55	35	8	2	1232	1217	0.99	0.89	1.21	0.96	986	1.23	1.09	1.17
	B2[b]	31.5	398	427	2890	65	81	16	2	1	1444	1213	0.84	1.03	0.76	0.93	1155	1.05	-	-
[38]	A1	40.2	291	644	162	51	57	21	2	20	443	412	0.93	0.89	1.03	0.49	354	1.16	1.24	1.47
	A2	40.2	291	388	162	51	62	23	2	13	408	380	0.93	1.09	1.12	1.01	326	1.16	1.15	1.35
	A3	40.2	291	644	480	55	68	16	1	15	485	412	0.85	0.89	0.83	0.47	388	1.06	3.05	1.47
[39]	J-HH[b]	32.1	382	578	867	57	67	12	9	12	780	725	0.93	0.83	0.82	0.63	624	1.16	-	-
	J-HO[b]	32.1	382	578	867	57	76	14	10	0	689	696	1.01	0.80	0.95	0.62	551	1.26	-	-
	J-OH[a]	32.1	382	578	867	57	74	13	0	13	709	642	0.91	-	-	-	568	1.13	-	-
	J-MM[b]	32.1	382	578	867	57	75	13	5	7	699	736	1.05	0.94	1.00	0.71	559	1.32	-	-
	J-MO[b]	32.1	382	578	867	57	80	14	5	0	654	752	1.15	0.96	1.15	0.74	523	1.44	-	-
	J-LO[b]	32.1	382	578	867	57	85	15	0	0	620	751	1.21	1.54	1.30	0.81	496	1.51	-	-
[40]	O1[a]	41.0	0	325	0	59	77	23	0	0	591	527	0.89	-	-	-	473	1.12	-	-
[41]	JXO-B1	21.3	307	371	307	53	79	15	2	4	386	282	0.73	0.80	0.77	1.05	309	0.91	1.37	1.07
[42]	A-1	19.3	324	356	353	50	73	22	5	0	443	495	1.12	0.84	1.24	0.76	355	1.40	6.34	1.42
[43]	I3	41.4	360	361	95	46	65	21	2	13	702	709	1.01	1.09	1.28	1.18	562	1.26	0.97	1.39
	I5	85.4	250	534	177	46	73	11	1	14	944	893	0.95	1.08	1.08	1.17	755	1.18	0.66	1.22
	I6	85.4	250	534	177	46	75	9	1	15	927	1005	1.08	1.13	1.22	1.11	741	1.36	0.75	1.37
[44]	B1	24.5	235	351	176	47	55	29	1	14	593	570	0.96	1.26	1.20	1.37	475	1.20	1.70	1.45

Author references	Specimen labels	f'_c (MPa)	f_{yh} (MPa)	f_{yv} (MPa)	N (kN)	θ_h (deg)	$V_{hc,ST1}$ (%)	$V_{hc,ST2-3}$ (%)	$V_{hs,h}$ (%)	$V_{hs,v}$ (%)	V_n (kN)	$V_{jh,test}$ (kN)	$\dfrac{V_{jh,test}}{V_n}$	$\dfrac{V_{jh,test}}{V_{n,Kim}}$	$\dfrac{V_{jh,test}}{V_{n,Wang}}$	$\dfrac{V_{jh,test}}{V_{n,Kassem}}$	V_d (kN)	$\dfrac{V_{jh,test}}{V_d}$	$\dfrac{V_{jh,test}}{V_{d,EC8}}$	$\dfrac{V_{jh,test}}{V_d,ACI}$
	B3	24.5	235	371	176	47	55	32	3	10	599	515	0.86	0.94	1.13	1.05	479	1.07	1.53	1.31
	A1	30.6	320	539	176	47	58	20	2	20	663	689	1.04	1.01	1.15	0.77	531	1.30	1.45	1.57
[45]	JE-0	27.0	364	345	0	47	57	34	2	7	492	477	0.97	1.00	1.43	1.17	393	1.21	0.99	1.55
[46]	JI0	27.0	456	456	821	61	69	17	7	7	858	876	1.02	0.86	0.95	0.77	687	1.28	2.00	1.14
[47]	JA [b]	33.7	484	484	1618	59	73	12	10	5	1266	1310	1.03	0.93	0.92	0.79	1013	1.29	-	-
	JB [b]	34.8	484	484	1670	59	67	17	11	5	1424	1331	0.93	0.85	0.88	0.66	1139	1.17	-	-
	JC [b]	32.5	461	484	1560	57	65	12	13	10	1455	1359	0.93	0.93	0.81	0.78	1164	1.17	-	-
	JD [b]	33.1	466	484	1589	57	63	11	16	9	1524	1491	0.98	0.98	0.83	0.78	1219	1.22	-	-
[48]	I [b]	26.2	409	457	1588	57	77	12	2	9	1141	1090	0.96	0.97	0.84	0.77	913	1.19	-	-
	II	41.8	409	449	1601	52	72	11	2	16	1612	1597	0.99	1.23	0.92	1.05	1289	1.24	4.22	1.68
	III [b]	26.6	409	402	1584	56	63	10	2	25	1402	1228	0.88	1.09	0.73	0.80	1122	1.09	-	-
	IV [b]	36.0	409	438	1615	62	78	11	5	6	1091	1455	1.33	1.22	1.20	1.02	873	1.67	-	-
	V	35.9	409	449	214	46	55	18	2	24	1275	1530	1.20	1.24	1.28	1.10	1020	1.50	1.56	1.73
	VI [b]	36.8	409	449	2682	60	79	7	2	12	1545	1646	1.07	1.32	0.81	1.04	1236	1.33	-	-
	VII [b]	37.2	409	438	2656	67	83	7	5	5	1138	1468	1.29	1.22	0.99	0.98	910	1.61	-	-
	XII [b]	35.2	423	449	1615	53	66	10	9	15	1595	1948	1.22	1.25	1.05	1.05	1276	1.53	-	-
	XIII	41.3	409	449	1570	52	69	11	5	15	1656	1557	0.94	1.02	0.85	0.92	1325	1.18	4.04	1.65
	XIV [b]	33.2	409	438	1615	62	70	10	15	5	1155	1539	1.33	1.12	1.10	0.92	924	1.67	-	-
[49]	OKJ-1	70.0	955	718	756	48	69	15	4	13	1148	1068	0.93	0.92	0.93	0.82	919	1.16	1.17	1.61
	OKJ-4	70.0	955	718	756	48	69	15	4	13	1148	1128	0.98	0.98	0.98	0.87	919	1.23	1.24	1.70
[50]	NO.2	34.1	354	354	180	46	64	27	0	9	655	485	0.74	1.10	1.04	1.13	524	0.92	0.86	1.05
	NO.4	34.1	354	354	180	46	71	19	0	10	594	542	0.91	1.22	1.16	1.26	476	1.14	0.96	1.17
[51]	J-1	81.2	638	638	834	48	72	14	2	12	1159	1150	0.99	1.08	1.00	1.04	927	1.24	1.04	1.49
	J-3	81.2	1456	1456	834	48	49	10	23	18	1694	1466	0.87	0.70	0.64	0.43	1355	1.08	1.32	1.90
	J-4	72.8	515	515	834	48	71	18	2	9	1143	1175	1.03	1.17	1.12	1.08	914	1.28	1.18	1.61
	J-5	72.8	839	839	834	48	69	14	3	15	1182	1320	1.12	1.13	1.09	0.95	946	1.40	1.33	1.81

Author references	Specimen labels	f'_c (MPa)	f_{yh} (MPa)	f_{yv} (MPa)	N (kN)	θ_h (deg)	$V_{hc,ST1}$ (%)	$V_{hc,ST2-3}$ (%)	$V_{hs,h}$ (%)	$V_{hs,v}$ (%)	V_n (kN)	$V_{jh,test}$ (kN)	$\dfrac{V_{jh,test}}{V_n}$	$\dfrac{V_{jh,test}}{V_{n,Kim}}$	$\dfrac{V_{jh,test}}{V_{n,Wang}}$	$\dfrac{V_{jh,test}}{V_{n,Kassem}}$	V_d (kN)	$\dfrac{V_{jh,test}}{V_d}$	$\dfrac{V_{jh,test}}{V_{d,EC8}}$	$\dfrac{V_{jh,test}}{V_d,ACI}$
	J-6	79.2	676	676	834	48	72	14	1	12	1152	1223	1.06	1.22	1.08	1.08	922	1.33	1.13	1.60
	J-8	79.2	370	370	834	48	66	20	1	13	1259	1385	1.10	1.31	1.18	1.04	1007	1.37	1.28	1.82
	J-10	39.2	700	700	417	48	61	19	3	17	873	875	1.00	0.98	1.08	0.78	698	1.25	1.47	1.63
	J-11	39.2	372	372	417	48	55	26	1	17	965	1029	1.07	1.20	1.26	0.81	772	1.33	1.72	1.92
[52]	JO-1	20.0	455	434	0	45	46	29	6	20	121	99	0.82	0.54	0.90	0.41	97	1.03	1.32	0.93
[53]	J0C-1	31.2	447	343	88	48	80	16	3	0	140	159	1.14	1.05	1.37	1.24	112	1.42	1.62	1.33
[54]	1	41.3	320	473	511	51	58	24	12	6	1194	1001	0.84	0.85	0.89	0.84	955	1.05	1.10	1.36
[55]	1	34.0	305	476	996	55	67	22	8	4	1095	966	0.88	0.92	0.94	0.88	876	1.10	2.82	1.44
	1 [a]	32.7	0	456	1557	63	85	15	0	0	946	985	1.04	-	-	-	757	1.30	-	-
	2 [a]	32.7	0	456	1557	63	85	15	0	0	946	969	1.02	-	-	-	757	1.28	-	-
[56]	3 [a]	30.4	0	486	1557	64	84	16	0	0	905	936	1.03	-	-	-	724	1.29	-	-
	4 [b]	31.9	300	518	1557	63	80	15	1	4	982	923	0.94	1.09	0.91	0.68	786	1.17	-	-
	5 [b]	29.8	300	455	1557	64	80	15	2	4	948	954	1.01	0.95	0.95	0.64	758	1.26	-	-
[57]	S3	28.0	390	450	100	46	56	24	2	18	601	731	1.22	1.15	1.41	1.01	481	1.52	1.56	1.74
[58]	J3B	23.7	448	480	207	44	54	21	7	18	542	438	0.81	0.77	0.82	0.76	434	1.01	1.82	1.30
[59]	Ho-JI1 [a]	27.0	0	541	0	45	63	23	0	14	829	893	1.08	-	-	-	663	1.35	-	-
	Ko-JI1 [a]	32.0	0	533	403	62	60	29	0	11	554	759	1.37	-	-	-	443	1.71	-	-
	BL1	28.8	407	528	1152	58	71	17	9	3	1083	1190	1.10	0.97	1.07	0.92	867	1.37	5.08	1.40
[60]	BL2 [b]	37.5	368	540	1800	59	77	12	8	3	1322	1267	0.96	0.90	0.88	0.81	1058	1.20	-	-
	BL3	29.8	464	444	1173	48	76	15	7	3	1283	1034	0.81	0.81	0.81	0.86	1026	1.01	3.88	1.33
	BL4	32.8	362	553	1312	58	73	16	8	3	1178	1038	0.88	0.81	0.86	0.76	942	1.10	3.12	1.22

[a] Joints without horizontal hoops

[b] Joints that did not satisfy both ACI Code and EC8 requirements

Table B3. Geometrical properties and reinforcement areas of the 28 specimens employed for the comparison between Eq. (78) and the expressions provided by Kim and LaFave (Eq. (79)), Wang et al. (Eq. (80)) and Kassem (Eq. (85)), and for the comparison between Eq. (91) and the shear strength formulae for interior joints provided by Eurocode 8 (Eq. (92)) and ACI 318-14 (Eq. (93)).

Author references	Specimen labels	b_b (mm)	h_b (mm)	b_c (mm)	h_c (mm)	δ_{b1} (mm)	δ_{b2} (mm)	δ_c (mm)	A_{sb1} (mm²)	A_{sb2} (mm²)	ϕ_1 (mm)	ϕ_2 (mm)	A_{sh} (mm²)	A_{sv} (mm²)
[61]	LIJ3	343	343	343	457	57	57	56	855	855	19.1	19.1	142	0
	LIJ4	343	343	343	457	54	54	56	633	633	12.7	12.7	142	0
[62]	X1	279	419	362	362	38	38	47	1551	1140	22.2	19.1	865	1013
	X2	279	419	362	362	38	38	47	1551	1140	22.2	19.1	1297	1013
	X3	279	419	362	362	38	38	47	1163	855	22.2	19.1	865	570
[63]	S1	350	500	500	460	53	53	55	2026	1013	25.4	25.4	1592	2026
[64]	C1-400	350	500	500	550	58	51	68	3020	1520	23.3	22.0	2123	2641
	C2-600	350	500	500	550	51	51	68	1900	1140	22.0	22.0	2123	2641
	C3-600	350	500	500	450	51	51	68	1900	1140	22.0	22.0	2123	2641
	C4-600	350	500	500	550	53	53	68	1963	981	25.0	25.0	2123	2641
[65]	PL-13	200	350	300	300	32	32	32	663	663	13.0	13.0	339	402
	PH-16	200	350	300	300	32	32	32	804	804	16.0	16.0	452	402
	PH-13	200	350	300	300	57	57	32	929	929	13.0	13.0	452	402
	PH-10	200	350	300	300	48	48	32	785	785	10.0	10.0	452	402
[66]	J1	300	400	350	350	57	57	55	2010	2010	16.0	16.0	942	2641
	BJ1	300	400	350	350	48	48	55	1206	1206	16.0	16.0	942	2641
	BJ2	300	400	350	350	48	48	55	1005	1005	16.0	16.0	628	2641
	BJ3	300	400	350	350	48	48	55	804	804	16.0	16.0	628	2641
[67]	BCJ2	203	305	254	254	27	25	27	506	285	12.7	9.5	127	760
	BCJ3	203	305	254	304	27	25	27	506	285	12.7	9.5	127	760
[68]	No. 1 [b]	250	350	350	350	38	38	34	1963	1963	25.0	25.0	471	2280
	No. 5 [b]	250	350	350	350	51	51	34	1407	1407	16.0	16.0	471	2280
[69]	C1	200	300	300	300	45	30	30	855	427	9.5	9.5	191	760
	J3	200	300	300	300	45	30	30	1013	507	12.7	12.7	899	760
[60]	CL1	350	500	400	400	38	38	38	1407	1206	16.0	16.0	1809	402
	CL2 [b]	300	500	400	400	52	40	40	1884	1256	20.0	20.0	2035	628
	CL3	250	400	350	450	54	36	36	1608	804	16.0	16.0	1356	402
	CL4	300	500	400	400	47	38	38	1608	1005	16.0	16.0	2035	402

[b] Joints that did not satisfy both ACI Code and EC8 requirements

Table B4. Mechanical properties, forces and results of the 28 specimens employed for the comparison between Eq. (78) and the expressions provided by Kim and LaFave (Eq. (79)), Wang et al. (Eq. (80)) and Kassem (Eq. (85)), and for the comparison between Eq. (91) and the shear strength formulae for interior joints provided by Eurocode 8 (Eq. (92)) and ACI 318-14 (Eq. (93)).

Author references	Specimen labels	f'_c (MPa)	f_{yh} (MPa)	f_{yv} (MPa)	N (kN)	θ_h (deg)	$V_{hc,ST1}$ (%)	$V_{hc,ST2-3}$ (%)	$V_{hs,h}$ (%)	$V_{hs,v}$ (%)	V_n (kN)	$V_{jh,test}$ (kN)	V_d (kN)	$\dfrac{V_{jh,test}}{V_n}$	$\dfrac{V_{jh,test}}{V_{n,Kim}}$	$\dfrac{V_{jh,test}}{V_{n,Wang}}$	$\dfrac{V_{jh,test}}{V_{n,Kassem}}$	$\dfrac{V_{jh,test}}{V_d}$	$\dfrac{V_{jh,test}}{V_{d,EC8}}$	$\dfrac{V_{jh,test}}{V_d,ACI}$
[61]	LIJ3	31.1	400	470	0	37	79	20	1	0	824	724	659	0.88	0.79	1.47	1.10	1.10	0.73	0.91
	LIJ4	34.3	400	470	0	37	79	20	1	0	900	789	720	0.88	0.91	1.52	1.46	1.10	0.71	0.93
[62]	X1	34.3	352	414	225	50	65	21	5	9	847	840	678	0.99	0.92	1.13	1.05	1.24	1.02	1.33
	X2	33.6	352	414	264	51	64	20	7	9	868	853	695	0.98	0.88	1.06	0.99	1.23	1.08	1.37
	X3	31.0	352	414	203	50	70	18	6	6	724	629	579	0.87	0.77	0.96	0.98	1.09	0.86	1.07
[63]	S1	38.3	496	452	0	47	66	15	7	12	1478	1419	1183	0.96	0.82	1.01	1.00	1.20	0.76	1.25
[64]	C1-400	32.0	446	510	0	42	55	22	7	16	1973	1860	1579	0.94	0.81	1.06	0.88	1.18	1.03	1.53
	C2-600	32.0	446	510	0	42	59	16	7	18	1841	1842	1473	1.00	0.80	1.05	0.88	1.25	1.02	1.52
	C3-600	32.0	446	510	0	48	56	17	9	18	1444	1853	1156	1.28	0.98	1.24	0.95	1.60	1.36	1.87
	C4-600	29.6	446	510	0	42	59	15	7	19	1724	1832	1379	1.06	0.85	1.07	0.96	1.33	1.12	1.59
[65]	PL-13	26.4	366	402	396	54	73	19	3	5	517	449	414	0.87	0.91	0.96	1.03	1.08	1.56	1.32
	PH-16	23.6	366	402	354	54	70	20	5	5	484	482	387	0.99	0.93	1.06	0.99	1.24	2.03	1.54
	PH-13	26.3	366	402	395	54	67	25	4	5	561	544	449	0.97	0.96	1.13	0.96	1.21	1.90	1.60
	PH-10	25.6	366	402	384	54	65	27	4	5	565	512	452	0.91	0.95	1.08	1.00	1.13	1.87	1.54
[66]	J1	40.0	510	514	0	49	44	29	5	22	1193	1604	955	1.34	1.25	1.52	0.99	1.68	1.70	2.36
	BJ1	40.0	510	514	0	49	49	20	6	25	1054	1237	843	1.17	1.12	1.17	1.10	1.47	1.31	1.82
	BJ2	40.0	510	514	0	49	52	17	4	26	997	1061	798	1.06	1.08	1.06	1.13	1.33	1.13	1.56
	BJ3	40.0	510	514	0	49	54	15	5	27	962	920	770	0.96	1.00	0.92	1.13	1.20	0.98	1.35
[67]	BCJ2	30.3	414	448	0	50	60	20	2	18	350	358	280	1.02	1.07	1.11	1.27	1.28	0.86	1.23
	BCJ3	27.4	414	448	0	45	61	20	2	18	419	394	335	0.94	1.01	1.09	1.32	1.17	0.86	1.22
[68]	No. 1 [b]	22.1	377	548	833	54	61	15	3	22	935	1148	-	1.23	1.19	1.13	0.75	-	-	-

Author references	Specimen labels	f'_c (MPa)	f_{yh} (MPa)	f_{yv} (MPa)	N (kN)	θ_h (deg)	$V_{hc,ST1}$ (%)	$V_{hc,ST2-3}$ (%)	$V_{hs,h}$ (%)	$V_{hs,v}$ (%)	V_n (kN)	$V_{jh,test}$ (kN)	V_d (kN)	$\dfrac{V_{jh,test}}{V_n}$	$\dfrac{V_{jh,test}}{V_{n,Kim}}$	$\dfrac{V_{jh,test}}{V_{n,Wang}}$	$\dfrac{V_{jh,test}}{V_{n,Kassem}}$	$\dfrac{V_{jh,test}}{V_d}$	$\dfrac{V_{jh,test}}{V_{d,EC8}}$	$\dfrac{V_{jh,test}}{V_d,ACI}$
	No. 5 [b]	21.6	377	548	833	54	59	17	3	21	940	1244	-	1.32	1.44	1.24	1.06	-	-	-
[69]	C1	26.6	324	422	183	47	61	26	1	11	571	436	457	0.76	0.95	0.95	1.13	0.95	1.05	1.27
	J3	24.0	367	374	173	47	58	23	8	10	554	576	443	1.04	0.88	1.12	0.90	1.30	1.62	1.81
[60]	CL1	35.5	407	528	1420	58	75	15	8	2	1237	1120	989	0.91	0.86	0.88	0.84	1.13	2.89	1.35
	CL2 [b]	38.2	368	540	1834	59	77	12	8	3	1337	1162	-	0.87	0.83	0.80	0.74	-	-	-
	CL3	34.3	464	444	1351	48	78	14	6	2	1409	945	1127	0.67	0.71	0.67	0.77	0.84	2.54	1.29
	CL4	30.2	362	553	1208	58	72	17	9	3	1118	947	894	0.85	0.76	0.83	0.70	1.06	3.49	1.36
													AVG	0.990	0.944	1.082	1.001	1.216	1.420	1.439
													DEV.ST	0.160	0.163	0.196	0.173	0.181	0.711	0.311
													COV	0.162	0.172	0.181	0.172	0.149	0.501	0.216
													UP	18	20	8	15	2	7	2

[b] Joints that did not satisfy both ACI Code and EC8 requirements